TRANSPORTATION RESEARCH RECORD 685

Geometrics, Hydraulics, and Hydrology

TRANSPORTATION RESEARCH BOARD

COMMISSION ON SOCIOTECHNICAL SYSTEMS
NATIONAL RESEARCH COUNCIL

NATIONAL ACADEMY OF SCIENCES
WASHINGTON, D.C. 1978

Transportation Research Record 685
Price $3.00

modes
1 highway transportation
3 rail transportation

subject areas
21 facilities design
22 hydrology and hydraulics
23 environmental design
54 operations and traffic control

Transportation Research Board publications are available by ordering directly from the board. They may also be obtained on a regular basis through organizational or individual supporting membership in the board; members or library subscribers are eligible for substantial discounts. For further information, write to the Transportation Research Board, National Academy of Sciences, 2101 Constitution Avenue, N.W., Washington, DC 20418.

Library of Congress Cataloging in Publication Data
National Research Council. Transportation Research Board.
Geometrics, hydraulics, and hydrology.

(Transportation research record; 685)

1. Roads–Design–Addresses, essays, lectures. 2. Roads–Accessories–Addresses, essays, lectures. 3. Road drainage–Addresses, essays, lectures. I. Title. II. Series.
TE7.H5 no. 685 [TE175] 380.5'08s [625.7'2] 79-9153
ISBN 0-309-02830-2

Sponsorship of the Papers in This Transportation Research Record

GROUP 2–DESIGN AND CONSTRUCTION OF TRANSPORTATION FACILITIES
Eldon J. Yoder, Purdue University, chairman

General Design Section
Lester A. Herr, Federal Highway Administration, chairman

Committee on Geometric Design
B. H. Rottinghaus, Howard Needles Tammen and Bergendoff, chairman
Alvin R. Cowan, Federal Highway Administration, secretary
W. L. Brittle, Jr., Sumner B. Chansky, Robert R. Coleman, Harold D. Cooner, Hugh G. Downs, John C. Glennon, Malcolm D. Graham, C. William Gray, William R. Hawkins, Peter J. Hunt, Max N. Jensen, Milton L. Johnson, Richard D. Johnson, Frank J. Koepke, Jack E. Leisch, Alex E. Mansour, J. Robert Moore, Thomas E. Mulinazzi, Geoffrey M. Nairn, Jr., George B. Pilkington II, Stanley L. Ring, Robert A. Snowber, W. A. Wilson, Jr.

Committee on Hydrology, Hydraulics, and Water Quality
Samuel V. Fox, Texas State Department of Highways and Public Transportation, chairman
Frank L. Johnson, Federal Highway Administration, secretary
Charles J. Allen, John J. Bailey, Jr., Harry H. Barnes, Jr., Lawrence D. Bruesch, Darwin L. Christensen, Earl C. Cochran, Jr., Allen L. Cox, Richey S. Dickson, John Joseph Duffy, Kenneth S. Eff, Philip F. Frandina, John L. Grace, Jr., Herbert W. Gregory, Lester A. Herr, J. Sterling Jones, Clinton E. Parker, Brian M. Reich, August R. Robinson, John E. Sandahl, William P. Somers, A. Mainard Wacker, Fred J. Watts, Henry B. Wyche, Jr.

Committee on Roadside Environment
L. E. Foote, Minnesota Department of Transportation, chairman
Kenneth A. Rickerson, Federal Highway Administration, secretary
Charles R. Anderson, Donald Appleyard, E. Leroy Brady, Jack E. Burton, Bernard L. Chaplin, Frank J. Cope, John F. Delay, Harold D. Dolling, Mil Fleig, James R. Gordon, Peter L. Hornbeck, Robert L. Jacobsen, Herman A. J. Kuhn, Thomas J. Mracek, William R. Nelson, Jr., Clarence R. Pell, E. Grover Rivers, G. I. Robertson, Jr., James Alton Saunders, Barbara M. Schaedler, W. A. Schmitz, John L. Snuggs, Leonard E. Wood

Lawrence F. Spaine, Transportation Research Board staff

Sponsorship is indicated by a footnote at the end of each report. The organizational units and officers and members are as of December 31, 1977.

Contents

Edge-of-Pavement Profiles

V. F. Hurdle, Department of Civil Engineering,
University of Toronto

When superelevation transitions occur within or adjacent to vertical curves, the profile of the edge of the road is sometimes distorted into shapes that are visually unpleasant or cause severe drainage problems, particularly on freeways or other wide roads. Such problems can be easily and quickly solved by simple algebraic methods that need no plotting of edge profiles to scale or resorting to curves more complicated than standard parabolic vertical curves if one takes advantage of the inherent simplicity of standard highway geometry. Methods for doing this are developed and demonstrated with a numerical example.

The horizontal and vertical alignment of highways has traditionally been thought of as a series of straight lines (tangents) connected together by curves. Probably as a carry-over from railway design—where horizontal curvature radically increases the force necessary to move the train—and for simplicity, most designers tried to keep the tangents as long as possible and the curves as short as possible. Roads built in hilly country 50 years ago were actually curvilinear (crooked) in spite of this design philosophy, but, as the introduction of motorized equipment lowered the cost of earthwork, the roads became straighter and straighter.

As Tunnard and Pushkarev (1) have documented so well with photographs, a frequent result was a type of long tangent, short curve alignment that not only seemed to exhibit a callous disregard for the integrity of the landscape, but tended to look silly in itself. To the extent that the general public reacted to this at all, the reaction was probably a sort of generalized objection to the building of roads and to the builders as well. Some professionals also reacted, however, and from this reaction a philosophy of curvilinear alignment developed wherein the designer fit long curves to the terrain and used short tangents as connecting elements.

In North America, this design philosophy suffered a severe setback during the rush of construction after World War II but eventually became commonly accepted, particularly during the period of emphasis on aesthetics of design in the United States in the mid-1960s. While many reference works on this type of design exist, I regard two (1, 2) as the most basic and comprehensive. Both reflect the ideas of progressive designers of the late 1930s (3).

Once one gets used to the idea of using curves rather than straight lines as the basic design elements, the design of curvilinear roads is not particularly difficult. Furthermore, the generous use of curvature allows a great deal of freedom in design, so one should be able to reduce construction costs by achieving a better fit to the terrain than is possible with a long-tangent, short-curve design.

The changeover is not completely without difficulties, however; a few new technical problems do arise. Perhaps the most obvious is that one must devote considerable attention to the provision of sufficient passing sight distance on two-lane roads. In addition, certain combinations of horizontal and vertical curvature can look very bad, so there has been considerable research into problems of the coordination of horizontal and vertical curvature and the general concept of the road as a three-dimensional object. Many books and papers (1, 2, 3) have devoted a good deal of attention to this subject, and some (4, 5) are entirely devoted to it.

A problem that has received much less attention, however, is the interaction of vertical curvature and superelevation transitions that occurs when vertical and horizontal curves of nearly equal length are superimposed to create a three-dimensional curve. The most obvious example of this interaction is the appearance of a little kink or dent in the edge of the roadway near the end of a superelevation transition, sometimes scarcely measurable, but very visible. Nearly every highway engineering manual and route surveying textbook contains a warning about this, usually coupled with the advice that a profile of the edge of the roadway should be plotted and examined for any irregularities. The advice is sound, but it should be obvious to any engineer who drives with a critical eye that the results often leave much to be desired.

An example of such a dent, along with the profile and superelevation diagram that produced it, is shown in Figure 1. The dent in the edge profile just to the left of km 10+000 is obvious in the figure and would be even more obvious on the ground, since the flat angle at which motorists view the roadway makes even very small undulations highly visible. The fact that the actual depth of the dent is tiny does not matter; the eye seems to be sensitive to irregularity of shape rather than to elevation.

To avoid such problems, many engineers abandon the superelevation diagram and design a smooth profile for each edge graphically with splines or French curves, a method recommended by the AASHTO Blue Book (8). This method is rather laborious, however, particularly since the resulting design can be included in contract plans only as a graphical curve or a series of grid point elevations. Splined curves are also positively guaranteed to produce indigestion if fed to a production-oriented computer program, so survey notes must be prepared by hand.

The basic premise of this paper is that an easier way is available. In many situations graphical methods are very desirable; in fact, I believe that engineers should use graphical methods more often than they do. In this particular case, however, an easier, quicker, and surer algebraic method is available. This method is hardly revolutionary; it really only amounts to understanding the basic geometry of the roadway and checking the values of certain critical parameters. There must be many engineers who have worked out similar methods. They are not, however, in common use in North America and appear in few, if any, of the standard texts and handbooks. A related but much less flexible approach has been used in the British computer program, JANUS (5).

VERTICAL CURVES

The first step in developing the method is to review the basic geometry of the parabolic vertical curves used in highway design. Two tangent grades, g_1 and g_2, are joined by a segment of a parabola defined by the quadratic equation

$$y(x) = y_0 + g_1 x + (r/2)x^2 \qquad (1)$$

where

$y(x)$ = elevation at a horizontal distance x from the beginning of the vertical curve (BVC),
y_0 = elevation at the beginning of the vertical curve,

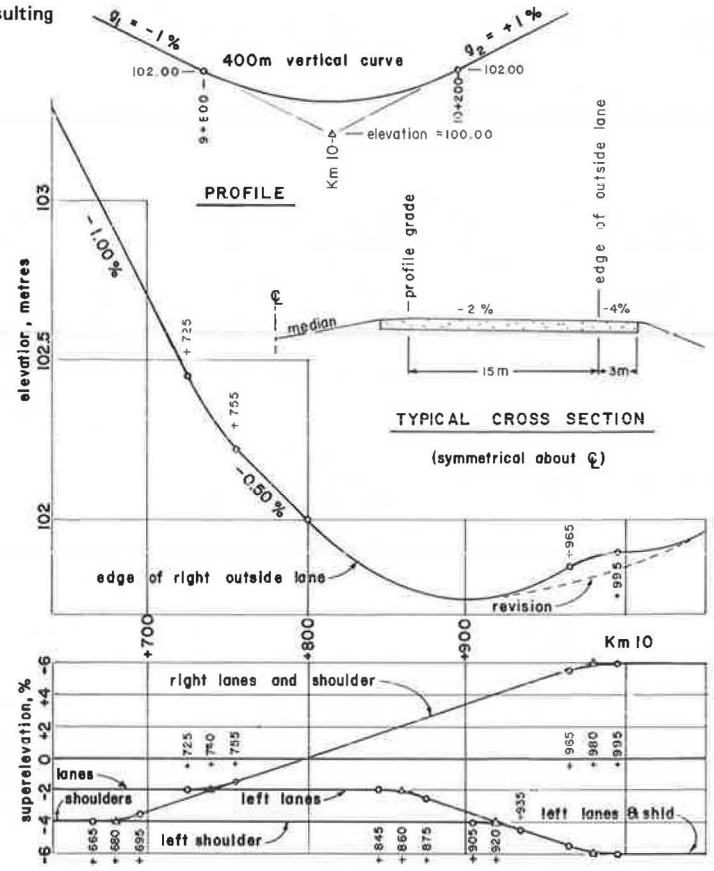

Figure 1. Superelevation diagram with 30-m curves and resulting edge-of-pavement profile for right lanes.

$r = (g_2 - g_1)/L$, and
L = horizontal length of the vertical curve.

The slope or grade at any point on the curve can be obtained by differentiating Equation 1:

$$dy(x)/dx = g_1 + rx \quad (2)$$

Of more interest in the problem considered here is the rate of change of grade:

$$d^2y(x)/dx^2 = r \quad (3)$$

That the rate of change of grade is constant is, of course, a fundamental property of a parabolic vertical curve (6). Instead of differentiating Equation 1 to obtain Equations 2 and 3, we could as well have postulated that a constant rate of change of grade was a desirable property, and then obtained Equations 2 and 1 by integration. Clearly this must be what happened historically: someone noted that a constant rate of change of grade not only was the simplest way to join two grades but also produced the shortest possible curve satisfying a criterion of the form $d^2y(x)/dx^2 \leq$ some number.

The value of r, or its reciprocal, can be used as a measure of curvature. Use of the reciprocal is, in fact, common and has an advantage in that a parabolic highway or railway curve with rate of change of grade r is very nearly the same curve as a circular curve with radius 1/r. The design handbooks listed in the references all use the reciprocal. Two European references (2, 10) identify 1/r as a radius and denote it by the symbols H and R_v, respectively. North American references (8, 9) instead use K = 1/100r, the distance required to accomplish a 1 percent change in grade.

In what follows we shall use r as our measure of curvature rather than K because the equations would be more complicated with K. Most design calculations, however, could be made just as easily with K as with r.

A NOTE REGARDING UNITS

This paper has been written at a rather awkward time so far as units are concerned; both the traditional system of feet and 100-foot stations and the metric system are in current use in North American practice. In Canada, in fact, one might find an engineer working on two projects concurrently, one measured in feet and the other in meters.

In general, this paper will use SI (Systeme International d'Unités) units, following in most details the usage recommended (7). Vertical distances will always be expressed in meters, but location along the centerline, or chainage, will be expressed as a distance in kilometers from some arbitrary zero point plus a distance in meters: a point 9 km from the starting point will be identified as km 9 or km 9+000 and a point 500.36 m farther from the starting point as km 9+500.36, for example.

Equations 1, 2, and 3 are unit free; they are valid in any units. The horizontal and vertical distances can be measured in meters, feet, chains, furlongs, fathoms, or even inches; it does not matter what the unit of measurement is, so long as the same unit is used throughout the calculation. It should be noted that the grades g_1, g_2, and dy(x)/dx are dimensionless ratios, so a grade of 0.02 means exactly the same thing in any system of units; the rate of change of grade r is not dimensionless, though, and has units of reciprocal meters (1/m) or reciprocal feet (1/ft). Typical values are of the order of 10^{-4} in either system.

Since numbers less than 0.1 are awkward to remem-

Figure 2. Cross section of simple one-lane road at location x.

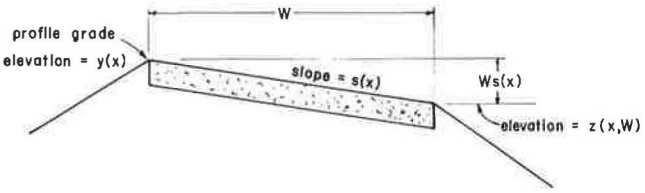

ber and use in mental calculations, it is common practice to express grades in percentages. The difficulty with too many zeros is obviously much more severe with the values of r normally encountered, so in this paper all values of r will be expressed as a multiple of 10^{-4}, for example 0.5×10^{-4}/m instead of 0.000 05/m. This can be thought of as 0.5 percent per hundred meters. In traditional units, 0.5×10^{-4}/ft can be thought of as 0.5 percent per station.

One additional warning about units is necessary for designers working with the AASHTO Blue Book (8) or RTAC metric standards (9). These handbooks express vertical curvature in terms of K, defined as the distance, in feet or meters respectively, to accomplish a 1 percent grade change. Thus the units of K are really ft/percent or m/percent, but table headings in the handbooks indicate that they are in feet and meters, respectively, because the percentage is included in the definition. The tabled values of K in these two reference books can, therefore, never be used directly in unit-free equations, but must always be converted to feet or meters by multiplying by 100.

SUPERELEVATION TRANSITIONS

The foregoing discussion of vertical curves used elementary calculus in order to clarify the concepts, but the mathematical methods used in ordinary practice are algebra and arithmetic. In treating superelevation, it is not even usual to use algebra; one simply draws a superelevation diagram such as the one shown in Figure 1 and reads the values graphically. As a matter of fact, this is a good approach. Since the diagram is easy to draw and provides adequate accuracy if an appropriate scale is used, why should one bother to write an equation?

In order to develop the relationship between vertical alignment and superelevation, however, we shall continue to use the language and notation of calculus because they provide an easy way to describe what is happening. For ordinary applications we shall revert to simple arithmetic.

To begin, let us suppose that our road has only one lane and no shoulders, with the profile along the left edge, as shown in Figure 2. This simple road could be a ramp or half of a two-lane road; the numerical example in Figure 1 is half of an eight-lane freeway. The width of the lane is W; the elevation of the left edge is, by definition, y(x); and we define a function s(x) = superelevation rate at location x to describe the superelevation. In the section on vertical curves, x was defined as the horizontal distance from the beginning of the vertical curve. In this section we shall not define it so precisely; x is simply a number that identifies our location, the horizontal distance along the centerline from some arbitrary zero point measured in the same units as all other distances. We shall never write an expression for s(x); it is simply a name for the function described by a superelevation diagram such as the numerical example in Figure 1. It is important to realize, however, that superelevation diagrams have the same mathematical form as profiles: straight lines joined together by parabolic curves.

To obtain the elevation z(x, W) of a point on the right edge of our one-lane road, a distance W right of a point on the centerline at location x, we simply read s(x) from the superelevation diagram, multiply by the width W, and add the product to the profile elevation g(x):

$$z(x, W) = y(x) + Ws(x) \tag{4}$$

Differentiating Equation 4 twice, we obtain

$$dz(x, W)/dx = dy(x)/dx + dWs(x)/dx \tag{5}$$

$$d^2z(x, W)/dx^2 = d^2y(x)/dx^2 + d^2Ws(x)/dx^2 \tag{6}$$

In this paper, it will always be assumed that the width of the road, W, is constant. For tapers, one must replace W with W(x) before differentiating.

From Equations 4, 5, and 6 we see that the shape of the edge of the lane, described by its elevation z(x, W), slope dz(x, W)/dx, and rate of change of grade $d^2z(x, W)/dx^2$, is simply the sum of the profile and the effect of the superelevation transition. For a numerical example, consider the right lanes of the road described in Figure 1. For the moment, we shall ignore the shoulders. Within the linear portion of the superelevation diagram,

$$dWs(x)/dx = (15\text{ m}) \times [+0.06 - (-0.02)]/240\text{ m} = +0.005 \tag{7}$$

The grade along the outside edge of pavement is 0.005 more than the grade along the profile at every point between km 9+755 and km 9+965. To make this calculation, we can use either of two mathematically equivalent approaches. The most direct is to rewrite the last term of Equation 5 as Wds(x)/dx, W times the slope of the superelevation diagram. The superelevation changes linearly from -2 to +6 percent in 240 m (ignoring the curves in the superelevation diagram for the moment) and from 0 to +6 percent in 180 m, so

$$Wds(x)/dx = (15\text{ m}) \times (+0.06 - 0)/180\text{ m} = +0.005 \tag{8}$$

However, Equation 5 was written with dWs(x)/dx rather than Wds(x)/dx because I do not usually make the calculation in such a straightforward mathematical way, but according to the following more physical logic. Between km 9+800 and km 9+980 the superelevation changes 6 percent. Since the pavement is 15 m wide, this is a $(0.06) \times (15\text{ m}) = 0.90$ m rise relative to the centerline. This rise is accomplished over a 180-m distance, so the grade necessary to accomplish it is

$$dWs(x)/dx = 0.90\text{ m}/180\text{ m} = +0.005 \tag{9}$$

To obtain the actual grade along the outside edge of pavement, we simply calculate the grade along the profile and add 0.005. For example, at km 9+820, we are 20 m into the profile vertical curve, so

$$dz(x)/dx = dy(x)/dx + 0.005 = g_1 + 20r + 0.005$$
$$= -0.01 + [20 \times (0.5 \times 10^{-4})] + 0.005 = -0.004 \tag{10}$$

Proceeding to the rate of change of grade, we can continue the same line of reasoning. Prior to km 9+965 the right edge of the road was rising at +0.005 relative to the centerline, but beyond km 9+995 it is parallel to the centerline. This -0.005 change is accomplished in a 30-m parabolic curve, so the rate of change of grade due to the superelevation transition must be $-0.005/30\text{ m} = -1.667 \times 10^{-4}$/m. If we call this rate of change of

grade due to the superelevation transition r_s, we can rewrite Equation 6 as

$$r_e = r + r_s \tag{11}$$

where $r_e = d^2z(x, W)/dx^2$ is the rate of change of grade along a line offset a horizontal distance W from the centerline. In Equation 11 it is clear that r_e is just the sum of the rate of change of grade due to the curves on the profile and on the superelevation diagram. In our example, r_e for the superelevation curve centered at km 9+980 is

$$r_e = r + r_s = +0.5 \times 10^{-4}/m - 1.667 \times 10^{-4}/m = -1.167 \times 10^{-4}/m \tag{12}$$

At this point, it should be very obvious why the profile of the outside edge of the right lanes in Figure 1 looks like a dented bowl. The dent is the portion from km 9+965 to km 9+995 where $r_e = -1.167 \times 10^{-4}$/m is negative, in contrast to the surrounding portion of the bowl where $r_e = r = +0.5 \times 10^{-4}$/m is positive. It is also quite obvious that we can eliminate the dent only by making r_e positive everywhere, which will happen if the absolute value of r_s is less than the absolute value of r. This can be accomplished either by lengthening the curve in the superelevation diagram or by shortening the curve in the profile. Usually, we prefer to do the former, although a situation occasionally arises where it is desirable or even necessary to change the profile.

In our example, we need to lengthen the curve in the superelevation diagram until $|r_s| < r = 0.5 \times 10^{-4}$/m, or $|-0.005/\ell| < 0.5 \times 10^{-4}$/m, where ℓ is the length of the curve in the superelevation diagram. Clearly we will achieve equality if $\ell = 100$ m and satisfy the inequality if $\ell > 100$ m. If we were to use $\ell = 100$ m, we would have $r_e = r + r_s = 0$ and the edge-of-pavement profile would be a straight line from km 9+930 to km 10+030.

The reader can see how this would look by laying a straight edge tangent to the edge-of-pavement profile at km 9+930 and km 10+030 on Figure 1. It eliminates the dent, but leaves a flat spot. Since flat spots on round bowls are usually considered undesirable, we shall usually insist on strict inequality. The dashed curve on Figure 1 has $\ell = 140$ m. This length was chosen rather arbitrarily to illustrate the effect of using $\ell > 100$ m; whether or not it was a good choice will be discussed in a later section. In any case, it is clear that the problem can be solved only by using a curve much longer than is standard practice. It should also be noted that any solution worked out graphically with a spline will involve a revision in the superelevation over a distance of at least 100 m.

MULTIPLE PLANES

Most modern roads have paved shoulders, so they cannot be considered a single plane. In addition, many highways are built with different cross slopes for each lane. The generalization of the preceding theory to cover multiple planes is straightforward.

Suppose that the road has several planes numbered 1, 2, 3, ... If plane number i has width w_i and superelevation $s_i(x)$ and we are interested in the shape of a line offset a distance $W = w_1 + w_2 + \ldots + w_n$ from the profile grade, then

$$z(x, W) = y(x) + \sum_{i=1}^{n} w_i s_i(x) \tag{13}$$

Taking derivatives as before,

$$dz(x, W)/dx = dy(x)/dx + \sum_{i=1}^{n} dw_i s_i(x)/dx \tag{14}$$

$$d^2z(x, W)/dx^2 = d^2y(x)/dx^2 + \sum_{i=1}^{n} d^2 w_i s_i(x)/dx^2 \tag{15}$$

Thus, we only need to add together the effects of what happens in each plane to obtain the total effect.

DESIGN EXAMPLE

To illustrate the analysis of multiple planes, we return to Figure 1, but we shall consider what happens to the edge-of-shoulder profile rather than the profile of the edge of the outside lane. This is the line we are really interested in, the actual physical edge of the roadway. It is not only the most clearly visible line, but also the one that determines the shape of the bridge rail if there is one.

Since we already know that there is a problem on the right side at km 9+980, we shall start there. The width W is now 18 m, but at this location we still have a single plane, since the shoulder and lanes all have the same superelevation. Thus the grade change caused by the superelevation transition is $dWs(x)/dx = (18\ m) \times (+0.06 - 0)/180\ m = +0.006$ and the rate of change of grade due to superelevation is $r_s = -0.006/30\ m = -2 \times 10^{-4}$/m. Since the profile grade is curving at $r = +0.5 \times 10^{-4}$/m, there will clearly be a dent in the edge of the shoulder unless we increase the superelevation curve length until $|r_s| \leq 0.5 \times 10^{-4}$ or $\ell > 0.006/(0.5 \times 10^{-4}/m) = 120$ m.

Usually we would choose to use a length greater than the minimum to avoid a flat spot, but this time we shall use $\ell = 120$ m. This will give us a 120-m straight line in the right edge of the shoulder profile on a grade of +0.2 percent, as shown in Figure 3. A short tangent might look bad, but 120 m seems long enough to stand on its own as a geometric element. Since we are on the high side of superelevation, the very flat grade will be acceptable, though some very careful gutter design might be necessary if the road were in excavation.

The next question to be asked is, Where else might there be dents in the edge of the shoulder profile? After a little reflection, it should be obvious that there are only two possibilities, both on the left roadway, at km 9+860 and at km 9+920. Notice that no calculations were necessary to reach this conclusion; these are the only other superelevation diagram curves that could cause dents, because all the other curves are either outside of the profile vertical curve or curve in the same direction as the profile. In the latter case r_s has the same sign as r, so the effect of the superelevation curve is to make the curvature sharper, not to change its direction.

To analyze the two possible trouble spots, it is not necessary to repeat all the calculations we made for the curve at km 9+980 on the right lanes. Instead, we observe that the curves at km 9+860 and km 9+920 look exactly the same on the superelevation diagram as the curve at km 9+980 on the right lanes. Therefore $ds(x)/dx$ and $d^2s(x)/dx$ are exactly the same as before; the only difference in the three curves is the width of the plane, W or w_1.

At km 9+860 only the lanes are curving, so W = 15 m. We found at km 9+980 that $|r_s|$ for a plane 18 m wide was 2.0×10^{-4}/m, so for W = 15 m, $|r_s| = (2.0 \times 10^{-4}/m) \times (15\ m/18\ m) = 1.667 \times 10^{-4}$/m and at km 9+920 where only the shoulder is curving due to superelevation $|r_s| = (2.0 \times 10^{-4}/m) \times (3\ m/18\ m) = 0.333 \times 10^{-4}$/m. Comparing these numbers with $r = 0.5 \times 10^{-4}$, we see that there will be a dent at km 9+860, but not at km 9+920.

When we change the length ℓ of the curve at km 9+860 to eliminate the dent, r_e will change in proportion to $1/\ell$, so we need to increase ℓ until $(1.667 \times 10^{-4}/\text{m}) \times (30\ \text{m}/\ell) \leq 0.5 \times 10^{-4}/\text{m}$ or $\ell \geq 100$ m. If we were to use 100 m, however, we would get the result shown schematically in Figure 4.

The negative value of r_e between km 9+905 and km 9+910 occurs because the lane curve at km 9+860 and the shoulder curve at km 9+920 now overlap. To eliminate this section of downward curvature by lengthening the curves, we would have to make the lane curve considerably longer than 100 m, but if it were longer than 120 m, it would extend outside of the profile vertical curve and again give us a short section where r_e was negative. This would not be too bad since it would be between a section with $r_e = 0$ and one with $r_e > 0$ rather than between two sections with $r_e > 0$, but it still seems worth avoiding. Sometimes a good solution to such a situation can be obtained only by changing the profile.

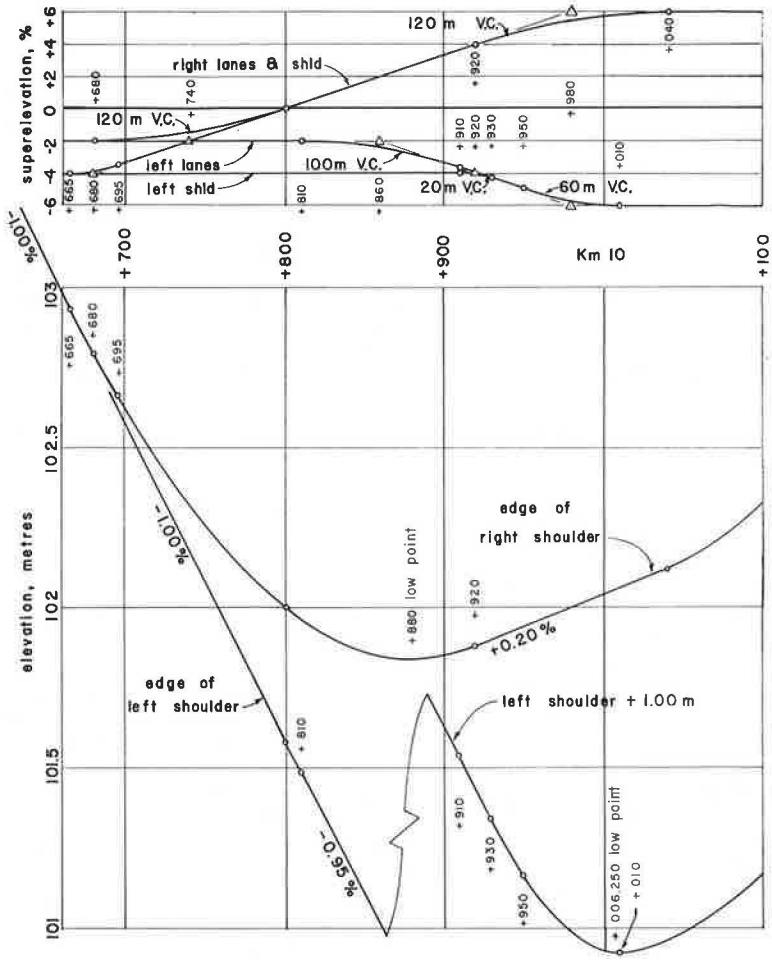

Figure 3. Redesigned superelevation diagram and resulting edge-of-shoulder profiles.

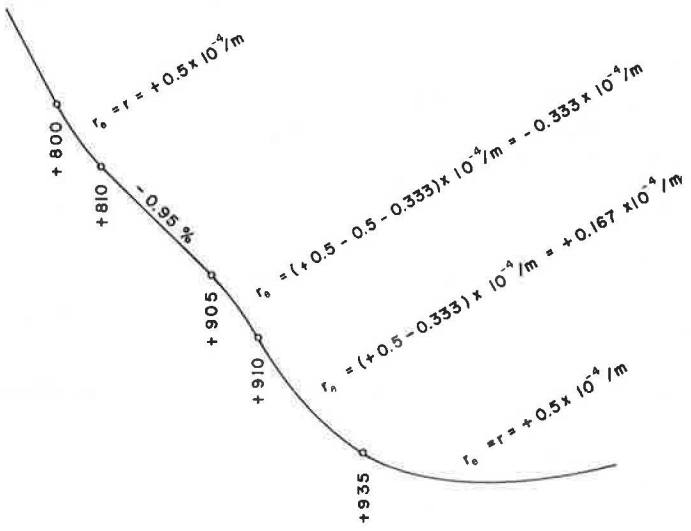

Figure 4. Sketch of left shoulder profile with 100-m curve at km 9+860 in superelevation diagram.

In this case, however, we have another option.

If we simply shorten the shoulder curve at km 9+920 to 20 m, as shown in Figure 3, it will not overlap a 100-m curve at km 9+860. This will give us $|r_s| = 0.5 \times 10^{-4}$/m at km 9+860 and $|r_s| = (0.333 \times 10^{-4}\text{/m}) \times (30\text{ m}/20\text{ m}) = 0.5 \times 10^{-4}$/m at km 9+920.

Interestingly enough (and quite by accident), both of these curves just exactly counteract the profile vertical curve, so the straight line on a -0.95 percent slope shown in Figure 4 will now extend all the way from km 9+810 to km 9+930. There will be no dents, but there is a 10-m curve in the edge of the lanes and shoulder centered at 9+805. Since the grade only changes 0.05 percent in this curve, it is a reasonably safe assumption that it will not show up at all; if it does, it will look like an angle point rather than a curve.

We have now eliminated all the dents but should still check the other superelevation curves to see if the design can be improved. On a two-lane road we would make the curve on the left side at km 9+980 the same length as the one on the right. On a freeway it is usually convenient to do so but not essential, and 120 m really does seem very long to use without a definite reason. On the other hand 30 m, though it does provide adequate sight distance for freeway speeds, is very short for such a wide road. Therefore, a 60-m curve will be used at km 9+980 as shown in Figure 3. This is probably about the shortest superelevation curve we should ever use for freeway lanes.

The subject of sight distance in superelevation transitions is complicated. In our example there is adequate sight distance because the profile vertical curve is very flat. If the profile had been designed to just satisfy sight distance standards, however, the 30-m curve would not have provided adequate sight distance in the outside lane. There can also be severe sight distance problems at crest curves in the superelevation diagram. On the high side of superelevation these problems are reduced because drivers can look diagonally across the lower lanes, but on the low side of superelevation in excavation the shoulder width may not be sufficient for this to be much help.

Wirasinghe of the University of Calgary has done some research on analytic methods for calculating the sight distance in superelevation transitions (11), but the complexity of his analysis of even very simple cases is discouraging. For practical purposes, it would seem that sight distance problems must be individually analyzed by graphical methods. Of course, a good understanding of the geometry of the roadway will be very helpful in identifying those cases where the likelihood of sight distance problems is sufficiently great to justify a graphical analysis.

The two curves that remain are at km 9+680 and km 9+740 on the right roadway, outside of the profile vertical curve. Nothing really needs to be done about these two curves, except possibly to lengthen the one at km 9+740 simply because 30 m is very short for a freeway curve. If we were to lengthen it to 60 m, however, we would be left with a 30-m straight line in the edge-of-shoulder profile between km 9+770 and km 9+800. To avoid this, I have used a 120-m curve so that the right edge-of-shoulder curves continuously from km 9+665 to km 9+920, as shown in Figure 3. This last change is admittedly a nicety rather than a necessity, but certainly a very inexpensive nicety.

DRAINAGE

So far, very little has been said about drainage, but it is often a major consideration in the design of superelevation diagrams. Figure 1 illustrates some of the problems that can arise. The figure shows the high edge of the road, but exactly the same things can happen on the low side where the shoulder is expected to function as a drainage channel. The most obvious potential drainage problem in Figure 1 is that the right edge profile has two points with zero grade, at km 9+900 and at km 10+000, with a very small hump between them. The second sag point was eliminated from the final design along with the dent centered at km 9+980.

Less interesting, perhaps, than the double sag points but very likely more serious is the danger of inadvertently creating grades that are too near zero for proper drainage. We have already seen that the 120-m tangent in the right shoulder profile in Figure 3 is on a grade of only 0.2 percent. To see what could have happened to us, suppose that g_1 and g_2 in Figure 1 had been -1.2 percent and 0.8 percent instead of -1.0 percent and 1.0 percent, respectively. Then the 120-m tangent would have been absolutely horizontal.

For an even more troublesome situation, suppose that g_1 and g_2 had been -0.6 percent and 1.4 percent. Then the 30-m straight line we considered using between km 9+770 and km 9+800 in the right edge of shoulder would have been horizontal. Since the superelevation at km 9+800 is also zero, a very hazardous pond would have formed on the roadway. To avoid this sort of ponding, it is necessary to design so that the resultant of the grade and the cross-fall is sufficiently large to keep the water moving. For example, Deitrich, Graff, and Rotach (10) recommend keeping $[g^2(x) + s^2(x)]^{1/2} \geq 0.005$, where $g(x)$ is the flattest longitudinal grade at any point on the cross section, i.e., the minimum value of $dz(x, W)/dx$ encountered for any W.

The analysis necessary to determine whether any drainage problems have been caused by a superelevation transition can be somewhat more complex than the analysis for the edge-of-shoulder dents but is never really difficult. It is not necessary to draw edge profiles to scale, but schematic drawings similar to Figure 4 are recommended for all situations where it is not immediately obvious that no problem exists. Solving the problems that already exist is likely to be more difficult. A solution can sometimes be obtained by changing the axis of rotation, but it is often necessary to change the profile. Only in unusually fortunate circumstances will changes in the length of the superelevation transition or its curves be sufficient to remedy serious drainage problems.

SUMMARY

As demonstrated in the numerical example, the simplicity of the mathematics of vertical curves and superelevation transitions can be exploited to very easily check whether a design will have undesirable features such as edge-of-shoulder dents, roller-coaster edge profiles, and a number of possible drainage and appearance problems. The arithmetic required to check the shapes is very simple and requires far less time than would be required to make the same checks graphically by plotting edge-of-shoulder profiles. In addition, the algebraic approach yields new designs that conform to the normal format of profile and superelevation diagrams and, hence, are compatible with standard computer programs.

ACKNOWLEDGMENTS

I first worked out the methods presented here in response to design problems encountered while working under the supervision of Gordon Chin and the late Walter Wong in a design department headed by W. Preston

Smith at the California Division of Highways in their San Francisco office. The basic idea that these things could be done was a faint memory from a summer in the mid-1950s when I, equipped with one year of college mathematics but no knowledge of surveying or highway geometry, worked under the supervision of Eric Stokes. He was then using methods similar to those presented here, but I am not familiar with the details of how he applied them. The encouragement of these four engineers, the many things they taught me, and the example presented by their great concern for quality in design are all gratefully acknowledged.

REFERENCES

1. C. Tunnard and B. Pushkarev. Man-Made America: Chaos or Control. Yale Univ. Press, New Haven, 1963, pp. 159-276.
2. Forschungsgesellschaft für das Strassenwesen. Richtlinien für die Anlage Von Landstrassen, Teil II: Linienführung, (RAL-L) Abschnitt 2: Räumliche Linienführung. Kirshbaum Verlag, Bonn-Bad Godesberg, 1970.
3. H. Lorenz and F. A. Finger, eds. Transsierungsgrundlagen der Reichsautobahnen. Volk und Reich Verlag, Berlin, 1943.
4. B. L. Smith, E. E. Yotter, and J. S. Murphy. Alignment Coordination in Highway Design. HRB, Highway Research Record 371, 1971, pp. 47-53.
5. A. B. Baker. The Design and Phasing of Horizontal and Vertical Alignments: Program JANUS. Transport and Road Research Laboratory, Crowthorne, England, Rept. LR 469, 1972.
6. C. J. Brownell. Rate of Change of Grade per Station. ASCE, Trans. 118, 1953, pp. 437-462.
7. RTAC Sector Committee 5.6. Guide to Metric Conversion of Highway Engineering. Roads and Transportation Association of Canada, Ottawa, 1976.
8. American Association of State Highway Officials. A Policy of Geometric Design of Rural Highways. Washington, DC, 1965.
9. Geometric Design Standards for Canadian Roads and Streets. Roads and Transportation Association of Canada, Ottawa, 1976.
10. K. Dietrich, V. Graf, and G. M. Rotach. Strassenprojektierung. Institute für Verkehrsplanung und Transporttechnik an der ETH Zurich, Zurich, 1975.
11. S. C. Wirasinghe. Sight Distance in Superelevation Transitions. Univ. of California, Berkeley, master's project, 1972.

Publication of this paper sponsored by Committee on Geometric Design.

Superelevation and Curvature of Horizontal Curves

Joseph Craus, Transportation Research Institute
Moshe Livneh, Civil Engineering Department, Technion-Israel Institute of Technology, Haifa

This paper deals with the various parameters required for design of a horizontal curve, namely the relation between superelevation rate and curve radius. These parameters are derived from the characteristics of a person-vehicle-environment system. The lateral acceleration that constitutes the physical output from this system determines the critical case, for which the radius is minimum. The data used here are taken from studies dealing with human factors and traffic characteristics. The maximum superelevation rate is determined by limiting the negative lateral acceleration for slow vehicles and by assuring safe driving for fast vehicles. The development of the relation between superelevation rate and curve radius for any constant design speed is based on driver expectation that the pressure exerted on the steering wheel will decrease with increasing curve radius. The findings are compared with the U.S. and German guidelines. The criteria developed here are concluded to be reasonable and the findings useful for design purposes.

The design guidelines of different countries recommend various correlations between horizontal curves and superelevation rates but display significant differences both in the permissible minimum radii and in the values of superelevation rates. Since horizontal curves constitute critical points along the entire road system, the need exists for determining consensus criteria prescribing the parameters required for the design of a horizontal curve.

The purpose of this work is to establish these criteria and the corresponding guidelines for the relation between the radius of the curve and the superelevation. The basic approach adopted is to choose parameters that express the desired values for attaining unforced driving—referred to as "natural" driving in this paper—in a horizontal curve for an actual driving-speed distribution.

The data employed to determine these values are taken from various studies of the human factor and traffic research. Such studies lead to indices that determine the norm for natural driving in a curve on one hand and to indices that determine actual speed distribution on the other. For this reason, the lateral friction factor does not constitute a leading parameter in establishing the sought correlation; however, data on road accidents in curves are important input data for the analysis.

The approach to the study of the subject, as formulated above, forms the justification for the present work. Clearly, knowledge of the criteria for deriving the radii and superelevation rates enables any designer to evaluate the various implications of their determination.

SUPERELEVATION FORMULA

A car moving in a circular horizontal curve is in an equilibrium of accelerations, as given by the following formula (see Figure 1):

$$a_r = a_c - a_e \quad (1)$$

Figure 1. Scheme of accelerations during travel in a horizontal curve.

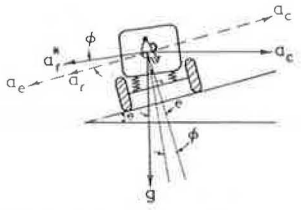

where a_r is the driver-perceived lateral acceleration, a_c is the centrifugal acceleration, and a_e is the superelevation acceleration. This formula is based on the fact that the value of the component of a_c acting in the direction of the superelevation slope is identical with the value of a_c itself, at a sufficient approximation. The expressions for the centrifugal acceleration and the superelevation acceleration are

$$a_c = V^2/R \tag{2}$$

$$a_e = ge \tag{3}$$

where V is the travel speed in the curve, R is the radius of the curve, e is the superelevation rate, and g is the gravity acceleration.

The assumptions inherent in the preceding equations are

1. The vehicle is a point mass,
2. The travel speed in the curve is constant,
3. The travel path of the vehicle has a constant radius identical with that of the curve itself, and
4. The longitudinal slope in the horizontal curve equals zero.

It is important to emphasize the difference between the real lateral acceleration, a_r, and the measured lateral acceleration, a_r^*. The latter is influenced by the angle of inclination of the car body (angle ϕ in Figure 1, denoted as body-roll angle). The real lateral acceleration is given by

$$a_r = a_r^* \cos \phi \tag{4}$$

where cos ϕ is defined with the aid of the body-roll spring rate, α, as follows:

$$\cos \phi = 1/(1 + \alpha) \tag{5}$$

or

$$a_r = a_r^*/(1 + \alpha) \tag{6}$$

The accepted value for α is 0.2.

Design speed represents a predicted distribution of speeds, usually characterized by the fact that 85-95 percent of actual travel speeds are lower. The validity of this speed distribution is subject to an examination of the superelevation equation, in which a constant travel speed equaling the design speed is substituted. The two parameters specified below constitute the examination tools.

The first parameter, defined as the superelevation coefficient β^2, is the ratio of the superelevation acceleration to the centrifugal acceleration:

$$\beta^2 = a_e/a_c \tag{7}$$

This coefficient expresses the degree of safety of vehicles traveling at speeds differing from the design speed. For instance, with increasing β^2 for a constant superelevation rate, the value of the centrifugal acceleration decreases. Clearly, this decrease corresponds to a higher degree of travel safety.

The second parameter is defined as the comfort speed V_0, for which the lateral acceleration equals zero:

$$V_0 = \sqrt{Rge} \tag{8}$$

This speed is sometimes called the "hands-off" speed, as the car is carried in a circular path without any pressure having to be exerted on the steering wheel. In contrast, traveling at a speed lower than V_0 forces the driver to press on the wheel in a direction opposite to that of the turn of the wheel; this represents an unnatural driving operation in a curve. The comfort speed, therefore, must be as close as possible to the minimum travel speed expected in a curve in order to prevent most drivers from constrained driving. The relation between the above-mentioned two speed parameters and the superelevation equation may be shown as follows:

$$V_0 = \beta V_D \tag{9}$$

where V_0 is the design speed. Also,

$$a_r = (V_0^2/\beta^2 R) - ge \tag{10}$$

Equation 10 is the superelevation equation, in which all basic parameters appear.

LATERAL ACCELERATION

Lateral acceleration comprises the physical output of the different variables for driving in a horizontal curve. Since the choice of travel speed is a result of the total person-vehicle-environment system, objective and subjective factors, such as qualifications, practical experience, and responses to stimuli, characterize the kinesthetic perception of the driver in conjunction with his or her visual perception. The output is, as mentioned above, the adopted lateral acceleration.

Some investigators—among them Ritchie, McCoy, and Welde (1); Leeming and Black (2); Moyer and Berry (3); and Kneebone (4)—have measured the value of the lateral acceleration of a vehicle in curves. The general trend of these measurements was that lateral acceleration value decreases with increasing travel speed (see Figure 2, which shows values of lateral acceleration corrected in accordance with Equation 6). This decrease results from drivers being overcautious when evaluating driving risk, which increases with increasing travel speed. The lateral acceleration values themselves were not uniform in the various measurements. However, the trend of these values when measured against travel speed is the same in almost all the measurements presented here.

The question that now arises is, from the complex of practical measurements, which correlation between design speed and lateral acceleration is recommended. The present work adopts the relation obtained by Ritchie, McCoy, and Welde, whose experiments involved 50 different drivers who drove an identical car along a fixed traveling course of 177 km with 227 curves (1).

Figure 3 shows the average lateral acceleration in these experiments for the entire driver population for the group of fastest drivers and for the group of slowest drivers. Analysis of these results shows that the correlation between lateral acceleration and curve speed for the entire population is closer to that for slow

Figure 2. Regression lines for the correlation between curve speed and the ratio a_r/g from different sources.

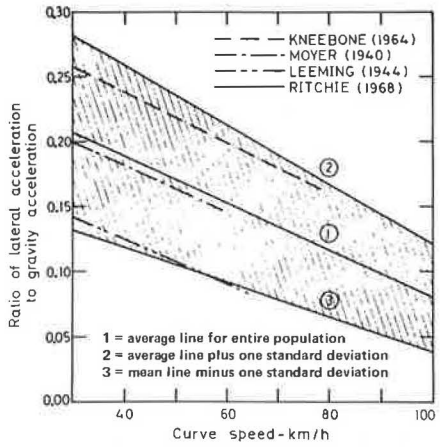

Figure 3. Regression lines for the correlation between curve speed and the ratio a_r/g from Ritchie, McCoy, and Welde's data.

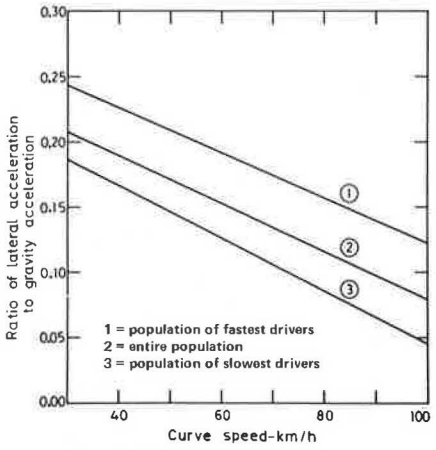

drivers than that for fast drivers. Stated another way, the average population adopts values of lateral acceleration that are closer to those of slow drivers. Which correlation is the most relevant for replacing the curve speed with the design speed?

It would seem that one should choose the speed for the population of slow drivers, since it contains the lowest acceleration values. However, the critical values normally are not taken as practical values for design; instead, the values chosen are those that are certain for the majority of, say, 80 percent of events. Therefore, the correlation between lateral acceleration and curve speed for the entire population is the one adopted here as the design relation between the lateral acceleration and the design speed. This correlation, furthermore, expresses the physical output of the input data of driving behavior, including the choice of a driving path with a radius not necessarily identical to the curve radius.

Adoption of the correlation obtained by Ritchie, McCoy, and Welde for the design of superelevation rates in horizontal curves receives added justification from the fact that it lies in the middle range of the various measurement results (see Figure 2). The distribution of the correlation over the range of standard deviation in each direction (in about 67 percent of the cases) shows the approximate limits of the above range.

The mathematical expression for the adopted correlation is

$$a_r/g = (0.262 - 0.001\,82\,V_D) \quad (11)$$

where a_r/g is the ratio of lateral acceleration to gravity acceleration, and V_D is the design speed in kilometers per hour.

Since this correlation is valid up to a speed of 100 km/h, extrapolated values are suggested for higher speeds by reducing by 25 percent the slope of a_r as a function of V_D. This reduction is based on the work of the Fourth Committee on Highway Design, operated jointly by Germany, France, and Switzerland (5). The design values of a_r as a function of design speed are presented in Table 1.

SUPERELEVATION DESIGN VALUE

As stated previously, the value of the superelevation coefficient β^2 is connected with travel safety. High values of β^2 are desirable for high travel speeds accompanying the design speed. Conversely, for low travel speeds accompanying the same design speed, low values of β^2 are desirable, as derived from Equation 9. These contrasting trends can be bridged by relating the values of β^2 to the value of the design speed. At high design speeds safety is a more severe factor for the fast vehicle, and it is thus logical that the β^2 values should increase with increasing design speed. As a consequence, the need exists for a superelevation rate that is independent of the design speed on one hand and has a suitable maximum value on the other. To achieve this, Equation 7 may be substituted in Equation 1:

$$\beta^2 = 1/[(a_r/a_e) + 1] \quad (12)$$

According to Equation 12, increasing β^2 is accompanied by a reduction in the value of a_r/a_e. Because lateral acceleration decreases with design speed, the increase in β^2 with the design speed is conditional on assigning to a_e at least a fixed value. Among the accepted maximum values of superelevation, i.e., in the range of 0.06 -0.10, one has now to choose a value satisfying the criteria advanced in the beginning of this section.

Since the choice of high values for the superelevation rate will result in a higher level of β^2 and, consequently, higher values of V_0 (see Equation 9), a value of 0.08 for the superelevation rate seems to ensure the maintenance of a reasonable limiting speed. In any case, a calculation check for the a_r values given in Table 1 and for e = 0.08 leads to the values of centrifugal acceleration, superelevation coefficient, and minimum radii, given in the same table. These values are checked by comparing the results of superelevation coefficient and centrifugal acceleration to commonly accepted values on one hand and to the reasonability of the derived speed distribution on the other.

As for the values of β^2 and a_e, it is important to mention the work of Spindler (6). Analysis of his observations proves that β^2 varies in the range from 0.3 to 0.5 when the values of centrifugal acceleration vary from 0.15 to 0.3 g. The horizontal curves that served for these experiments had radii varying from 30 to 500 m. Comparison of these findings with the results in Table 1, within the range of relevant radii, proves the reasonability of the values of both superelevation and lateral acceleration for this part of the check.

Table 1. Values of lateral acceleration for design, centrifugal acceleration, superelevation coefficient, and minimum radii as functions of design speed.

Design Speed (V_D) (km/h)	Ratio of Lateral to Gravity Acceleration (a_r/g)		Ratio of Centrifugal to Gravity Acceleration (a_e/g)	Superelevation Coefficient (β^2) ($\frac{f}{f}$)	Curve Radius (R) (m)
	Value	Standard Deviation			
30	0.207	0.075	0.287	27.9	25
40	0.189	0.070	0.269	29.7	47
50	0.171	0.066	0.251	31.9	78
60	0.153	0.061	0.233	34.3	122
70	0.135	0.056	0.215	37.2	179
80	0.116	0.051	0.196	40.8	257
90	0.098	0.046	0.178	44.9	358
100	0.080	0.041	0.160	50.0	492
110	0.075	0.038	0.155	51.5	615
120	0.071	0.036	0.151	53.0	751
130	0.067	0.034	0.147	54.5	905
140	0.063	0.032	0.143	56.0	1080

Figure 4. Correlation between curve radius and vehicle speeds, on the basis of measured speed distributions.

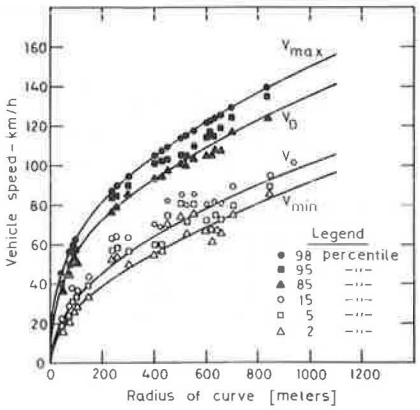

As for the speed distribution, the following two assumptions are made: first, the "low critical speed" (V_{min}) is defined as that corresponding to a negative lateral acceleration of 0.02 g, which is equivalent to a lateral acceleration of 0.02 g, with an opposite direction to a_e for a car traveling on a straight line with a normal crown of 0.02 cross-fall; second, the "high critical speed" (V_{max}) is defined as that corresponding to the design lateral acceleration increased by one standard deviation (see Table 1). Calculation of these speeds based on the data in Table 1 and Equation 9 is given in Table 2.

The check of the suitability of the speed distribution shown in Table 2 is based on the following procedure. Different sources (7, 8, 9, 10, 11) cite actual distributions of travel speeds along straight sections. From these sources one can determine the values of the speeds corresponding to the following percentiles: 98, 95, 85, 15, 5, and 2. These are shown in Figure 4. Their dependence on the radius value is expressed by comparing the actual travel speed that corresponds to the 98th percentile with the high critical speed (V_{max}) given in Table 2. In other words, the calculated correlation between V_{max} and the curve radius comprises the position of the points representing the actual travel speed corresponding to the 98th percentile; the remaining points, representing the other speed percentiles, are indicated relative to that position. Figure 4 also shows the calculated correlations between the design speed (V_D), the comfort speed (V_o), the low critical speed (V_{min}), and the curve radius.

It is seen from this figure that the speed distribution derived from the superelevation calculations indeed approaches the actual speed distribution.

It should be pointed out that the design speed (V_D) is obtained as the speed corresponding to the 85th-95th percentile, that the comfort speed (V_o) is obtained as the speed corresponding to the 5th-15th percentile, but that the low critical speed (V_{min}) is obtained as the speed corresponding to the percentile below 5. The findings given here are highly significant and strengthen the recommendations in this section.

Still one more check is made to prove that a superelevation of 0.08 is preferable to superelevation rates of 0.10 and 0.06: First, if β^2 values are calculated for a superelevation of 0.06 up to a design speed of 80 km/h, they will be found to be lower than the recommended value of 0.3. This means that application of this superelvation rate does not ensure driving safety at the high travel speeds accompanying the design speeds. Second, it can be proved that V_o accompanying a superelevation of 0.10 equals V_{min} accompanying a superelevation of 0.08. Thus, application of a superelevation of 0.10 would result in negative radial accelerations for a greater proportion of vehicles and would not ensure driving safety at low travel speeds accompanying the design speeds. In conclusion, the application of a superelevation of 0.08 reflects the correct balance between the low superelevation of 0.06 and the high superelevation of 0.10.

CORRELATION BETWEEN RADIUS OF CURVE AND SUPERELEVATION RATE

The previous discussion and the numerical values given in Table 2 relate to the critical case only, where the curve radius assumes the absolute minimum value. The correlation between design speed and lateral acceleration (Equation 11) can serve only that case, since it is based on the average of the lateral acceleration values obtained in Ritchie, McCoy, and Welde's experiments. This average represents the maximum value of lateral acceleration that can still be considered tolerable during driving in a horizontal curve. It thus serves to establish the minimum curve radius. The radii given in Table 2 should, therefore, be considered as the absolute minimum radii for the different design speeds at a constant superelevation rate of 0.08.

Calculation of the superelevation for radii exceeding the absolute minimum is based on the criterion described below.

A road designed according to a design speed must satisfy the common expectation of drivers that the

Table 2. Distribution of speeds as a function of design speed.

Design Speed (V_D) (km/h)	Curve Radius (R) (m)	Low Critical Speed (V_{min}) (km/h)	Comfort Speed (V_0) (km/h)	High Critical Speed (V_{max}) (km/h)
30	25	13.8	15.8	33.9
40	47	18.9	21.5	45.0
50	78	24.4	28.3	56.0
60	122	30.5	35.2	67.5
70	179	36.9	42.7	78.5
80	257	44.3	51.5	89.8
90	358	52.5	60.3	101.0
100	492	61.2	70.7	112.0
110	615	69.3	78.9	122.8
120	751	78.0	87.4	133.6
130	905	87.3	96.0	144.3
140	1080	97.4	104.8	155.0

Table 3. Correlation between a number of factors and $(\beta_{max}/\beta_{min})^2$.

$(\beta_{max}/\beta_{min})^2$	Δ_0		R_{max}/R_{min}	a_{r1}/g	a_{r2}/g
	V_D = 60 km/h	V_D = 120 km/h			
1.0	0	0	4	0	-0.005
1.2	10	19	4.8	-0.003	-0.008
1.4	17	34	5.6	-0.006	-0.009
1.6	25	49	6.4	-0.008	-0.010
1.8	36	64	7.2	-0.010	-0.012

Figure 5. Relation between curve radius and superelevation rate, including absolute minimum radii.

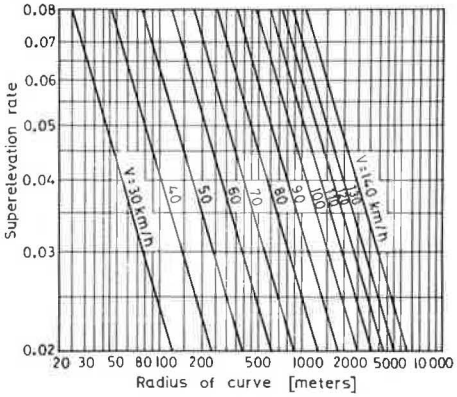

Figure 6. Comparison of curve radius and superelevation rate with AASHO values.

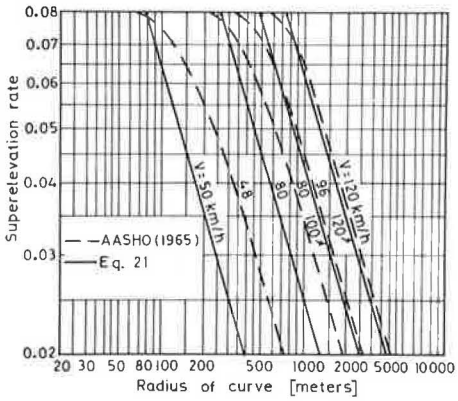

pressing effort on the steering wheel during driving in a curve will decrease with the increasing radius of the curve. The superelevation factor β^2 constitutes a measure of the extent of pressing effort on the wheel: the higher its value, the smaller the effort. An analysis of β^2 values in Table 1 proves that the pressing effort still considered tolerable by the driver population decreases with increasing travel speed in the critical cases, when curve radii are minimum.

Clearly, for a minimum radius corresponding to a given design speed, β^2 is as given in Table 1, but its value has to increase with increasing curve radius, and its maximum value is reached with the maximum radius (R_{max}), defined here as the radius for which the superelevation rate is 0.02. It is obvious that β should not be allowed to increase beyond a given value for the reason that this would lead to an increase in the comfort speed (V_0) and, consequently, in the frequency of occurrence of negative lateral acceleration (pressing the steering wheel in a direction opposite to that of the turn) in vehicles traveling at speeds slower than the design speed.

The implications of the variation of β with the curve radius for a given design speed (denoted as β_r) were examined with respect to (a) the increase in the number of vehicles developing negative lateral acceleration and (b) the value of negative lateral acceleration for the case where the curve radius equals R_{max}. For the purpose of this examination, it is assumed that the cumulative distribution of travel speeds is linear between the values (according to Table 3) of V_0, corresponding to the 15th percentile, and V_D, corresponding to the 85th percentile.

If, then, Δ_0 denotes the increase in the percentage of vehicles that develop negative lateral acceleration, one obtains

$$\Delta_c = [(85\text{-}15)/(V_D - V_0)]\ (\beta_r V_D - V_0) \qquad (13)$$

After appropriate substitution with $V_0 = \beta_{min} V_D$, the value of Δ_c is

$$\Delta_c = 70\beta_{min}/(1 - \beta_{min})\ [(\beta_{max}/\beta_{min}) - 1] \qquad (14)$$

where β_{min} is the value corresponding to the critical case (Table 1) and β_{max} is the value corresponding to the case where the curve radius equals R_{max} with a superelevation rate of 0.02.

The value of lateral acceleration (a_{r1}) that develops at a travel speed of V_0 in a curve where the radius equals R_{max} with a superelevation of 0.02 is given as

$$a_{r1} = (V_0^2/R_{max}) - 0.02\ g \quad (15)$$

and, by appropriate substitutions, one gets

$$a_{r1} = \{[0.08/4(\beta_{max}/\beta_{min})^2] - 0.02\}\ g \quad (16)$$

The negative lateral acceleration developed for the proportion of vehicles Δ_o varies from zero to the value of a_{r1} given in Equation 16. It is obvious that, for the proportion of cars traveling at a speed lower than V_0 (about 15 percent), the value of negative lateral acceleration will be larger, reaching the value of a_{r2} at a speed of V_{min}, as defined in Table 3, and as given in the following equation:

$$a_{r2} = \{[0.06/4(\beta_{max}/\beta_{min})^2] - 0.02\}\ g \quad (17)$$

The values of a_{r1}, a_{r2}, Δ_o, and R_{max}/R_{min} are summarized in Table 3 to show their dependence on $(\beta_{max}/\beta_{min})^2$.

Table 3 permits a consideration of the design value for $(\beta_{max}/\beta_{min})^2$. The maximum value of this expression is governed both by the extent of negative acceleration and by the magnitude of the additional proportion (Δ_o) of vehicles expected to acquire negative acceleration. As a reasonable maximum value of negative lateral acceleration (a_{r1}), one can adopt the value of -0.005 g. Thus, it was established that $(\beta_{max}/\beta_{min})^2$ equals 1.25. In addition, it should be pointed out that the sensitivity to the change in superelevation rate with radius for values exceeding 1.25 but less than 1.4 is insignificant. This strengthens the choice of the design value.

The expected additional proportion of vehicles (Δ_o) for which negative lateral acceleration will vary from 0 to -0.004 g is only about 20 percent.

The correlation between β_r and any radius can be expressed by the following equation:

$$(\beta_r/\beta_{min})^2 = (R/R_{min})^{0.14} \quad (18)$$

For R_{max}/R_{min}, $(\beta_{max}/\beta_{min})^2$ equals 1.25. Under this condition it can be proved that R_{max}/R_{min} equals 5. The correlation can now be found between the superelevation rate and the curve radius for any given design speed.

It can be proved that

$$a_r = \beta_r^2\ V_D^2/R \quad (19)$$

By making the various substitutions, the following results:

$$a_e = 0.08\,g\,(R_{min}/R)^{0.86} \quad (20)$$

The values of β^2_{max} and R_{min} are given in Table 1 as a function of the design speed.

The above correlation between curve radius and the superelevation rate constitutes a straight line on a logarithmic plot; thus

$$\log e = \log 0.08 + 0.86 \log R_{min} - 0.86 \log R \quad (21)$$

This correlation is displayed graphically in Figure 5.

COMPARISON WITH OTHER SOURCES

In order to evaluate the quality and reasonability of the findings derived here, a comparison was made with design guidelines existing in the United States (12) and Germany (13)(RAL-73).

Comparison With AASHO Guidelines

It may be seen from Figure 6 that the superelevation values according to the AASHO guidelines exceed those proposed in the present work up to a design speed of 100 km/h. Above this speed, the values are essentially equal. This fact results in higher negative values of lateral acceleration in slow vehicles traveling on curves designed according to AASHO. Figure 7 presents the correlation between negative lateral acceleration and curve radius for the following design speeds: 48, 80, and 120 km/h, and a traveling speed V_0 (comfort speed) corresponding to each case. The figure indicates two important phenomena: (a) the correlation reaches a peak, and the increase from the minimum radius to the radius corresponding to this peak does not comply with the driver's expectation (i.e., with a desired decrease in pressure on the steering wheel with increasing curve radius) and (b) the values of negative acceleration largely exceed the limiting value of 0.05 m/s^2 proposed in this work, and they even reach a value of 0.28 m/s^2 at a design speed of 48 km/h and a value of 0.19 m/s^2 at a design speed of 120 km/h. This requires high pressure on the wheel, with the pressure itself exerted in the unnatural direction. Thus, the values of negative lateral acceleration calculated from AASHO guidelines may be subject to question.

It is also important to point out that Δ_o varies from 50 percent for a design speed of 80 km/h to 35 percent for a design speed of 120 km/h. These values of Δ_o were determined by using Equation 14 and the values of β_{min} and β_{max} calculated from the AASHO data. Comparison of these Δ_o values with those appearing in Table 3 for $(\beta_{max}/\beta_{min})^2 = 1.25$ shows that the former are greater and that the difference increases with decreasing design speed. This is in agreement with the principle that the lateral acceleration is zero or a higher value for a travel speed equal to the average running speed that corresponds approximately to the 70th percentile, on which the AASHO guidelines are based.

Another point is that the minimum radii of AASHO are significantly smaller than those given here for a design speed of 80 km/h or higher.

Considering the facts presented in this section, it seems reasonable to apply the data developed here in actual practice.

Comparison With RAL-73

Figure 8 shows that the superelevation values according to RAL-73 are essentially similar to those proposed in this work. The differences in the superelevation rates reach a limiting value of 0.005; the RAL-73 superelevation rates for small radii are lower and those for large radii are higher than the values presented here. The advantage of the data in the present work lies in the fact that the radii corresponding to a superelevation rate of 0.08 exceed those obtained from RAL-73. (The RAL-73 values for a superelevation rate of 0.08 are obtained by extending the curves in Figure 8 beyond 0.07, which is the maximum value in the German guidelines.) This fact is mentioned because a maximum superelevation of 0.08 is definitely appropriate for many conditions.

SUMMARY AND CONCLUSIONS

The present work adopts clear criteria for establishing the correlation between superelevation rates and curve radius. These criteria are derived from those factors that contribute to natural and unconstrained driving in a horizontal curve and to the distribution of travel speeds

Figure 7. Comparison of negative lateral acceleration and curve radius with AASHO values at a travel speed of V_o.

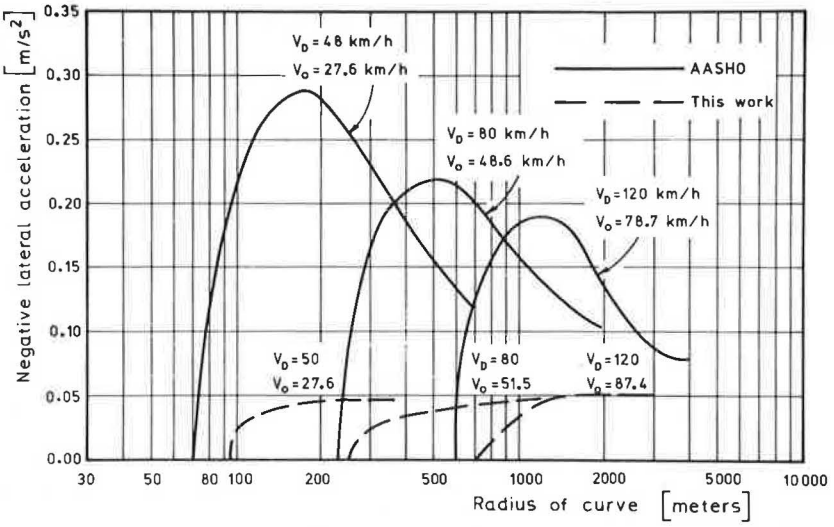

Figure 8. Comparison of curve radius and superelevation rate with RAL-73 values.

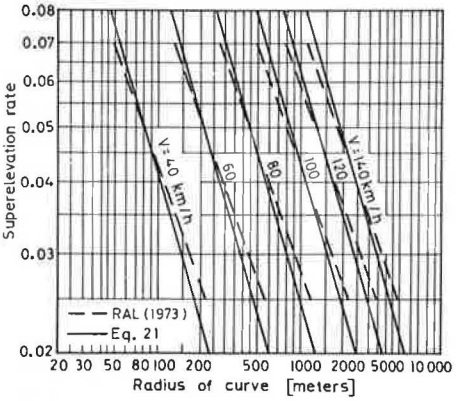

accompanying each given design speed.

The critical case, in which the radius is minimum, is defined by the maximum permissible lateral acceleration, which constitutes the physical output of the different input variables of driving parameters connected with the person-vehicle-environment system. The maximum superelevation rate derived from this case must permit natural driving for any actual speed distribution. Thus, the requirement for a slow vehicle is that the negative lateral acceleration, causing pressure on the steering wheel in a direction opposite to that of the turn, shall not exceed 0.2 m/s^2 for about 95 percent of all vehicles.

The correlation between superelevation rates and radius for a constant design speed is defined by the decrease in pressure exerted on the steering wheel with increasing curve radius. This pressure is expressed with the aid of an index, β^2, whose value increases with increasing curve radius. The function for this increase in β^2 also ensures a reasonable negative lateral acceleration in slow vehicles: 0.05 m/s^2 or less for 85 percent of all vehicles.

The results of the present work have been compared with AASHO and RAL-73 guidelines, and it appears that the criteria developed here are reasonable and that the findings are useful for design purposes.

REFERENCES

1. M. L. Ritchie, W. K. McCoy, and W. L. Welde. A Study of the Relation Between Forward Velocity and Lateral Acceleration in Curves During Normal Driving. Human Factors, Vol. 10, No. 3, June 1968, pp. 255-258.
2. J. J. Leeming and A. N. Black. Road Curvature and Superelevation: Experiments on Comfort and Driving Practice. Journal of the Institute of Municipal and County Engineers, Vol. 71, No. 5, Dec. 1944, pp. 137-149.
3. R. A. Moyer and D. S. Berry. Marking Highway Curves With Safe Speed Indications. Proc., HRB, Vol. 20, 1940, pp. 399-428.
4. D. C. Kneebone. Advisory Speed Signs and Their Effect on Traffic. Proc., Australian Road Research Board, Vol. 2, Pt. 1, 1964, pp. 524-541.
5. G. A. Breevord. De Ontwerpsnelheid in Bogen. Wegen, No. 705, Aug. 1974, pp. 223-228.
6. W. von Spindler. Untersuchung uber Kurvenfahrt und Ubergangsbogen. Forschungen fur die Sicherheit im Strassenverkehr, Frankfurt am Main, pp. 23-29.
7. H. G. Krebs. Bewertungskriterien zum Begriff der Richtgeschwindigkeit. Strassenbau und Strassenverkehrstechnik, Vol. 126, 1972.
8. Arizona Department of Transportation. Annual Speed Study. Highways Division, Traffic Operations Service, Oct. 1974.
9. A. C. Sarna and B. M. Sharma. Speed Studies on National Highways. Central Road Research Institute of India, Road Research Paper No. 112, Oct. 1970.
10. Highway Capacity Manual. HRB, Special Rept. 87, 1965.
11. Strassen-projektierung. Institut fur Verkehrsplanung und Transporttechnik ETHZ, Zurich, Oct. 1975.
12. American Association of State Highway Officials. A Policy on Geometric Design of Rural Highways. Washington, DC, 1965.
13. Richtlinien fur die Anlage von Lanstrassen Teil 11, Linienfuhrung (RAL-L): Strassenbau von A-Z. Erich Schmidt Verlag, Berlin, 1973.

Publication of this paper sponsored by Committee on Geometric Design.

Cost-Effectiveness of Driveway Slope Improvements

Edward R. Post and Patrick T. McCoy, Department of Civil Engineering, University of Nebraska, Lincoln
Richard J. Ruby and David O. Coolidge, Nebraska Department of Roads

In the development of roadside safety improvement programs, many types of obstacles have been identified as being hazardous. However, little attention has been given to the hazard of driveway slopes along noncontrolled and limited-access roadways. It was the purpose of this study to assess the hazard posed by such driveway slopes and to determine the cost-effectiveness of flattening them. The degree of hazard was measured in terms of the expected number of injury (fatal or nonfatal) accidents per year resulting from a vehicle traversing the slope. The probability of injury in a run-off-the-road encroachment of a driveway slope, which was used to compute the degree of hazard, was derived from severity indexes computed from results obtained from the highway vehicle object simulation model to simulate a standard-sized automobile traversing driveway slopes under encroachment conditions of 92-km/h (55-mph) speed and 10° encroachment angle in a free-wheeling steering mode. The results of this study indicate that (a) driveways are a roadside hazard, (b) the most cost-effective driveway slope design standard is 8:1, and (c) flattening to an 8:1 slope is the most cost-effective driveway slope improvement. The cost-effectiveness methodology used in this study provides a common basis for comparing driveway slope improvements with other types of improvements in the management of roadside safety improvement programs.

During the past two decades a considerable amount of attention has been devoted to improving roadside safety by removing, relocating, or reducing the impact severity of obstacles along roadsides. Many types of obstacles have been identified as being hazardous, and, as a result, comprehensive safety improvement programs have been undertaken. However, very little attention has been given either to the hazard of driveway slopes along the roadside of noncontrolled or limited-access roadways or to the cost-effectiveness of improving driveway slopes.

The purpose of this study was threefold. First, the degree of hazardousness of a typical driveway slope configuration along the roadside of a modern noncontrolled access, or limited-access, roadway facility was assessed. Second, the most cost-effective design standard for driveway slopes was determined. And, third, the cost effectiveness of improving driveway slopes from 3:1 to flatter slopes was evaluated.

The probability of injury in a run-off-the-road encroachment of a driveway slope must be determinable in order to conduct a cost-effectiveness analysis. The severity of such an event can be expressed as the ratio of the resulting automobile accelerations to the resulting accelerations "tolerable" to an unrestrained occupant. This ratio, commonly referred to as a severity index, was computed from the results obtained by a mathematical computer model simulation program named the highway vehicle object simulation model (HVOSM). The methodology used to express severity indexes in terms of probability of injuries is also discussed in this paper.

DESCRIPTION OF DRIVEWAY SITE

The driveway used in this study was chosen as a typical rural-suburban example. It is located along a four-lane divided rural highway section that is in a rural-urban transition area. The driveway site is shown in Figure 1.

The speed limit posted in the area of the driveway is the current national standard of 92 km/h (55 mph). The design speed of the highway section is 108 km/h (65 mph), and the horizontal and vertical alignments through the study area are both tangent. The topography traversed is flat and level.

The section has a variable width median, two 7.3-m (24-ft) lanes in each direction surfaced with portland cement concrete, a 3.7-m (12-ft) shoulder section on the outside with a 3.0-m (10-ft) wide surface of asphalt concrete. The foreslope is 6:1 to a minimum of 9.1 m (30 ft) from edge of pavement. Beyond 9.1 m, the foreslope is 4:1 to the 3.0-m flat-bottom ditch. The backslope is uniformly 4:1 from ditch bottom to original terrain elevation.

The actual driveway geometrics include 3:1 fill slopes with an 18.3-m (60-ft) wide grading top, for future intersection development, and an essentially tangential grade line from the shoulder point to the original terrain. The driveway used for this research did have drainage; however, based on prior research on flared end-sections and bar grates, no special consideration was given to this area; the main thrust of the research was directed to the driveway fill slopes. The geometric connection of driveway embankment to roadway embankment is basically defined by intersecting planes with a variable but limited amount of rounding.

COMPUTER SIMULATION MODEL

HVOSM was used to study the dynamic motion of an automobile traversing the ditch and driveway configurations described in the preceding section. HVOSM was developed by McHenry (1, 2) of the Cornell Aeronautical Laboratories and modified for specific field applications by the Texas Transportation Institute (3).

A standard-sized automobile was used in this study. The properties of the selected automobile were defined in previous research work conducted by Ross and Post (4, 5) and Weaver, Marquis, and Olson (6) on sloping grates in medians and roadside embankment slopes.

The roadway, shoulder, and soil were assigned friction coefficient values of 0.8, 0.6, and 0.2, respectively, and the soil was assigned a stiffness value of 580 kPa (4000 lbf/in^2). Terrain contact was only monitored at the two corners of both the front and rear bumpers.

No attempt was made to steer and brake the automobile during any of the driveway simulations. This free-wheeling condition would be representative of an inattentive driver.

PROBABILITY OF INJURY

The criteria used in the majority of the research work conducted during the past decade for evaluating the safety aspects of roadside hazard improvements were based on levels of vehicle deceleration that would be tolerable to an unrestrained occupant. An attempt was made in this study to expand the existing technology to include the probability of occurrence of injury accidents. This task was required in order to determine the cost-effectiveness of making driveway slope improvements.

Figure 1. Driveway site.

Severity Index Concept

The severity index concept attempts to take into consideration the combined and simultaneous effects of the longitudinal (x-axis), lateral (y-axis), and vertical (z-axis) accelerations of the automobile at its center of mass. The severity index is computed as the ratio of the measured or computed resulting automobile acceleration to the resulting tolerable automobile acceleration that defines an ellipsoidal surface. This ratio can be expressed mathematically by Equation 1. An in-depth discussion on the development of Equation 1 has been presented elsewhere (6, 7).

$$SI = \sqrt{(G_{LONG}/G_{XL})^2 + (G_{LAT}/G_{YL})^2 + (G_{VERT}/G_{ZL})^2} \quad (1)$$

The relationship between the accelerations experienced by an occupant and the accelerations of an automobile at its center of mass during a run-off-the-road collision or maneuver are largely dependent on the degree of restraint. In other words, the greater the degree of restraint the more similar are the accelerations experienced by an occupant and the accelerations of the automobile. At the present time, however, accident data show that in the majority of the accidents occupants were unrestrained. The tolerable accelerations suggested (6) for use in the severity index equation are presented in the table below.

Degree of Occupant Restraint	Acceleration (*g*)		
	G_{YL}	G_{XL}	G_{ZL}
Unrestrained	5	7	6
Lap belt only	9	12	10
Lap belt and shoulder harness	15	20	17

The severity index computations in what follows will be based on accelerations tolerable to an unrestrained occupant, and the automobile accelerations will be averaged over a time duration of 50 ms.

Severity Index and Injury Probability

In 1967, Michalski (8) of the National Safety Council statistically established, from the results of a study involving 951 automobile traffic accidents, that the incidence of occupant injury was directly related to the position of impact and the corresponding magnitude of vehicle damage. The severity of damage to a vehicle was rated on a seven-point photographic scale (9) by police officers and researchers at the scene of an accident.

The work of Michalski was applied and extended by Olson and Post (10) to include vehicle decelerations. Selecting vehicles damaged in full-scale tests conducted by California, New York, and the Texas Transportation Institute, Olson had research engineers rate the severity of vehicle damage using the National Safety Council's seven-point photographic scales. The corresponding average vehicle decelerations could then be computed knowing the impact conditions of the tests, vehicle dimensions, and the types of objects hit. The results of that study are shown in Figures 2 and 3.

An insight into establishing a relationship between severity index and injury probability can be obtained based on the combined work of Michalski (8) and Olson (10) for an angle-type collision such as a traffic barrier. In this type of collision in which vehicle snagging was minimized, it was determined that the average longitudinal vehicle decelerations (G_{long}) were equal to

$$G_{long} = \mu G_{lat} = \mu(10\ P) \quad (2)$$

where

μ = coefficient of friction between vehicle body and traffic barrier,
G_{lat} = average lateral decelerations = 10 P (Figure 2), and
P = injury probability.

On substituting Equation 2 into the severity index equation (Equation 1) and assuming that (a) the vertical accelerations are negligible, (b) the occupants are unrestrained, and (c) the friction coefficient is 0.3, one obtains the following relationship:

$$SI = \sqrt{(G_{long}/G_{x1})^2 + (G_{lat}/G_{y1})^2} = \sqrt{(10\mu P/7)^2 + (10P/5)^2} = 2.0P \quad (3)$$

Further insight into the relationship between severity indexes and injury probability can be obtained by combining the later work of Young, Post, and Ross (11) with that of Michalski (8) and Olson (10). In 1971, Young conducted a research study on the rigid Texas concrete median barrier, which is similar in design to the General Motors (GM) (12) traffic barrier that has inclined surfaces. HVOSM was used in that study, and several full-scale tests were conducted for validation purposes. Severity indexes were computed to compare the severity of one test, or simulation, with another and to serve as an aid in making decisions concerning roadside modifications that should effect a reduction in occupant injury and loss of life.

The combined work of Michalski, Olson, and Young is presented in Figure 4. In addition, Michalski statistically established the angle impact relationships shown in Figure 4 between mean vehicle damage ratings (R) and those accidents in which (a) R = 1.99 and vehicles were drivable, (b) R = 4.08 and vehicles were not drivable, (c) R = 2.49 and no injuries occurred, and (d) R = 4.73 and injuries occurred.

The average lateral vehicle decelerations, G_{lat}, that correspond to these mean damage ratings were obtained from Figure 2. The deceleration levels, in turn, were expressed as a function of the impact speed and angle using an equation contained in Olson's work. Referring to Figure 4, the following conclusions were reached:

1. The severity index curves exhibit the same characteristic shape as the deceleration level curves generated independently by Olson.
2. The no-injury prediction by Michalski and Olson agrees well with the tests run on the GM traffic barrier using a live driver who received no injuries and remained in complete control of his vehicle during 83-km/h (50-mph) and 8° collisions. It must be kept in mind, however, that even during this type of collision resulting in low levels of deceleration there exists a low probability for injury.
3. The injury prediction by Michalski and Olson corresponds to a severity index of 1.3 and an injury proba-

Figure 2. Curve relating lateral deceleration, proportion of injuries, and damage-rating scale.

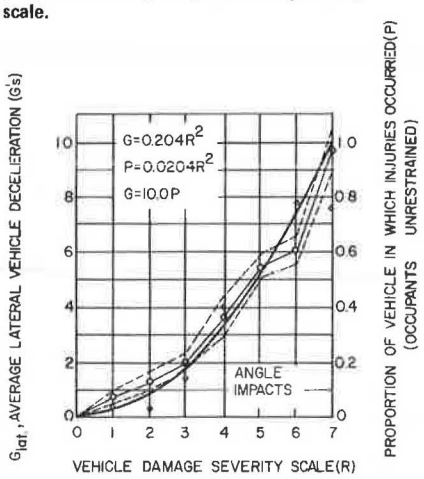

Figure 3. Curve relating longitudinal deceleration, proportion of injuries, and damage-rating scale.

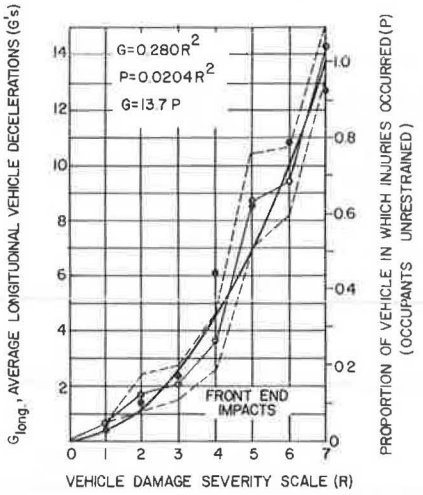

bility of about 50 percent. No attempt was made by Michalski to classify the severity of an injury. However, it is our opinion that this condition may approximately define the division between minor and serious injuries.

4. The not-drivable prediction by Michalski and Olson corresponds to an injury probability of about 35 percent and a severity index of 1.0, which was defined by Weaver, Marquis, and Olson (6) as representing a safe run-off-the-road maneuver or a collision.

5. The relationship between severity index and injury probability defined by Equation 3 agrees reasonably well with the results presented in Figure 4.

Based on the findings discussed above and realizing the complexity of the problem at hand, we reached a decision to define injury probabilities for fatal and nonfatal accidents over six broad categories of severity index. This relationship, shown in the table below, will be used in the subsequent cost-effectiveness evaluation.

Figure 4. Relations among impact conditions and vehicle lateral accelerations, severity index, and probability of injury during collision with Texas concrete median barrier.

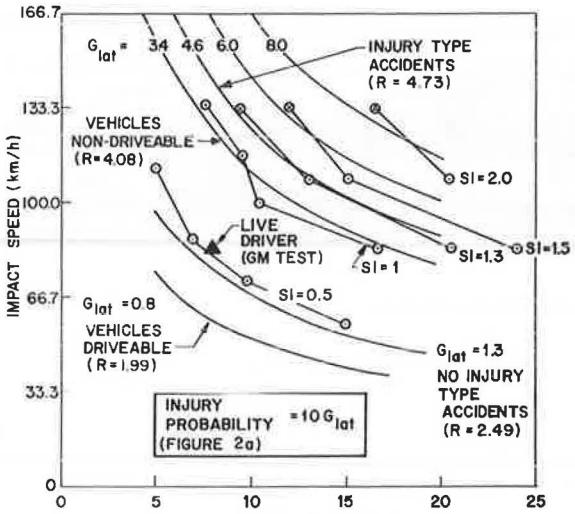

Note: 1 km/h = 1.61 mph.

Severity Index	Probability of Injury Accident
SI ≤ 0.5	0.1
0.5 < SI ≤ 1.0	0.3
1.0 < SI ≤ 1.5	0.5
1.5 < SI ≤ 2.0	0.7
2.0 < SI ≤ 2.5	0.8
2.5 < SI	1.0

SIMULATION RESULTS

Twenty-seven computer simulation runs were made in this study on driveway slopes of 3:1, 4:1, 6:1, and 8:1. The automobile was assumed to encroach on the roadside from the center of the outside lane at a speed and angle of 92 km/h (55 mph) and 10°. Simulations were made across the entire width of the driveway slope in increments of roughly 3.0 m (10 ft), which was considered adequate for making a cost-effectiveness analysis. The paths of the center of gravity of an automobile traversing 3:1 and 8:1 driveway slopes are shown in Figures 5 and 6.

The position of a vehicle along its path where the severity index was computed is marked by an "x". In the majority of the runs this occurred near the intersection of the ditch slope and driveway front slope, before the automobile was abruptly airborne, and at or slightly beyond the point where the automobile touched down.

The dotted portion along a vehicle's path defines the area and distance over which the automobile was airborne. Similarly, a large single dot along the vehicle's path defines the position where the roll angle was approximately 90° and rollover was imminent. Other than being reflected in the severity index, no attempt was made to evaluate the significance of the automobile being airborne for the driver's response.

COST-EFFECTIVENESS ANALYSIS

The cost-effectiveness analysis conducted in this study was based on the cost-effectiveness approach formulated by Glennon (13) and implemented in Texas for managing roadside safety improvement programs on both noncontrolled roadways and freeways (14). The cost-effectiveness measure used in this approach was annual cost that eliminated one injury (fatal or nonfatal)

Figure 5. Driveway 3:1 slope computer simulations of automobile center-of-gravity paths.

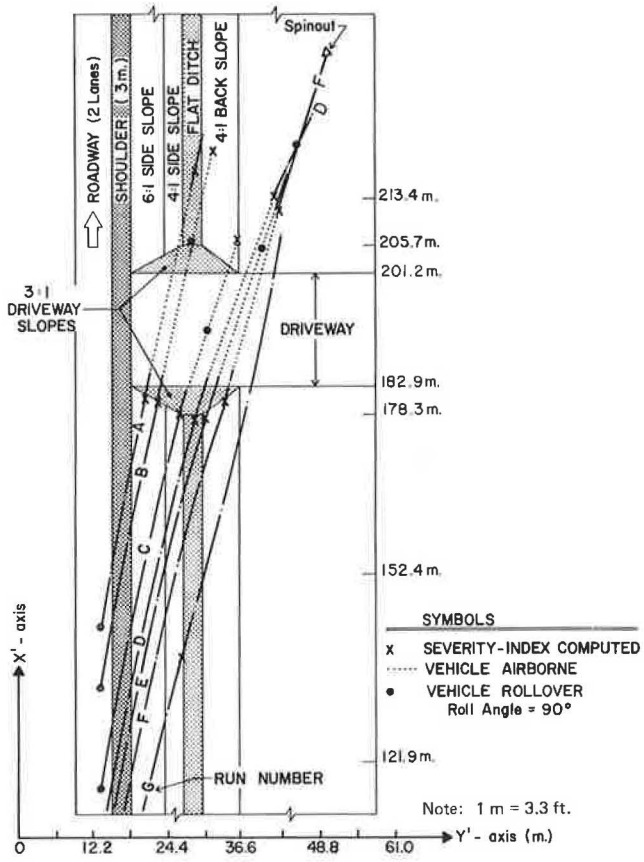

Figure 6. Driveway 8:1 slope computer simulations of automobile center-of-gravity paths.

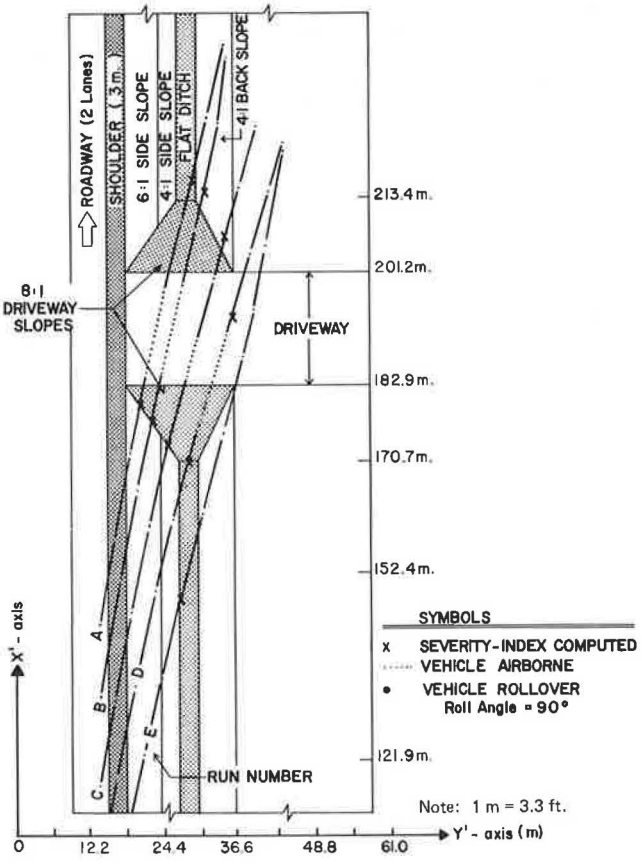

accident per year. The measure of effectiveness was defined as the difference between the hazard indexes before and after an improvement expressed in terms of number of fatal and nonfatal accidents per year. Thus, in order to apply the cost-effectiveness approach, it was necessary to compute the hazard index for each driveway slope alternative and its annual cost.

Hazard Index

The hazard index was computed for each driveway slope alternative using the following equation:

$$H_i = E_f[P(C/E)]\,[P(I/C)_i] \quad (4)$$

where

H_i = hazard index for driveway slope i or expected number of injury (fatal or nonfatal) accidents per year (i = 3:1, 4:1, 6:1, 8:1, 10:1),
E_f = encroachment frequency or number of encroachments per 1.6 km (1 mile) per year,
$P(C/E)$ = probability that a driveway slope will be traversed given that an encroachment has occurred, and
$P(I/C)_i$ = probability of an injury (fatal or nonfatal) accident given that a driveway slope i has been traversed.

A brief discussion of how each of the independent variables in this equation was computed follows.

Encroachment Frequency

Knowledge of the frequency with which vehicles encroach on the roadside of noncontrolled facilities is extremely limited. Therefore, the encroachment frequency used by Glennon (13) was assumed to be applicable for the purposes of this analysis.

Probability of Traversing Driveway

The probability that a driveway slope will be traversed given that an encroachment has occurred is proportional to the longitudinal length of the roadway within which the path of an encroaching vehicle would intersect a driveway slope. For the conditions simulated in this study (encroachment angle of 10°), it was determined that this length was about 61 m (200 ft) per driveway. Due to the lack of data on the effects of roadway conditions on the frequency and nature of encroachments, it was assumed that the longitudinal distribution of encroachments was uniform.

Probability of Injury Accident

The probability of an injury accident given that a driveway slope has been traversed was computed for each driveway slope using the following procedure:

1. For each driveway slope, the maximum severity index and potential for rollover were determined from the simulation results on each of five encroachment paths (A, B, C, D, and E).
2. For each driveway slope, the probability of an

injury accident was determined for each encroachment path as follows: (a) if rollover occurred, a probability of one was assigned; (b) if rollover did not occur, a probability was assigned on the basis of the maximum severity index experienced on the encroachment path using the relationship presented in the second table.

3. For each of the five encroachment paths, the probability that it would be the path of an encroaching vehicle was derived from the distribution of lateral displacements of encroaching vehicles generated by Glennon (13). These encroachment path probabilities were determined as follows: (a) for each encroachment path, the lateral distances between the edge of the traveled way and the point at which the path intersects each driveway slope were calculated, and the range of these values was determined, (b) the probabilities of the lateral displacements of vehicle encroachments being within each of these ranges were determined.

4. The expected probability of an injury accident for each driveway slope was calculated by using the following equation:

$$P(I/C)_i = \sum_{j=A}^{E} P(j)\,[P(I/j)] \quad (5)$$

where

$P(I/C)_i$ = probability of an injury accident given that driveway slope i has been traversed,
$P(j)$ = probability that encroaching vehicle will follow encroachment path j (j = A, B, C, D, E), and
$P(I/j)$ = probability of an injury (fatal or nonfatal) accident given that the encroaching vehicle follows path j.

The results of this step are presented below.

Driveway Slope	Probability of Injury Accident
3:1	0.9
4:1	0.8
6:1	0.7
8:1	0.3
10:1	0.3

Table 1. Driveway construction costs.

Driveway Slope	Driveway Type Costs ($): With No Underdrainage	With One 0.6-m-Diameter Underdrain	With Two 0.6-m-Diameter Underdrains
3:1	320	1890	3460
4:1	340	2060	3790
6:1	380	2400	4420
8:1	420	2730	5040
10:1	460	3070	5670

Note: 1 m = 3.3 ft.

Table 2. Driveway slope improvement costs.

Slope Improved To	Slope Improvement Cost ($): From 3:1 C[a]	E[b]	C/E[c]	From 4:1 C[a]	E[b]	C/E[c]	From 6:1 C[a]	E[b]	C/E[c]	From 8:1 C[a]	E[b]	C/E[c]
4:1	100	250	400	-	-	-	-	-	-	-	-	-
6:1	240	690	1140	140	440	740	-	-	-	-	-	-
8:1	380	1120	1860	280	870	1460	140	430	720	-	-	-
10:1	530	1560	2600	430	1310	2200	290	870	1460	150	440	740

[a]C = with no underdrainage.
[b]E = with one 0.6-m (2-ft) diameter underdrain.
[c]C/E = with two 0.6-m (2-ft) diameter underdrains.

Table 3. Cost-effectiveness of alternate driveway slope design standards with no underdrainage.

Slope Improved To	Slope Improvement: From 3:1 C[a] ($)	E[b]	C/E[c] ($)	From 4:1 C[a] ($)	E[b]	C/E[c] ($)	From 6:1 C[a] ($)	E[b]	C/E[c] ($)	From 8:1 C[a] ($)	E[b]	C/E[c] ($)
4:1	2	0.03	70	-	-	-	-	-	-	-	-	-
6:1	6	0.05	120	4	0.02	200	-	-	-	-	-	-
8:1	6	0.15	70	8	0.12	70	4	0.10	40	-	-	-
10:1	14	0.15	90	12	0.12	100	8	0.10	80	4	0	Infinite

[a]C = annualized cost of improvement using 8 percent interest rate, 20-year service life, and zero salvage value.
[b]E = difference between the hazard indexes before and after improvement.
[c]C/E = cost to eliminate one injury (fatal or nonfatal) accident.

Table 4. Cost-effectiveness of alternate driveway slope improvements with no underdrainage.

Slope Improved To	Slope Improvement: From 3:1 C[a] ($)	E[b]	C/E[c] ($)	From 4:1 C[a] ($)	E[b]	C/E[c] ($)	From 6:1 C[a] ($)	E[b]	C/E[c] ($)	From 8:1 C[a] ($)	E[b]	C/E[c] ($)
4:1	10	0.03	330	-	-	-	-	-	-	-	-	-
6:1	24	0.05	480	14	0.02	700	-	-	-	-	-	-
8:1	38	0.15	250	28	0.12	230	14	0.10	140	-	-	-
10:1	53	0.15	350	43	0.12	360	29	0.10	290	15	0	Infinite

[a]C = annualized cost of improvement using 8 percent interest rate, 20-year service life, and zero salvage value.
[b]E = difference between the hazard indexes before and after improvement.
[c]C/E = cost to eliminate one injury (fatal or nonfatal) accident.

Cost

Construction costs and slope improvement costs of the driveways studied were estimated by using 1977 average unit cost data obtained from the Nebraska Department of Roads. In each case, three cost estimates were made to reflect the effects of different drainage requirements. The estimated construction costs and slope improvement costs are shown in Tables 1 and 2 respectively.

Analysis

An incremental cost-effectiveness analysis was conducted to identify (a) the most cost-effective driveway slope design standard and (b) the most cost-effective driveway slope improvement. In the design-standard evaluation, the cost of the flatter slope provided by a higher standard was assumed to be equal to the difference in the driveway construction costs given in Table 1 for the two slopes involved and the particular drainage requirements under consideration. In the analysis of driveway slope improvements, the costs shown in Table 2 were used. The costs were made annual by using an 8 percent interest rate, 20-year service life, and zero salvage value.

The hazard indexes were computed by using Equation 4 and the probabilities of an injury accident given previously. An average daily traffic count of 3000 was assumed, which corresponds to an annual encroachment frequency of six per 1.6 km (1 mile).

Results

The results of the incremental cost-effectiveness analyses of driveway slope design standards and driveway slope improvements for driveways with no underdrainage are presented in Tables 3 and 4 respectively, also based on the 3000 annual daily traffic and six encroachments per year per 1.6 km (1 mile). For both design standards and improvements, the alternative with the lowest cost to eliminate one injury accident per year was the 8:1 driveway slope. Although the costs to eliminate one injury accident per year were higher for driveways with one or two 0.6-m (2-ft) diameter underdrains, the results were similar to those of driveways without underdrainage. Thus, in every case, the most cost-effective driveway slope design standard was 8:1 and the most cost-effective driveway slope improvement was 8:1.

CONCLUSIONS

The results of this study indicate the following:

1. Driveway slopes do present a roadside hazard,
2. The most cost-effective driveway slope design standard is 8:1, and
3. The most cost-effective driveway slope improvement is to flatten the slope to 8:1.

Of course, the higher the ADT of the roadway, the greater the degree of hazard and the more cost effective the 8:1 slope becomes.

REFERENCES

1. R. R. McHenry and D. J. Segal. Determination of Physical Criteria for Roadside Energy Conversion Systems. Cornell Aeronautical Laboratory Rept. VJ-2251-V-1, July 1976.
2. R. R. McHenry and N. J. DeLeys. Vehicle Dynamics in Single Vehicle Accidents: Validation and Extension of a Computer Simulation. Cornell Aeronautical Laboratory Rept. VJ-2251-V-3, Dec. 1968.
3. H. E. Ross and J. E. James. HVOSM User's Manual. Texas Transportation Institute, Texas A&M Univ., College Station, Research Rept. 140-9, Aug. 1974.
4. H. E. Ross and E. R. Post. Tentative Criteria for the Design of Safe Sloping Culvert Grates. HRB, Highway Research Record 386, 1972, pp. 101-110.
5. H. E. Ross and E. R. Post. Full-Scale Embankment Tests and Comparisons With a Computer Simulation. TRB, Transportation Research Record 488, 1974, pp. 53-63.
6. G. D. Weaver, E. L. Marquis, and R. M. Olson. Selection of Safe Roadside Cross Sections. NCHRP, Rept. 158, 1975.
7. H. E. Ross and E. R. Post. Criteria for Guardrail Need and Location on Embankments—Volume One, Development of Criteria. Texas Transportation Institute, Texas A&M Univ., College Station, Research Rept. 140-4, April 1972.
8. C. S. Michalski. Model Vehicle Damage Scale: A Performance Test. Traffic Safety, Vol. 12, No. 2, June 1968.
9. Vehicle Damage Scale for Traffic Accident Investigators. Traffic Accident Data Project, National Safety Council, TAD Project Technical Bull. No. 1, 1968.
10. R. M. Olson, E. R. Post, and W. F. McFarland. Tentative Service Requirements for Bridge Rail Systems. NCHRP, Rept. 86, 1970, pp. 12-16.
11. R. D. Young, E. R. Post, and H. E. Ross. Simulation of Vehicle Impact With Texas Concrete Median Barrier: Test Comparisons and Parameter Study. HRB, Highway Research Record 460, 1973, pp. 61-71.
12. L. C. Lunstrom, P. C. Skeels, and B. R. Englund. A Bridge Parapet Designed for Safety. HRB, Highway Research Record 83, 1965, pp. 169-187.
13. J. C. Glennon. Roadside Safety Improvement Programs on Freeways: A Cost-Effectiveness Priority Approach. NCHRP, Rept. 148, 1974.
14. G. D. Weaver, D. L. Woods, and E. R. Post. Cost-Effectiveness Analysis of Roadside Safety Improvements. TRB, Transportation Research Record 543, 1975, pp. 1-15.
15. J. W. Hutchinson and T. W. Kennedy. Medians of Divided Highways—Frequency and Nature of Vehicle Encroachments. Engineering Experiment Station, Univ. of Illinois, Bull. No. 487, 1966.

Publication of this paper sponsored by Committee on Geometric Design.

Abridgment

Pavement Width Standards for Rural Two-Lane Highways

Patrick Shannon, Department of Management and Finance, Boise State University
Alohn Stanley, Idaho Transportation Department

For a number of years, Idaho's pavement policy has included full-width pavement with shoulders paved the same thickness as the roadway. Overall widths have conformed generally to AASHTO standards. These standards were accepted in the absence of a formal analysis of local conditions suitable for establishing width criteria.

This study was undertaken to analyze local data and to obtain relationships among pavement width, construction and maintenance costs, and accident costs for rural two-lane highways. The investigation included two major phases: first, a statistical analysis of accident records to investigate the effects of width and other factors and, second, using accident trends determined from the first part of the study, economic analyses to evaluate the overall economic effects of different pavement widths in various average daily traffic ranges.

ACCIDENT ANALYSIS

Accident records from 1972, 1973, and 1974 were analyzed. Urban sections, unpaved roads, sections with more than two lanes, and sections with average daily traffic (ADT) greater than 3000 vehicles were excluded. A total of 664 highway sections in Idaho and 332 sections in Washington were studied. Very few of the sections had edgeline paint stripes during the study period. Section length varied between 1.6 and 16 km (1 and 10 miles). Study sections were further classified according to ADT and terrain type, using six levels of ADT and, initially, three levels of terrain. Accident rates in terms of accidents per 1.6 million vehicle-km (1 million vehicle-miles) were separated into three categories: property damage only, personal injuries or fatalities, and total accidents.

Statistical analysis of the accident data followed a procedure somewhat similar to an earlier Oregon study (1). Two steps were involved. First, product-moment correlations and partial correlations were employed to measure the extent of the linear relationship between accident rates and pavement widths. In the second step, variance and covariance procedures were used to determine whether there were statistically significant differences among accident rates in the different width classes.

The Pearson product-moment correlation technique was used to measure the extent of linear correlation between accident rate and terrain type, pavement width, section length, and ADT in each of six ADT ranges. Terrain and pavement width were found to be considerably more significant in a statistical sense than were section length and within-group ADT variation.

Table 1 shows the correlation coefficients in the various ADT ranges, considering total accident rates only. The positive signs on the significant terrain coefficients indicate increasing accident rate as the terrain becomes more severe. The negative signs on the width coefficients indicate decreasing accident rate as width increases. The effects of section length and within-group ADT are generally less significant than terrain and pavement width. This analysis only indi-

Table 1. Product-moment correlations.

ADT Range	Terrain	Width	Length	ADT	No. of Cases
0-249.99	-0.0203	-0.1457	0.1399	-0.0038	52
250-399.99	0.4022[a]	-0.2819[a]	-0.2027	0.0873	78
400-749.99	0.1833[a]	-0.1335[a]	-0.0423	-0.1418[a]	205
750-999.99	0.4526[a]	-0.2855[a]	-0.3545[a]	0.1014	123
1000-1999.99	0.1035	-0.3942[a]	-0.0417	-0.1657[a]	338
2000-2999.99	-0.0851	-0.3855[a]	-0.2167[a]	-0.0054	200

[a]Significant at the 0.05 level.

Table 2. Partial correlations.

ADT Range	Terrain	Width	Length	ADT	No. of Cases
0-249.99	-0.007 56	-0.103 85	0.098 87	0.023 74	52
250-399.99	0.395 85[a]	-0.288 40[a]	-0.155 72	0.140 21	78
400-749.99	0.148 03[a]	-0.127 35	-0.081 91	-0.087 61	205
750-999.99	0.417 01[a]	-0.200 09[a]	-0.354 14[a]	-0.076 62	123
1000-1999.99	0.086 65	-0.395 25[a]	-0.108 73[a]	-0.143 09[a]	338
2000-2999.99	0.074 76	-0.408 38[a]	-0.265 34[a]	-0.000 40	200

[a]Significant at the 0.05 level.

Table 3. Analysis of variance.

Source of Variation	Mean Accident Rate	Sum of Squares	Degrees of Freedom	Mean Square Error	F
Paved width (m)					
4.9-6.7	3.10				
7.9-14.0	2.16				
		158.398	1	158.398	75.78[a]
ADT range					
0-249.99	2.9531				
250-399.99	2.5204				
400-749.99	2.3409				
750-999.99	2.8909				
1000-1999.99	2.6116				
2000-2999.99	2.2497				
		68.379	5	13.67	6.54[a]
Interaction		16.551	5	3.31	1.58
Residual (error)		1584.508	756	2.09	
Total		1827.836	767		

Note: 1 m = 3.3 ft.
[a]Significant at any reasonable confidence level.

Table 4. Analysis of covariance.

Source of Variation	Mean Accident Rate	Sum of Squares (adjusted)	Degrees of Freedom	Mean Square Error	F
Paved width (m)					
4.9-6.7	3.099				
6.7-7.9	2.738				
7.9-14.0	2.159				
		143.763	2	71.881	29.821[a]
Error		2386.307	990	2.410	
Total		2530.070	992		

Note: 1 m = 3.3 ft.
[a]Significant at any reasonable confidence level.

Figure 1. Present-worth investment return analysis for a cost of $10 000 per accident.

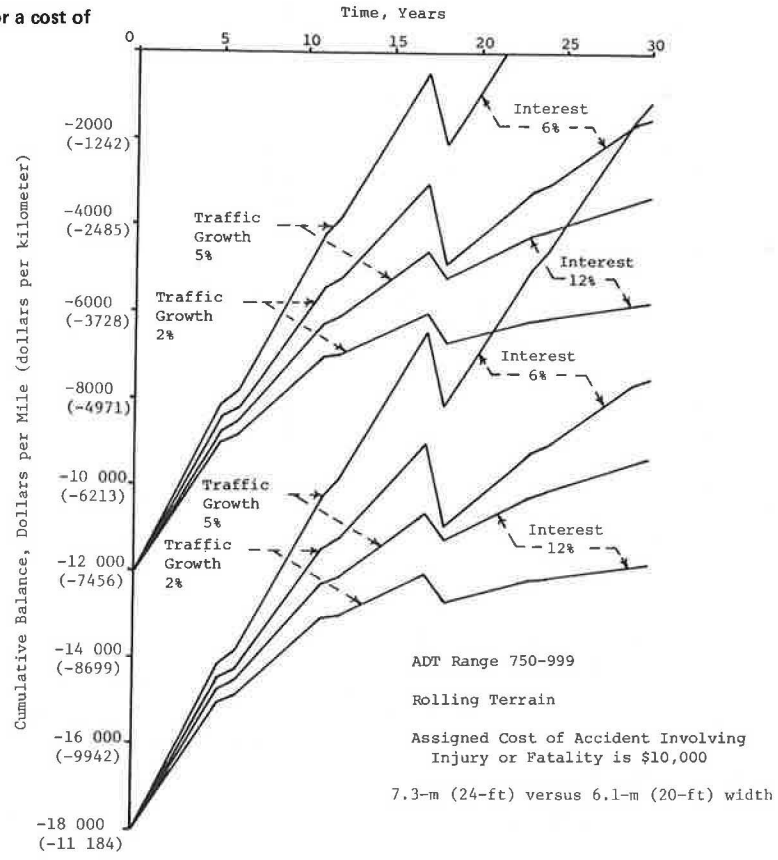

Notes: Values in parentheses are cumulative dollar balances per kilometer.
This example uses Idaho data only.

Figure 2. Present-worth investment return analysis for a cost of $12 000 per accident.

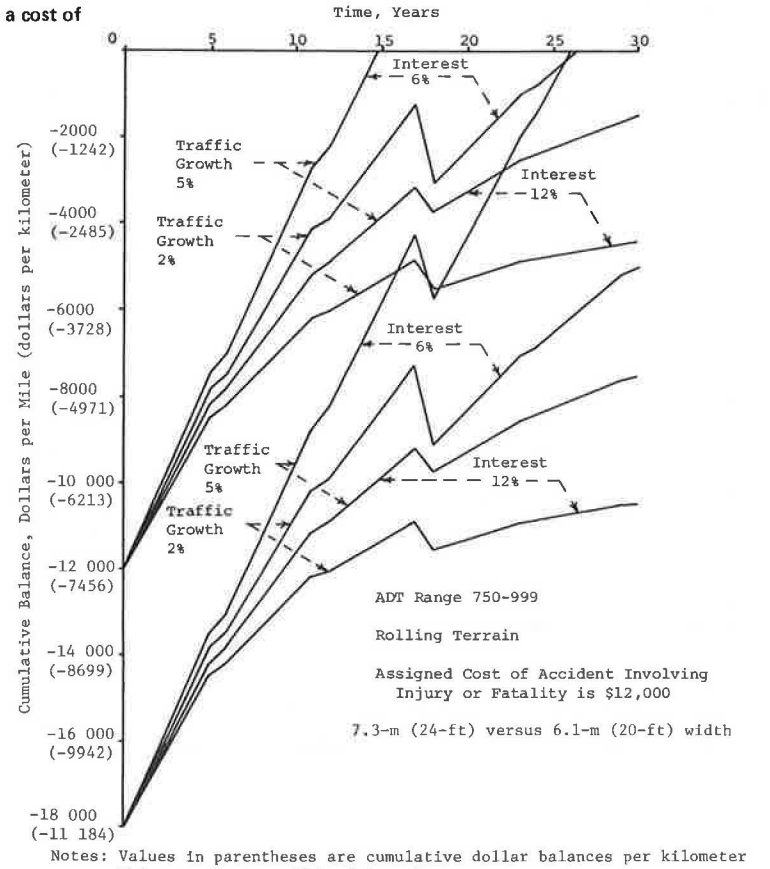

Notes: Values in parentheses are cumulative dollar balances per kilometer
This example uses Idaho data only.

cates that the linear relationship is significantly different from zero but does not necessarily imply direct cause and effect between variables.

Partial correlation was next attempted, partly because the trends revealed by the product-moment correlation had to be verified and partly because partial correlation has the additional feature of determining whether a causal relationship exists. Table 2 summarizes the partial correlations.

The preceding tables indicate that a basic linear pavement-width and accident-rate relationship can be inferred with high confidence in some ADT ranges but not in others, based on the data used in this study. A second observation is that the significant terrain coefficients are often numerically larger than the corresponding width coefficients, indicating that terrain constraint sometimes has a stronger linear relationship with accident rate than does pavement width.

Next a factorial analysis of variance was performed. The factorial design allows study of interactions among the variables involved. Only pavement width and ADT range were investigated in this portion of the study. Section length was not considered, because the preceding analysis showed its effect to be small. Terrain type was eliminated partly because it was not the variable of primary interest and partly because of small sample sizes in some terrain categories in certain ADT ranges. Table 3 lists mean total accident rates for two width ranges and six ADT ranges. Statistical variance testing indicated with a high degree of confidence that the observed differences in accident rates were significant.

The final type of statistical analysis performed was analysis of covariance, which has the advantage of controlling secondary factors so the true effect of the primary factor can be determined. Table 4 shows the mean accident rates for three levels of pavement width. The covariance analysis controlled all other effects so only pavement width and an error factor remained as sources of variation. The analysis indicated with a high degree of confidence that variations in accident rates resulted from the differences in pavement width.

ECONOMIC ANALYSIS

The accident study revealed a tendency for accident rates to decrease with increased pavement width, but of course highway cost increases with increased pavement width. It is desirable to evaluate the cost of wider pavement in comparison with potential cost savings resulting from accident reductions associated with wider pavement. For this purpose we chose a present-worth evaluation similar to that used in a North Carolina study (2). Interest rates of 6 and 12 percent were used to cover a range of representative values.

Construction costs were estimated using 1975 Idaho Division of Highways contractor bid prices. Construction cost increases for a 1.2-m (4-ft) wide strip of additional fill material, base, and paving were estimated to be $7085/km ($12 000/mile) on flat ground and $11 184/km ($18 000/mile) in more difficult terrain. Proportionate costs were calculated for other width changes.

Major maintenance operations were assumed to be chip seal coats at 6-year intervals and a 9.1-m (0.3-ft) thick overlay at 18 years. Estimated costs were $373/km ($600/mile) for seal coating and $3728/km ($6 000/mile) for the overlay on a 1.2-m (4-ft) wide strip.

Routine maintenance cost differences were estimated using data supplied by the Nevada Department of Highways. Computerized records covering 1 year and 4 months during 1973-1974 indicated routine maintenance costs for 3701/km (2300/miles) of 7.3-m (24-ft) pavement were about $31.06/km ($50.00/mile) lower than for 2253/km (1400/miles) of 6.1-m (20-ft) pavement. This relatively small difference was found to have no significant effect on the overall economic analysis.

Economic values associated with individual accidents were initially assumed to be $500 for an accident involving property damage only and $10 000 for an accident involving injury or loss of life. The effect of assuming values up to $20 000 as the average cost of an injury or fatality accident was also investigated. Average accident costs per kilometer were computed separately for six ranges of ADT and six nominal pavement widths. Initially, separate computations were made for each terrain type, but all terrain types were later merged to increase the number of roadway sections in each study category. Furthermore, eliminating terrain type facilitated comparisons with existing Idaho Division of Highways width standards, because minimum pavement widths are now the same for all terrain types. Only minimum standards for speed, foreslope steepness, curvature, grade, and stopping sight distance are changed to reflect terrain type.

For each study category, a weighted average accident

Table 5. Number of years required to pay back costs of wider pavement based on accident cost savings.

Initial Cost Difference ($/km)	Annual Interest (%)	Annual Traffic Growth (%)	No. of Years to Pay Back Costs by Construction-Year ADT					
			0-249	250-399	400-749	750-999	1000-1999	2000-2999
11 184	6	2	–[a]	–[a]	–[a]	–[b]	13	9
		5	–[a]	–[a]	–[a]	26	11	8
	12	2	–[a]	–[a]	–[a]	–[b]	–[b]	14
		5	–[a]	–[a]	–[a]	–[b]	16	11
16 776	6	2	–[a]	–[a]	–[a]	–[b]	25	15
		5	–[a]	–[a]	–[a]	–[b]	16	12
	12	2	–[a]	–[a]	–[a]	–[b]	–[b]	–[b]
		5	–[a]	–[a]	–[a]	–[b]	–[b]	23

Note: 1 km = 0.62 mile.

[a]The wider [10.4-m (34-ft)] pavement had a higher accident rate than the narrower [8.5-m (28-ft)] pavement.

[b]The narrower pavement had the higher accident rate but the costs were not paid back for 30 years.

Table 6. Comparison between existing Idaho minimum pavement widths and suggested minimums.

Range of Current ADT	Average 20-Year ADT of Sample Sections in the Given Range of Current ADT (2% growth)	DHV (assume 13% of 20-year ADT)	Suggested Minimum Width (m)	Idaho Minimum Width for Primary Highways (m)	Idaho Minimum Width for Secondary Highways (m)
0-249	246		6.1	7.9-8.5	7.9-8.5
250-399	467		6.1	10.4	8.5
400-749	851	111	7.3	10.4	10.4
750-999	1294	168	8.5	10.4	10.4
1000-1999	2124	276	10.4	12.2	12.2
2000-2999	3643	474[a]	12.1	13.4	13.4

Note: 1 m = 3.3 ft.

[a]Idaho design standard calls for four-lane design when DHV exceeds 400.

rate was computed for a 1.6-km (1-mile) section, using the accident records for that category. Future ADT was estimated for each of the next 30 years, using both 2 and 5 percent annual traffic growth. The 30-year period was estimated to be a reasonable interval during which no major reconstruction would likely be required. For each of the 30 years, a cumulative summation of costs and benefits was made under each combination of assumptions about traffic growth, interest rate, and initial cost difference. Accident rate was assumed constant over the 30 years.

Figures 1 and 2 illustrate the general features of the analysis. Traffic growth is 2 percent annually for both figures. The point at which the curve crosses the horizontal axis is the year in which the savings due to accident reductions would repay the added cost associated with the wider paved road. Comparison between the two figures illustrates that the analysis is somewhat sensitive to changes in the economic value assigned to each injury or fatality accident. A condensed form of data presentation was used in evaluating the results of the computations. This is illustrated in Table 5 for one set of conditions.

CONCLUSIONS

Using the foregoing type of analysis, a table of suggested minimum paved widths was prepared. Table 6 compares the suggested minimums with existing Idaho Division of Highways standards. Because the analysis is relatively sensitive to injury or fatality accident cost, the suggested minimums should be reevaluated if the average cost of such accidents increases significantly, or if accident trends change significantly.

ACKNOWLEDGMENTS

Major funding for this study was provided by the Pacific Northwest Regional Commission. The cooperation of the state highway agencies of Nevada, Oregon, and Washington is gratefully acknowledged.

REFERENCES

1. R. C. Blensly and J. A. Head. Statistical Determination of Effect of Paved Shoulder Width on Traffic Accident Frequency. HRB, Bulletin 240, 1960.
2. C. L. Heimbach, W. W. Hunter, G. C. Chao, and T. W. Griffin. Investigation of the Relative Cost-Effectiveness of Paved Shoulders on Various Types of Primary Highways in North Carolina for the Purpose of Establishing Priority Warrants. North Carolina State Univ., Raleigh, 1972.

Publication of this paper sponsored by Committee on Geometric Design.

Earth Berms and Their Actual and Perceived Effects on Noise and Privacy in Adjacent Neighborhoods

Kumares C. Sinha, School of Civil Engineering, Purdue University, West Lafayette, Indiana
Neil R. Wienser, Milwaukee District, Wisconsin Division of Highways

The purpose of this paper is to compare and assess the measured and calculated attenuations obtained from earthen sound berms and also to assess the perceived effects of selected berms on adjacent residential neighborhoods by means of an attitudinal survey. Simultaneous sound readings were taken before and after construction of the berms. It was found that they produced median sound-level attenuations of 5 dB(A) at the right-of-way line and 3 dB(A) at a distance corresponding to the front sidewalk of the homes along the freeway. The attitudinal survey, conducted before and after the construction of sound berms, indicated that residents immediately adjacent to the freeway perceived a reduction in sound levels and increased privacy both indoors and outdoors. The study concluded that even minor attenuations of freeway noise of 5 dB(A) or less are discernible within adjacent neighborhoods and, based on the subjective responses of the attitudinal survey, are perceived to be greater than actually measured. Also, the increased privacy afforded by sound berms should be a consideration in the evaluation of proposals for the construction of future sound-attenuating devices.

In the fall of 1971 the Milwaukee metropolitan district office of the Wisconsin Division of Highways undertook a series of safety improvement projects, particularly concrete median barriers, on the interstate freeways within its jurisdiction. During the design of these barriers it became evident that there would be an excessive amount of earth material that would have to be removed from the project sites. It was decided that, rather than waste this material on private dumping areas, it could be used to develop experimental acoustical barriers at selected sites along the freeway that were near the sites. It was felt that the barriers would serve two purposes: They could be used as sound deflectors to reduce freeway noise levels for land uses along the freeway and they could function as privacy shields between the freeway and the adjacent land developments.

Because the use of such berms was experimental, it was felt that a study should be done to obtain first-hand information on the benefits and design of these barriers. Consequently, a before-and-after study was undertaken to determine the effectiveness of the earth berms in sound attenuation and to serve as a guide for future design and construction of these devices.

The initial intent of the before-and-after study was a series of sound-level readings to measure the actual attenuation realized from the barriers. However, a literature search revealed a number of studies that had already measured attenuation of barriers of this nature (1, 2, 3, 4). All of these studies, nevertheless, indicated

Figure 1. Typical earth berm cross sections.

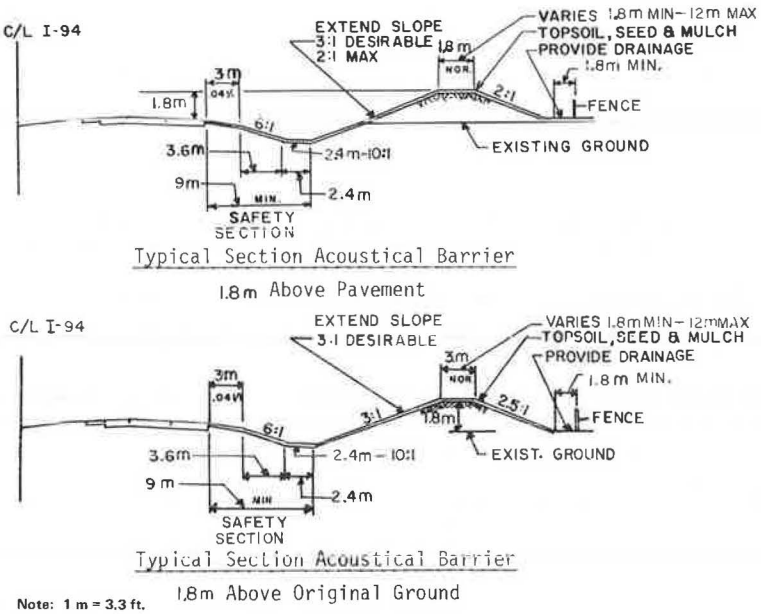

Note: 1 m = 3.3 ft.

Figure 2. Typical sound sample and point location.

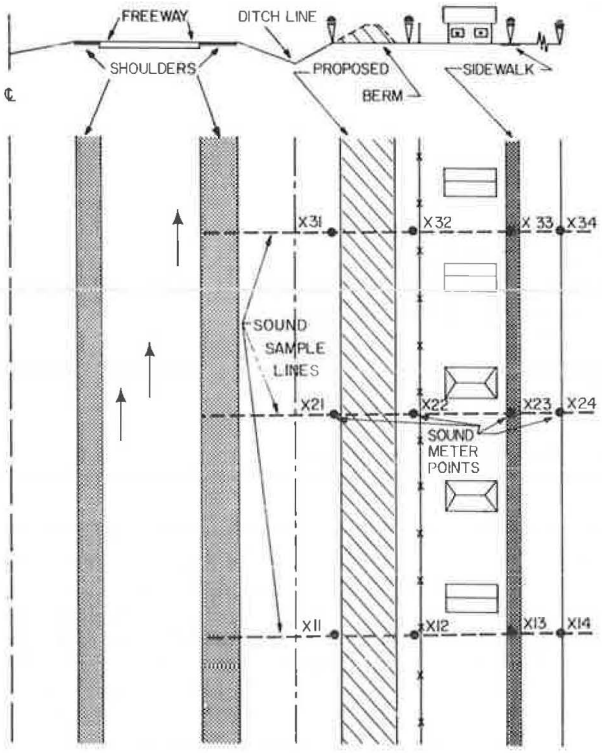

that, although measured attenuations were well documented, there appeared to be a lack of information concerning the perceived attenuation and the acceptance of such barriers by the adjacent land users. Furthermore, it was felt that even if the barriers did not afford a significant amount of attenuation they would provide privacy to the adjacent neighborhoods. It was therefore decided to conduct a thorough study (6) that would not only measure the resulting attenuation of these barriers through a series of simultaneous before-and-after sound-level readings, but that would also produce information concerning the perceived effects and acceptance of the barriers by the residents in adjacent neighborhoods, through an attitudinal survey, to be administered before and after the construction of the barriers.

SOUND-BARRIER DEVELOPMENT

The earth berms were constructed entirely on existing highway right-of-way land. Six sites were located along the North-South Freeway, I-94, in Milwaukee County. Because the safety improvement projects were extended to a portion of the East-West Freeway in Waukesha County, two additional barrier sites for construction of acoustical barriers were selected.

As the material became available for construction of each berm from the excavation for the median safety barriers on the freeways, it was put in place. The contractor responsible for a few of the berms decided to construct the center of the berm with removed concrete curb and gutter. This material was covered with the adequate earth material taken from the median area of the adjacent freeway. It was intended, in the location of each barrier, that the haul distance for the median soil be kept to a minimum.

In Figure 1 typical cross sections of the sound berms constructed are shown. Actual design in a specific site depended upon several factors, including considering the continuation of existing slopes, minimum width of a relatively level top, and maximum slopes for safe maintenance. Minimum distances from right-of-way fences for any future maintenance vehicles were also taken into consideration. In addition, adequate provision had to be made in the berm design for proper cross drainage of trapped water. A thorough landscaping plan was developed that included not only seeding but also extensive placement of bushes and trees. Before the placement of any berms, existing trees and bushes were carefully removed from the areas and preserved for use in the final landscaping.

The landscaping plan primarily included fast-growing species of bushes that could be planted in drifts rather than singly. The landscaping was completed in the spring of 1973, the year after berm construction. Because the plants used in landscaping were very young and the bushes that were removed and later replanted on the berms had only been planted in recent years and were not yet mature, the immediate impression of landscaping did not appear extensive. However, over the next

several years the full extent of the landscape work will become evident as the plants and bushes reach their maturity.

FIELD MEASUREMENTS OF SOUND BEFORE CONSTRUCTION

A sampling procedure was developed through several trial methods that could be followed by field technicians and that was subsequently shown to be accurate to ±1.75 dB(A) at a 95 percent confidence level. Along with the measuring of changing sound levels, traffic volume and classification were also recorded.

While the adopted sampling method measured a sound level at any one point, it could not be used to measure an attenuation at a single location on a before-and-after survey because it is nearly impossible to duplicate the sound source that existed during the initial survey. Therefore, measured attenuation was obtained through simultaneous readings at fixed points from the freeway that included points along the freeway side of the future berm and several points on the other side of the berm at various distances away from the freeway. Figure 2 shows a layout of typical sound-sample lines and point locations.

This method in the initial survey produced attenuations that reflected changes in sound levels due to distance and other terrain parameters. In the after survey the measured attenuations with the addition of the barrier between the sound source and the observers beyond the barrier, with the distance and other terrain parameters unchanged, were compared to the initial attenuations. The comparison between the before-and-after attenuations resulted in the attenuation caused by the introduction of the earth berm in the path of the sound.

All sets of sound-level readings were taken simultaneously in order to negate the effect of changing the traffic parameters. It was observed that along the freeway the sound levels varied from 80 to 86 dB(A) on the North-South Freeway and from 84 to 88 dB(A) on the East-West Freeway at the edge of roadway. Corresponding sound ranges at point 2 were 74-80 dB(A) and 78 dB(A) without variation; at point 3 the range varied from 60 to 75 dB(A) and from 66 to 71 dB(A); and at point 4, which was measured on the North-South Freeway only, the range varied from 54 to 68 dB(A).

It can be seen from the difference in the ranges that, although the same identical traffic did not pass during each of the sample periods on a sample line, the L_{10} sound level remained fairly uniform along the freeway but a greater range was observed at the more distant locations. It may be noted that the sound levels farther from the freeway appeared to be more susceptible to activities within the neighborhoods—children playing, subdivision traffic, and lawn care.

FIELD MEASUREMENTS OF SOUND AFTER CONSTRUCTION

The same procedures developed for the initial study were followed in the sound study after the berms were constructed.

In the after survey it was observed that along the freeway the sound levels varied from 81 to 88 dB(A); at point 2 the sound level varied from 68 to 79 dB(A); at point 3 the range was from 63 to 71 dB(A); and at point 4 the range went from 57 to 70 dB(A). Although the ranges of sound levels were sometimes higher in the after survey than in the before survey, this did not indicate a loss of attenuation due to the sound berms.

Traffic volumes and classification mix that were different during the final survey produced basic sound levels different from the initial survey. For proper consideration of sound attenuation the sound data were analyzed by comparing before-and-after sound readings from point 1 with those at the other sampling points along the sample line; this procedure does not allow the results to be affected by the variations in traffic volumes during, before, and after sound surveys.

An established method (4) was used to calculate all sound-berm attenuations for a general check of measured values. These attenuations appeared to be satisfactory and generally what would be expected. Table 1 summarizes the measured and calculated attenuations obtained at location 4. The resulting median ambient sound level L_{10} at that location is given below (1 m = 3.3 ft):

Condition	L_{10} by Distance to Edge of Near Freeway Lane [dB(A)]		
	20-27 m (point 1)	40-53 m (point 3)	76-98 m (point 4)
Measured	72	63	65
Calculated	74	64	62

ATTITUDINAL SURVEY

Before Construction

The initial attitudinal survey was conducted before the berms were constructed to investigate the opinions of the residents in adjacent residential neighborhoods who would be affected by the future sound berms. The survey included a questionnaire constructed to judge the current attitudes on a number of neighborhood characteristics.

In addition to the future berm areas, the survey included a control area that would not be affected by the construction of future sound berms. By comparing the responses from the initial and final questionnaires, the control area information could be used as a basis for judging any outside influences during the period between the two surveys that might have caused an appreciable change in the attitudes of the residents of the study area.

Identical questionnaires were handed out in both the control and study areas. The questionnaires were designed to be cross checking; that is, the opinions concerning the effects and extent of freeway noise in the neighborhood were asked in several different questions. In this way it was felt the consistency and validity of the responses could be checked.

Because it was believed at the beginning of the survey that the berms would provide not only a sound attenuation for the adjacent neighborhoods but also increased privacy for the residents, several questions were included that would evaluate the respondents' attitudes toward the possible invasion of their privacy by the adjacent freeway. The survey questionnaires and a summary of the responses to the questions are available elsewhere (6).

Five of the eight proposed sound berms were located immediately adjacent to residential subdivisions. Three of these berms were located so that they would affect approximately 415 dwelling units. The control area included approximately 195 dwelling units. In Figure 3 is shown the aerial view of the sound berm along I-94. A review of the 1970 census information showed that the age of the survey area population was predominantly in the range of 25-40 years. Valuation of the homes ranged from $24 000 to $34 000.

The survey questionnaires were delivered personally by the study group and were collected after a few days from the respondents at their homes. A cover letter in-

Table 1. Attenuation L_{10} in dB(A) for 2680-4480 vehicles/h and 20 percent trucks.

Line	Type of Attenuation	Attenuation by Distance to Edge of Near Freeway Lane [dB(A)] 20-27 m (point 2)	40-53 m (point 3)	76-98 m (point 4)	Barrier Height (m)	Distance to Nearest End of Berm (m)
41	Measured	5	5	1	2.9	24.4[a]
	Calculated	6	4	1		
42	Measured	9	17	14	1.8	18.3
	Calculated	11	8	6		
43	Measured	7	8	4	1.7	21.3
	Calculated	10	7	3		
44	Measured	2	4	2	1.5	43.0[a]
	Calculated	5	3	1		
45	Measured	1	-3	-3	3.1	12.2
	Calculated	0	2	1		

Note: 1 m = 3.3 ft.

[a]Break in barrier between sound sample lines.

Figure 3. Alignment of tiers in study area.

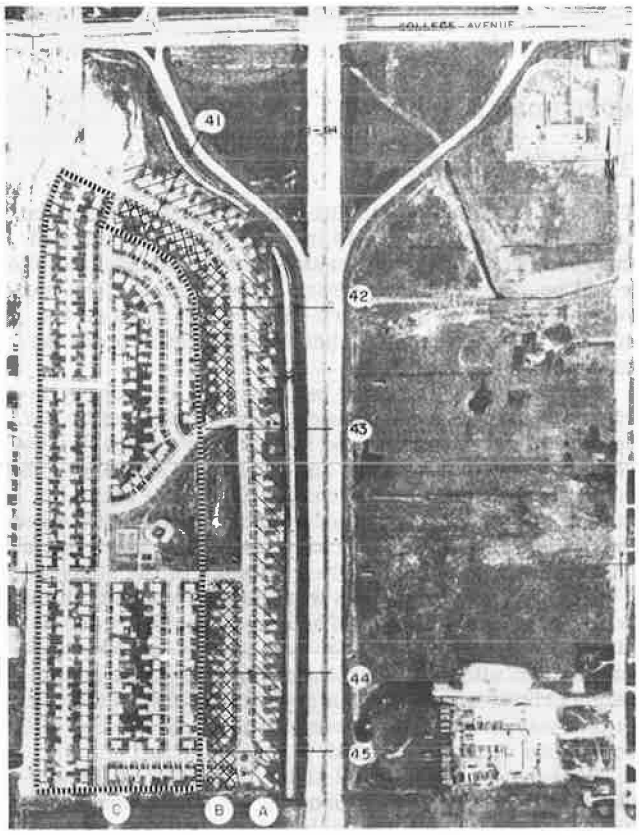

formed the respondents of the nature of the survey, why it was being conducted, and how the completed survey forms would be collected. A total of 417 questionnaires were distributed in the study area; the response rate was 45 percent. At the control area, 195 questionnaires were distributed; the response rate was 32 percent.

In the development of the attitudinal survey it was felt that responses would be different depending on the location of the respondent in relation to the freeway. Accordingly, a record was kept to indicate the location of the home of each respondent; the locations are identified as tier A if the homes are situated directly adjacent to the freeway, tier B if the homes are situated one lot away from the freeway, and tier C if the homes are situated at two or more lots away from the freeway. The responses to the questions relevant for this study were summarized by the location of tiers. The alignment of tiers in the area is shown in Figure 3.

The survey showed 63 percent of the respondents in the study area and 83 percent in the control area moved into their homes during or after the construction of the freeway. The percentage of the respondents who indicated that they were either "very satisfied" or "just satisfied" living in the study area and control area are 92 percent and 81 percent respectively. The majority of the respondents in both the study and control areas considered their neighborhood to be "noisy" or "slightly noisy". The location in the study area within tiers A, B, or C was found to be significant with respect to the responses to neighborhood noise. A chi-square test with grouped data indicated no significant difference in the responses from the study and control areas. All tests were conducted with a 1 percent level of significance.

Table 2 presents the responses obtained from the study area with respect to the question on "noticing noise". Through chi-square tests it was observed that, although the perception of noise inside the home was not significant with the location of tier, it was significant outside the home. This result can be attributed to the sound attenuation offered by the dwelling unit.

The respondents were observed to be annoyed by the freeway traffic noise, and again this annoyance varied significantly from tier to tier. Table 3 shows the degree of annoyance by freeway traffic noise in the study area.

In general, the respondents felt they had "enough privacy"; however, as shown in Table 4, there was some lack of privacy resulting from the layout of houses, lack of bushes and trees, and freeway exposure. As expected, the lack of privacy due to freeway exposure was significantly affected by tier location with respect to freeway.

After Construction

The final attitudinal survey was conducted in October 1973 in the same manner as the initial survey. However, the questionnaires were modified to include questions concerning the berms that had been placed in the study area in the meantime. Out of a total of 494, 156 responses were obtained in the study area, while in the control area 93 questionnaires were returned out of 210.

In the study area 53 percent of the respondents felt that the sound berms were effective in reducing traffic noises heard out of doors in their neighborhoods. This was slightly higher, 58 percent, in tier A than for the entire study area. Indoors, 52 percent felt that the sound berms were effective in reducing freeway noise; there was an increase in this response in tier A from the out-of-doors results in that 66 percent felt that there was a decrease in noise. The tabulation of the responses is shown in Table 5.

With respect to privacy, 68 percent of the respondents in tier A of the study area and 28 percent of the total respondents felt that there was an increase in household out-of-doors privacy due to the berms. This result is entirely understandable considering that generally privacy would be affected mainly for the respondents adjacent to the freeway or, at the most, one tier of lots removed from the freeway. The indoors response indicated that 55 percent of the respondents in tier A and 21 percent of the respondents overall felt there was an increase in indoor privacy. The tabulation of the responses is shown in Table 6.

Fifty-four percent of the total respondents indicated that there was a positive effect from the berms. Moreover, the percentage of respondents in tier A who felt the berm had improved privacy and reduced noise was 71 percent. In analyzing the responses by tiers, tier C indicated that the predominant effect was less freeway

noise, while in tier A both the reduction in freeway noise and the increased household privacy were mentioned as the predominant effect in approximately an equal number of responses.

Table 2. Perception of neighborhood noise.

Response	Number of Responses							
	Outside				Inside			
	Tier A	Tier B	Tier C	Total	Tier A	Tier B	Tier C	Total
Not noticeable	2	0	5	7	4	4	28	36
Slightly noticeable	8	4	49	61	23	17	53	93
Very noticeable	25	31	60	116	5	12	25	42
Total	35	35	114	184	32	33	106	171

Table 3. Annoyance by freeway noise.

Response	Number of Responses			
	Tier A	Tier B	Tier C	Total
Not annoyed	8	3	42	53
Slightly annoyed	10	18	38	66
Very annoyed	17	15	22	54
Total	35	36	102	173

Table 4. Neighborhood conditions negatively affecting personal privacy.

Response	Number of Responses			
	Tier A	Tier B	Tier C	Total
Layout of houses	14	18	48	80
Lack of bushes and trees	13	8	31	52
Heavy traffic	6	2	8	16
Neighbors	5	10	18	33
Freeway exposure	19	8	10	37
Children	6	9	22	37
Others	1	2	10	13
Total	64	57	147	268

ATTITUDINAL SURVEY COMPARISONS IN CONTROL AREA

A detailed statistical comparison of the responses from the before-and-after surveys in the control area was made in order to determine any changes that might have affected responses in the study area as to the effects of the sound berms.

A series of chi-square tests was performed with respect to length of residence, respondent's satisfaction with neighborhood, the characteristics liked most and least, consideration of noise in the neighborhood, degree of annoyance from noise, consideration of privacy in the neighborhood, and sex and age group of the respondent. It was concluded that there had not been a statistically significant change in attitude concerning the noise or privacy level in the control area in the period between the two surveys.

As the study area was in the general vicinity of the control area it was felt that the responses related to the berms in the study area were not affected by any attitudinal changes since the initial survey. This conclusion was further validated by determining that the characteristics of the respondents in the study area did not change.

MEASURED ATTENUATION AND PERCEIVED EFFECTS

Sound levels are measured as decibels on the A scale. The decibel is a log measurement of sound intensity or acoustical energy. The relationship between sound-level change and acoustical energy and corresponding change of relative loudness (5) is shown below.

Sound-Level Change [dB(A)]	Acoustical Energy Loss (%)	Relative Loudness
0	0	Reference
-3	50	Perceptible change
-10	90	One-half as loud
-20	99	One-quarter as loud
-30	99.9	One-eighth as loud

To compare measured and perceived attenuation, further discussion of audible sounds is necessary. Peak hearing ability is observed during the ages of 10-20 years. Before that age hearing ability increases, and after it hearing ability decreases. During the peak hearing periods

Table 5. Effectiveness of berms on freeway noise reduction.

Response	Number of Responses							
	Outside				Inside			
	Tier A	Tier B	Tier C	Total	Tier A	Tier B	Tier C	Total
Much less noise	4	1	8	13	7	3	16	26
Slightly less noise	18	12	38	68	18	9	28	55
No effect	15	11	39	65	9	13	43	65
Slightly more noise	-	1	2	3	1	1	1	3
Much more noise	1	3	1	5	3	2	1	6
Total	38	28	88	154	38	28	89	155

Table 6. Effectiveness of berms on increasing privacy.

Response	Number of Responses							
	Outside				Inside			
	Tier A	Tier B	Tier C	Total	Tier A	Tier B	Tier C	Total
Much more privacy	12	3	2	17	0	1	2	11
Slightly more privacy	14	3	8	25	13	2	5	20
No effect	9	20	71	100	13	23	74	110
Slightly less privacy	2	1	3	6	3	-	3	6
Much less privacy	1	1	-	2	1	2	-	3
Other	-	-	1	1	-	-	1	1
Total	38	28	85	151	38	28	85	151

Table 7. Study area attenuation L_{10} in dB(A) for 2680-6790 vehicles/h and 11-20 percent trucks.

Type	Attenuation by Distance From Freeway [dB(A)]			Berm Height (m)
	20-43 m (point 2)	40-125 m (point 3)	76-98 m (point 4)	
Median				
Measured	5	3	1	2.1
Calculated	5	2	1	
Range				
Measured	1-10	0-8	0-6	1.5-4.3
Calculated	0-11	1-8	0-6	

Note: 1 m = 3.3 ft.

humans can distinguish intensity of noise difference of 2-3 dB(A). After the age of peak hearing, a 3-4 dB(A) intensity difference is required for the normal person to distinguish a difference in sound levels. When a person is not looking for the difference in sound levels, the change in level would have to be in the range of 4-6 dB(A) to notice the difference.

COMPARISON OF SOUND-LEVEL ATTENUATION

The final attitudinal survey in the study area obtained the subjective attitude of the respondents in relation to the decrease in neighborhood noise attributable to the sound berm. In tier A, 47 percent indicated "slightly less noise", 11 percent indicated "much less noise". Based on the definition of audible sound it can be concluded that "slightly less noise" could correspond to a sound that is audible to a typical respondent in the 30-40 age bracket, in the range of 4-6 dB(A). "Much less noise" can be considered to be in the range of 8-10 dB(A). In tier B, 33 percent indicated a "slightly less noise" response. This could also correspond to a 4-6 dB(A) reduction in noise level at tier B.

Table 7 summarizes the measured and calculated attenuations within the study area. The calculated attenuations were derived on the basis of the procedure given elsewhere (4).

A review of the above measured attenuations with the subjective responses indicated that the respondents to the survey felt that there was a slightly greater attenuation than shown in the measured survey. Approximately half (47 percent) of the respondents in tier A indicated that there was a 4-6 dB(A) reduction in noise for their living activities, whereas the measured attenuations indicate that, while at the right-of-way line there was a median attenuation of 5 dB(A), the attenuations at the sidewalk line were 3 dB(A). This is slightly less than the subjective attitudinal attenuations. Also, 11 percent indicated "much less noise", which is somewhat higher than the actual attenuation. In tier B, 33 percent indicated a "slightly less noise" attenuation of 4-6 dB(A); however, the measured attenuations indicated a median attenuation at approximately the sidewalk line of tier B of 1 dB(A), indicating that there was a perceived or subjective attitudinal attenuation for a third of the respondents in tier B of approximately 3-5 dB(A) higher than the measured attenuation.

This comparison indicates that a berm of the given design and layout would give an attitudinal attenuation slightly higher than what would be obtained in reality. This would mean that, although a berm would be expected to result in a relatively small calculated attenuation, the benefit achieved in the minds of the people affected would be potentially greater. This is important because even a slight anticipated attenuation could be considered worthwhile as an overall effect.

PRIVACY CONSIDERATION

The attitudinal survey in the study area after the berms were constructed indicated that 68 percent of the respondents in tier A felt that they had experienced an increase in privacy in their neighborhood because of the sound berms. The majority of the responses indicating a positive "most significant effect of the sound berms" in tier A was related to both freeway noise and increased household privacy with some additional responses indicating just "increased household privacy" as a most significant effect. It can, therefore, be concluded that the increased household privacy is a major benefit to the residents in tier A who are, in fact, the households most affected by the freeway.

DESIGN CONSIDERATIONS

A series of photographs was taken at various points in the study area before and after the construction of the sound berms. A review of these photographs indicated that, after the berms were placed, the tops of the adjacent homes could be seen from the freeway but the direct line of sight for a person standing on his or her property was blocked from the freeway. Observations made from within the study area after the berms were placed indicated that the tops of heavy trucks and their exhaust systems were visible from the adjacent properties.

The result of the attitudinal survey revealed that 69 percent of the respondents in tier A and 49 percent of all respondents felt that the berm should have been constructed higher. Of these responses 70 percent in tier A and 65 percent in all tiers indicated that the berms should have been constructed 0.61-1.8 m (2-6 ft) higher. The computations done on calculated attenuations showed that this additional height would have increased attenuation by 2-4 additional decibels, resulting in the median attenuation of 8 dB(A) for the residents in the adjacent area.

In the design factors it appears that berms should be constructed with regard to the adjacent land use considering the height of development occupying that land, in order to separate the entire development from freeway sight. Also, reductions or breaks in the berm should be given careful consideration, as they adversely affect its overall usefulness.

CONCLUSIONS

A group of major conclusions can be drawn from this study. These conclusions are discussed in the following paragraphs.

1. A measured and calculated median attenuation of 5 dB(A) was obtained for the sound berms in this study; the range of attenuation was 1-10 dB(A).
2. The attitudinal responses related to the effect of sound berms on noise compared well with the measured levels of attenuation. However, it appeared that the perceived attenuations tended to be higher than measured values, indicating that people affected by sound berms judged the benefits to be greater than actually measured.
3. An important consideration in the location of sound barriers should be an increase in privacy for the adjacent land users. This was indicated in the attitudinal survey and should be given equal consideration when only minimum noise attenuation is anticipated from a proposed sound barrier, resulting in questionable justification for construction.
4. On existing freeways the cost of sound berms as a prime item of a construction contract appears to be

significantly high. However, if material is available from nearby freeway construction improvement work and the cost of material removal from the right-of-way is anticipated to be high, construction of sound berms appears to be a desirable highway policy.

5. Sound barriers should be designed and constructed with major consideration for the topography of the freeway and adjacent land, for the existing or planned development of the neighboring land, and for the effects of height and length of the barriers on anticipated results.

6. From the negative comments concerning berm construction it was concluded that sufficient public relations should be performed in the development stage of sound barriers to obtain sufficient information to properly locate the barriers and inform the public of anticipated results of the barriers.

REFERENCES

1. J. T. Broch. Acoustic Noise Measurements. Bruel and Kjaer, K. Larsen and Son, Soborg, Denmark, 2nd Ed., Jan. 1971.
2. M. B. Harmelink and J. J. Hajek. Performance Testing of Freeway Noise Barriers. Paper presented at the ASCE National Transportation Engineering Meeting, Milwaukee, July 17-21, 1972.
3. W. J. Galloway, W. E. Clark, and J. S. Kerrick. Highway Noise: Measurement, Simulation, and Mixed Reactions. NCHRP, Rept. 78, 1969.
4. C. G. Gordon, W. J. Galloway, B. K. Kugler, and D. L. Nelson. Highway Noise: A Design Guide for Highway Engineers. NCHRP, Rept. 117, 1971.
5. Fundamentals and Abatement of Highway Traffic Noise. National Highway Institute, Federal Highway Administration, Rept. FHWA-HHI-HEV-73-7976-1, June 1973.
6. N. R. Wienser. A Study of the Effects of Earthen Attenuation Devices in Reducing Noise and Improving Privacy in Neighborhoods Adjacent to Urban Freeways. College of Engineering, Marquette Univ., Milwaukee, 1974; NTIS, Springfield, VA, PB 244 053, 1974.

Publication of this paper sponsored by Committee on Geometric Design and Committee on Roadside Environment.

Abridgment

Hydraulic and Safety Characteristics of Selected Grate Inlets

P. H. Burgi, U.S. Bureau of Reclamation, Denver
D. E. Gober, U.S. Forest Service, Laramie

With the recent increase in the number of bicycles on our nation's highways and streets, there has been a corresponding increase in the number of bicycle accidents. Some of these accidents are related to highway grate inlets. The purpose of the comprehensive study summarized in this paper was to identify, develop, and analyze selected grate inlets that maximize hydraulic efficiency and bicycle safety.

Fifteen grate inlet designs were initially selected for consideration. They included seven steel-fabricated grates and eight cast grates.

The test program was conducted using two test facilities. The bicycle safety tests were conducted on an outdoor test site consisting of a 6.7-m (22-ft) wide, 152-m (500-ft) long abandoned roadway. A 2.44-m (8-ft) wide, 18.3-m (60-ft) long hydraulic test flume was constructed in the U.S. Bureau of Reclamation, Hydraulic Research Laboratory, and used as a test facility for the hydraulic efficiency tests.

ANALYSIS OF STRUCTURAL INTEGRITY

Figure 1 illustrates the basic grate inlet designs that were structurally analyzed and the reticuline grate that was not structurally analyzed because it is commercially available and the manufacturer's publications provide vehicle load tables based on AASHTO specifications.

The general-purpose computer program STR5 was used to perform the structural analysis of the selected grates. In some cases it was determined by a preliminary analysis that the bearing bars of the grate acted independently as simple supported beams. In those cases, a simple beam analysis was performed.

The grates tested have been code-named to standardize the names. The first symbol refers to the grate design (parallel bar grate P, curved vane grate CV, 45° or 30° tilt bar grate 45 or 30, and reticuline R). The second number is the nominal center-to-center longitudinal bar spacing. The last number is the nominal center-to-center transverse bar spacing. Therefore, the P-48-102 (P-1⅞-4) grate refers to a parallel bar grate with center-to-center spacing of the longitudinal bars of 48 mm (1⅞ in) and center-to-center spacing of the transverse bars of 102 mm (4 in).

ANALYSIS OF BICYCLE AND PEDESTRIAN SAFETY

Bicycle and pedestrian safety tests were performed on 11 grate inlets to preselect safe grate inlets for the hydraulic testing phase of the study. The grate size of 0.61 × 1.22 m (2 × 4 ft) was selected for use in the bicycle safety tests. Table 1 presents principal features of the grates evaluated in the test program and gives their bicycle safety rankings.

Two grates were tested in the hydraulic efficiency tests that were not tested in the bicycle safety tests. The curved vane grate CV-83-108 (CV-3¼-4¼) design was very similar to the 45-83-102 (45-3¼-4) grate, which satisfactorily passed the bicycle safety tests. The parallel bar grate with transverse spacers P-29 (P-1⅛) was tested independently for bicycle safety (1).

The transverse spacing of grate bars is a critical factor in bicycle safety performance. It is a more critical factor than whether the grate is of the reticuline, 45° tilt bar, curved vane, or parallel bar with

Figure 1. Basic grate designs.

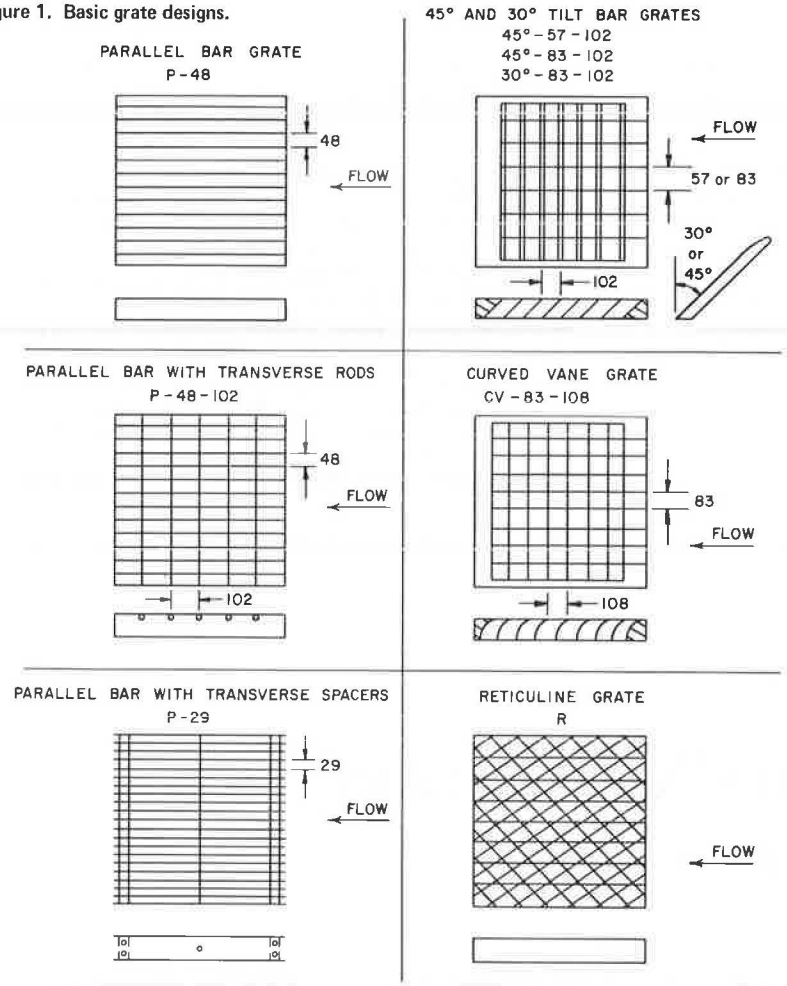

Table 1. Principal grate dimensions and bicycle safety ranking.

Type	Longitudinal Spacing[a] (mm)	Longitudinal Bar Width (mm)	Transverse Spacing[b] (mm)	Transverse Bar Width (mm)	Bicycle Safety Ranking
Reticuline	67[d]	6.4	127[c]	4.8	3
Parallel bar	48[d]	6.4	102	9.5 rod	2
	48[d]	6.4	152	9.5 rod	8
	48[d]	6.4	203	9.5 rod	11
	60[d]	6.4	102	9.5 rod	6
45° tilt-bar	57[e]	13	76	19	7
	57[e]	13	102	19	4-5
	57[e]	13	159	19	9
	83[e]	13	76	19	1
	83[e]	13	102	19	4-5
	83[e]	13	159	19	10

Note: 1 mm = 0.39 in.

[a]Center-to-center spacing of bars parallel to direction of flow.
[b]Center-to-center spacing of bars transverse to direction of flow.
[c]Center-to-center spacing of rivets, reticuline grate only.
[d]Fabricated steel grate.
[e]Grates made of white oak to simulate cast grates.

transverse rod type. The analysis suggests that deterioration in bicycle safety performance begins as transverse spacings are increased somewhat above 102 mm (4 in). Keeping the grates wet increased the chances of skidding.

TEST FACILITY AND EXPERIMENTAL APPROACH

To accurately investigate the hydraulic characteristics of grate inlets, the decision was made to use a full-scale test facility. The width of the roadbed selected for the test facility was 2.4 m (8 ft) including a 0.61-m (2-ft) gutter section and one-half of a 3.7-m (12-ft) traffic lane, generally considered the allowable width of flow spread. The test roadbed was 18.3 m (60 ft) long with the grate inlet test section located 12.2 m (40 ft) from the headbox. The facility was designed and constructed to accommodate the following test conditions: (a) longitudinal slopes, S_o = 0.5-13 percent; (b) cross slopes, 1/Z = 1:48-1:16; (c) maximum gutter flow, Q_T = 0.16 m^3/s (5.6 ft^3/s); and (d) Manning roughness factor, n = 0.016-0.017.

For each grate design, size, longitudinal slope, and cross slope, five different gutter flows were tested. The maximum gutter flow was limited by either the pump capacity of 0.16 m^3/s (5.6 ft^3/s) or width of spread limited to T′ = 2.3 m (7.5 ft). The minimum gutter flow was the flow that was completely captured by the grate inlet or provided a flow spread of T′ = 0.61 m (2 ft). The five data points obtained were sufficient to develop curves relating hydraulic efficiency (E = intercepted gutter flow/total gutter flow, $E = Q_i/Q_T$) to gutter flow (Q_T) and width of spread (T′) for each combination of longitudinal and cross slopes.

DISCUSSION OF TEST RESULTS

The preliminary structural analysis and bicycle-pedestrian analysis led to the selection of eight grate designs for the hydraulic tests. They included a steel-fabricated parallel bar grate that was not bicycle safe but provided an excellent standard for hydraulic efficiency with which to compare other grate inlet designs. Three

Table 2. Grate inlet classification.

Debris	Safety	Hydraulics		Composite Selection	
		Favorable Gutter Flow Conditions	Unfavorable Gutter Flow Conditions	Favorable Gutter Flow Conditions	Unfavorable Gutter Flow Conditions
Class I (high performance)					
CV - 83 - 108	P - 48 - 102	P - 48 - 102	CV - 83 - 108	P - 48 - 102	CV - 83 - 108
30 - 83 - 102	Reticuline	P - 29	P - 29	P - 29	P - 29
				Reticuline	
45 - 83 - 102	P - 29	Reticuline		45 - 83 - 102	
Class II (low performance)					
P - 48 - 102	45 - 83 - 102	CV - 83 - 108	45 - 83 - 102	CV - 83 - 108	45 - 83 - 102
45 - 57 - 102	45 - 57 - 102	45 - 83 - 102	P - 48 - 102	45 - 57 - 102	P - 48 - 102
Reticuline	CV - 83 - 108	45 - 57 - 102	45 - 57 - 102	30 - 83 - 102	45 - 57 - 102
P - 29	30 - 83 - 102	30 - 83 - 102	30 - 83 - 102		Reticuline
			Reticuline		30 - 83 - 102

other steel-fabricated grates were also tested: parallel bar grate with transverse rods at the surface, P-48-102 (P-1⅞-4); parallel bar grate with spacers, P-29 (P-1⅛); and a reticuline grate (R). Four cast grates were tested. They included two 45° tilt bar grates, 45-83-102 (45-3¼-4) and 45-57-102 (45-2¼-4); a 30° tilt bar grate, 30-83-102 (30-3¼-4); and a curved vane grate, CV-83-108 (CV-3¼-4¼) design. The test results are covered in detail elsewhere (2).

For a constant gutter flow, all the grates show some increase in hydraulic efficiency if the cross slope is held constant and the longitudinal slope is increased. At steeper longitudinal slopes, the same gutter flow occupies a smaller cross-sectional area; therefore, a greater percentage of the flow passes over the grate inlet. If no flow splashes completely across the grate, intercepted flow is greater and, hence, hydraulic efficiency is higher. All of the grate inlets, except the parallel bar and the curved vane grate, had splashing occurring under some flow conditions. The other six grates showed a decrease in hydraulic efficiency above a limiting longitudinal slope, related to grate design, size, and cross slope.

The seven bicycle-safe grate designs (discounting the parallel bar grate) can be classified in three hydraulic efficiency performance groups at the steeper longitudinal and cross slopes. The CV-83-108 (CV-3¼-4¼) and P-29 (P-1⅛) grates are consistently superior to the other bicycle-safe grates tested. The 0.61 × 1.22-m (2 × 4-ft) sizes of these two grates are within 3-4 percent of the parallel bar grate for the same test conditions.

At the other extreme, the reticuline grates generally rank last. At higher gutter flows with steep longitudinal and cross slopes, the reticuline grates usually had the lowest efficiency of the grates tested (for longitudinal slopes less than 3 percent, the reticuline grate is as efficient as the other grates). The remaining grates, the 45-57-102 (45 -2¼-4), the 45-83-102 (45 -3¼-4), P-48-102 (P-1⅞-4), and the 30-83-102 (30 -3¼-4), tend to have hydraulic efficiencies very close to each other. They rank somewhat better than the reticuline grates, but far below the CV-83-108 (CV-3¼-4¼) and the P-29 (P-1⅛) grates.

Tests to determine debris-handling capability showed a definite debris-handling advantage for grates with the 83-mm (3¼-in) longitudinal bar spacing over those with smaller longitudinal bar spacing.

SUMMARY AND CONCLUSIONS

In applying the three major test criteria for grate inlets, hydraulic efficiency, safety, and debris-handling ability, it is clear that the safety and debris-handling characteristics of a grate inlet are not as dependent on longitudinal slope, S_o, as the hydraulic characteristics. The hydraulic test results indicate that above certain longitudinal slopes, S_o, the hydraulic efficiency, E, of several grate inlets is adversely affected by the high-velocity flow striking the transverse bar members and splashing over the inlet. The specific longitudinal slopes depend on such variables as cross slope, 1/Z, gutter flow, Q_T, and grate length, L, but can be identified in two generalized categories as favorable and unfavorable gutter flow conditions.

Results of the debris tests indicate that the wider the longitudinal bar spacing, the better the debris-handling ability of a grate inlet.

The bicycle safety tests suggest that the deterioration in bicycle safety performance begins as transverse bar spacing is increased above 102 mm (4 in). In addition, grates having large, nearly square openings of 83 × 102 mm (3¼ × 4 in) are also judged to pose some potential danger to pedestrians.

Table 2 is a summary of the test results for debris, safety, and hydraulic efficiency considerations. An attempt has been made to classify the selected grates into high- and low-performance groups for the three major areas of consideration. The high-performance (class I) grates for bicycle safety are low performers (class II) with respect to debris-handling capabilities. For favorable gutter flow conditions (no splashing), the class I grates are slightly more efficient (less than 6 percent) than the class II grates. For the unfavorable gutter flow conditions, hydraulic efficiencies vary as much as 34 percent between class I and class II grates for a 0.61-m (2-ft) grate length and 15 percent for a 1.22-m (4-ft) grate length. The composite selection in the table is our overall classification of the selected grates tested.

ACKNOWLEDGMENTS

The study was conducted by the U.S. Bureau of Reclamation at their Engineering and Research Center, Denver, Colorado, for the Federal Highway Administration. We would like to acknowledge the help of Daniel Smith of DeLeuw, Cather and Company in directing the bicycle-pedestrian safety phase of the study.

The project was monitored by D. C. Woo, Contract Manager, Environmental Design and Control Division, Federal Highway Administration.

REFERENCES

1. Evaluation of Three Types of Catch Basin Grates for Streets With Bicycle Traffic. Los Angeles County Flood Control District, Systems and Standards Group, Design Division, Jan. 1973.
2. P. H. Burgi and D. E. Gober. Bicycle-Safe Grate Inlets Study. Vol. 1: Hydraulic and Safety Characteristics of Selected Grate Inlets on Continuous Grades. Federal Highway Administration, FHWA-RD-77-24, June 1977.

Publication of this paper sponsored by Committee on Hydrology, Hydraulics, and Water Quality.

Abridgment

Determining Design Flows for Culverts and Bridges on Ungauged Streams: A Watershed Rationale

John F. Orsborn, Department of Civil and Environmental Engineering,
Washington State University, Pullman

The determination of the characteristic low, average, and flood flows of ungauged perennial streams is a continuing problem for hydrologists. The acquisition of streamflow records has improved the reliability of flows at or near gauging sites, but at a distant site, say just upstream of the first major tributary, we rapidly lose our prediction confidence.

Methods for predicting ungauged streamflows come in three categories of input-output models: deterministic, rational, and regression. Numerous references that describe their development and use are available (1, 2, 3). Characteristic flows are considered to be "average" low, annual, and flood flows. Knowledge of these flows and their variability at an ungauged site, coupled with the duration curve characteristics at gauges in the province, makes it possible to create a flow duration history for the ungauged site.

The basic concept behind this geohydrologic watershed rationale is that the watershed integrates precipitation and yields flows with certain statistical characteristics. Further, the outflows form channels with geometric characteristics, and the kinetic energy (velocity), channel width, and channel depth can be related to the flow in the channel (4). Thus, in a total geohydrologic analysis of a watershed one should be able to relate flows to watershed characteristics and flows to channel characteristics and thus determine channel characteristics from basin characteristics and vice versa. If these concepts are physically correct, there should be little scale effect between large and small watersheds within the dominant range of sizes that generate perennial streams requiring culverts or bridges. Application of similar concepts to intermittent streams is under investigation.

The three characteristic flows of perennial streams considered here are

1. Q7L2: the 7-day average low flow with a 2-year recurrence interval,
2. QAA: the average annual flow, and
3. QF2P: the peak flood with a 2-year recurrence interval.

These three flows are representative statistical and arithmetic averages and are quite stable over periods of 30-50 years. In addition, the 20-year low flow Q7L20 can be determined and coupled with Q7L2 to yield the low flow recurrence interval graph. When the 50-year flood flow QF50P is determined, a flood recurrence graph can be developed. These five flows, plus the deviation of QAA, give a band of duration curves that describes the usual history of flows at a site.

The three average flows—Q7L2, QAA, and QF2P—will be used to describe watershed parameter relationships. Details of the procedures for estimating these ungauged flows are presented elsewhere (5, 6, 7). The remainder of this paper covers five topics: (a) watershed parameters and their analogies used in streamflow estimation; (b) relationships between the characteristic flows Q7L2, QAA, and QF2P; (c) correlations between watershed parameters and characteristic flows; (d) channel width, depth, velocity, and discharge relationships; and (e) the combination of c and d to yield channel characteristics in terms of watershed parameters.

WATERSHED PARAMETERS AND THEIR ANALOGIES IN STREAMFLOW ESTIMATION

The geohydrologic output:output watershed rationale for streamflow estimation uses four primary watershed linear geometric characteristics. These are summarized in Figure 1 as

1. LS: length of perennial streams of various orders where LT is the total,
2. A: drainage basin (watershed area),
3. LB: basin axis length, and
4. H: basin relief, or differential elevation between the headwaters and the outlet (the gauged or ungauged flow site).

The stream length (LS) is analogous to the linear interface between the groundwater supply and the stream that the aquifer supplies. Drainage area (A) is analogous to the watershed's ability to capture precipitation. The axis length of the basin is combined with the derived mean basin width (WB = A/LB) to give a watershed aspect ratio of LB/WB. This aspect ratio is analogous to the time of concentration when estimating floods. The basin relief (H) represents the driving force, or potential energy, for flow from the watershed. Precipitation is directly related to elevation (relief) in some regions.

RELATIONSHIPS AMONG CHARACTERISTIC FLOWS

A study of low, average, and flood flows in Washington, Oregon, and Idaho (8) has shown that there is a fundamental 1, 2, 3 power relationship between the three characteristic flows of

$$Q7L2 = C(QAA^3/QF2P^2) \quad (1)$$

The coefficient (C) in Equation 1 varies between hydrologic provinces, but for natural flows and no severe geologic anomalies the coefficient is very consistent within provinces. For the sample area of southwest Washington (8) shown in Figure 2, the coefficient in the form of Equation 1 has an average value of about 10.0; the minimum theoretical value is 1.0.

Figure 1. Watershed parameters and their flow analogies.

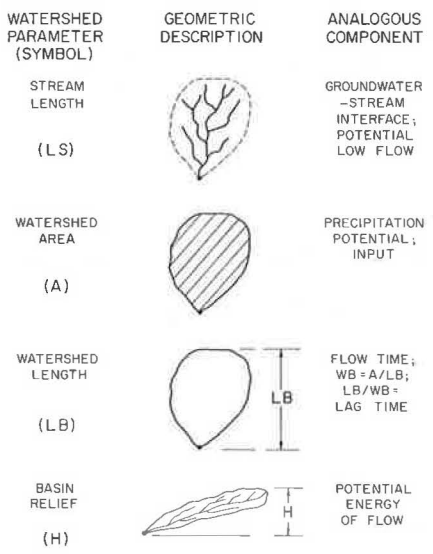

Figure 2. Average flood related to average annual and low flows for data sample from southwestern Washington.

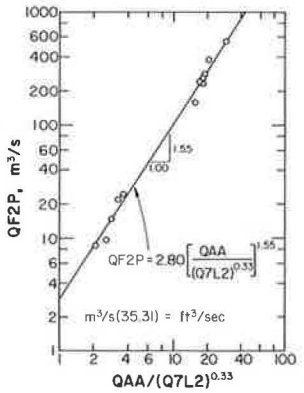

CORRELATIONS BETWEEN WATERSHED PARAMETERS AND CHARACTERISTIC FLOWS

The low, average, and flood flows used in Equation 1 were estimated for ungauged streams by using correlations developed from the gauged watersheds in the hydrologic province. Examples are drawn from a study of the Lake Coeur d'Alene watershed in northern Idaho (9).

Low Flows

The best combination of watershed characteristics (best basin parameters) for making the first estimate of low flows in the Coeur d'Alene province is $(LT)(H)^{0.5}$. For the average low flow (the coefficient 23.30 is 0.32 in EGS units)

$$Q7L2 = 23.35[LT(H)^{0.5}] \quad (2)$$

Average Annual Flows

Provincial relationships between average annual streamflow records and the average annual volume of precipitation are highly correlated. In equation form

$$QAA = C(P \cdot A) \quad (3)$$

where C is a coefficient that varies as a function of climatic region and is larger for areas with greater values of P, P is the average annual precipitation, and A is the watershed drainage area.

Flood Flows

Within hydrologic provinces, average annual floods have been found to be a consistent multiple of the average annual flow (10). In equation form,

$$QF2P = C(QAA) \quad (4)$$

In many provinces a stronger relationship has been found between QF2 and QAA raised to some power

$$QF2P = C(QAA)^n \quad (5)$$

For northern Idaho watersheds (9),

$$QF2P^2 = 1687(QAA)^{1.7} \quad (6)$$

Noting the similarity between Equations 1 and 6 and rearranging Equation 1 yield

$$QF2P = C(QAA^3/Q7L2)^{0.5} \quad (7)$$

For example, the results of the Coeur d'Alene study (9) show, as in Equation 1, that

$$Q7L2 = 8.0QAA^3/QF2P^2 \quad (8)$$

This may be combined with Equation 2, $Q7L2 = 23.35[(LT)(H)^{0.5}]$, and with Equation 3

$$QAA = 1.85(10^{-4})(P \cdot A) \quad (9)$$

Also, total stream length (LT) is related to drainage area (A) by

$$LT = 2.08(A)^{0.98} \quad (10)$$

Substituting Equations 2 and 9 into Equation 8 and rearranging give

$$23.35[LT(H)^{0.5}] = [1.85^3(10^{-4})^3(P \cdot A)^3]/QF2P^2 \quad (11)$$

$$QF2P^2 = 2.71[(P \cdot A)^3/LT(H)^{0.5}](10^{-9}) \quad (12)$$

Substituting Equation 10 into Equation 12, the 2-year peak flood is

$$QF2P = 3.60(P^{1.50}A/H^{0.25})(10^{-5}) \quad (13)$$

The combination of terms on the right side of Equation 12, $(P \cdot A)/[LT(H)]$, tends to be a constant within hydrologic provinces. Thus, after a provincial correlation is developed, average annual precipitation can be determined for an ungauged watershed by measuring drainage area, relief, and total stream length.

CHANNEL WIDTH, CHANNEL DEPTH, VELOCITY, AND FLOW RELATIONSHIPS

Numerous investigators have demonstrated that channel width (W), depth (D), and mean velocity (V) each can be expressed in terms of average annual flow (QAA) or other flows up to bankfull conditions (4).

$$W = a(QAA)^b \quad (14)$$

Table 1. Width, depth, and velocity related to discharge in typical stream channels, Little Brush Creek, Utah.

Station No.	Width Equation (m)	Depth Equation (m)	Velocity Equation (m/s)
1[a]	$W = 1.22(Q)^{0.65}$	$D = 0.304(Q)^{0.30}$	$V = 1.480(Q)^{0.16}$
2	$W = 27.09(Q)^{0.10}$	$D = 0.082(Q)^{0.52}$	$V = 0.440(Q)^{0.38}$
3	$W = 59.13(Q)^{0.04}$	$D = 0.092(Q)^{0.59}$	$V = 0.184(Q)^{0.37}$

Notes: 1 m = 3.3 ft.
Data derived from Chrostowski (11).
[a]Exponents do not total 1.00 at station 1 because of a sharp change in section shape from triangular to rectangular between stage 1 and stage 0.

Table 2. Comparison of predicted and measured channel widths based on annual precipitation volume and relief.

Station No.	State	Stream	Channel Width (WAC) (m) Predicted: Equation 21 or 22	Predicted: Equation 26	Measured[a]
06 0195	Montana	Ruby	17	14	13
0330		Boulder	13	10	13
0375		Madison	29	21 (34)	27
0485		Bridger	8	5[b] (10)[c]	7
0615		Prickley Pear	9	7	7
0735		Dearborn	20	12 (20)	21
0770		Sheep	8	7	8
0905		Belt	18	16 (21)	19
1185		Musselshell	12	10 (15)	14
2890	Wyoming	Little Bighorn	14	12	15
3145		N.F. Crazy Woman	6	5	8
6160	Colorado	N.F. Michigan	5	5	6
7165		Clear	13	13	18

Notes: 1 m = 3.3 ft.
Data derived from Hedman and Kastner (12).
[a]From Hedman and Kastner (12).
[b]Small basin; $(H)^{0.16}$ is probably less than 1.0.
[c]If P = 69.3 cm (27.3 in) is used as published by SCS rather than 38.1 cm (15.0 in) of Weather Bureau as used elsewhere (12), then the value of WAC in parentheses is given by Equation 26 in column 4.

$$D = c(QAA)^d \quad (15)$$

$$V = e(QAA)^f \quad (16)$$

Exponents b, d, and f must total 1.0, and the multiple of coefficients a, c, and e must be 1.0.

Channel shapes can range only between the extremes of perfectly triangular and rectangular, assuming various combinations of rectangular, triangular, and trapezoidal shapes depending on the stage of flow between low and bankfull conditions. Some width, depth, and velocity relationships for typical channels are presented as a function of streamflow in Table 1.

CHANNEL CHARACTERISTICS, FLOOD FLOW, AND WATERSHED PARAMETERS

A series of expressions for average annual flows and floods for streams in Montana, Wyoming, and Colorado has been developed (12). One such equation for average annual flow is

$$Q_A = 37.7 W_{AC}^{2.00} \quad (17)$$

where W_{AC} is the active channel width that carries bankfull and lesser flows. In terminology used thus far

$$QAA = 0.170(WAC)^2 \quad (18)$$

where QAA is Q_A in cubic meters per second and WAC is in meters.

Using Equation 3 and substituting the data from Hedman and Kastner (12, Table 1)

$$QAA = 0.95(P \cdot A)(10^{-4}) \quad (19)$$

$$QAA = 1.85(P \cdot A)(10^{-4}) \quad (20)$$

Setting Equations 18 and 19 and 18 and 20 equal to each other, the following expressions emerge for active channel widths in the eastern Rocky mountains:

$$WAC_{0.95} = 2.36(P \cdot A)^{0.5}(10^{-2}) \quad (21)$$

$$WAC_{1.85} = 3.30(P \cdot A)^{0.5}(10^{-2}) \quad (22)$$

where 0.95 and 1.85 are runoff coefficients in Equations 19 and 20.

One flood equation (12) in standard units is

$$Q_2 = 0.87 W_{AC}^{1.579} A^{0.162} \quad (23)$$

and in metric units is

$$QF2P = 5.52(WAC)^{1.58}(A)^{0.16} \quad (24)$$

By setting Equations 24 and 13 equal to each other and solving for WAC,

$$5.52(WAC)^{1.58}(A)^{0.16} = 3.60(P)^{1.50}(A)/(H)^{0.25}(10^{-5}) \quad (25)$$

$$WAC = 5.22\{[(P)^{0.94}(A)^{0.53}]/(H)^{0.16}\}(10^{-4}) \quad (26)$$

Applying Equations 21, 22, and 26, widths of the active channels were predicted for the set of stations in Table 2 by two equations and compared with the measured widths from Hedman and Kastner (12), where relief (H) was not given but $(H)^{0.16} \rightarrow 1.0 \pm 10$ percent within normal ranges.

This brief example derived for Orsborn and Deane (13) has shown how relationships between basin characteristics and streamflow, and channel characteristics and streamflow, can be combined to predict channel characteristics in terms of basin characteristics. It therefore completes the development of the two tenets basic to the watershed rationale: the integrative effects of the watershed on outflows and the channel characteristics that result from those flows.

SUMMARY

A watershed rationale that assumes that outflows are integrated by the watershed to yield floods and low flows with certain provincial correlations has been explored. The provincial correlations use combinations of various watershed geomorphic characteristics, including stream length and watershed area, length, and relief. A 1, 2, 3 power relationship among average low, flood, and annual flows opens new opportunities for flood flow predictions.

The possibility of being able to predict flood flows in terms of channel characteristics has been presented. To complete the integrated watershed rationale, channel characteristics have been predicted in terms of watershed characteristics by setting two flood flow equations from different mountainous regions equal to each other. The only input term used in the analysis is the average annual watershed precipitation. Floods have been shown to be strongly dependent on watershed area, relief, and stream length—those geomorphic parameters that are analogous to certain physical hydrologic processes and that make the integrated watershed rationale possible.

REFERENCES

1. F. F. Snyder. Synthetic Flood Frequency. Proc., ASCE, Journal of Hydraulics Division, Vol. 84,

No. HY5, Paper No. 1808, Oct. 1958.
2. D. M. Thomas and M. A. Benson. Generalization of Streamflow Characteristics From Drainage-Basin Characteristics. U.S. Geological Survey, Water Supply Paper 1975, 1970.
3. B. O. Benn. Regional Planning Potential of Deterministic Hydrologic Simulation Models. Proc., Seminar on Hydrologic Aspects of Project Planning, HEC, Corps of Engineers, Davis, CA, March 7-9, 1972, pp. 13-26.
4. L. B. Leopold and T. Maddock, Jr. The Hydraulic Geometry of Stream Channels and Some Physiographic Implications. U.S. Geological Survey Professional Paper 252, 1953.
5. J. F. Orsborn. A Geomorphic Method for Estimating Low Flows. ASCE, Annual Meeting, Denver, Nov. 3-7, 1975.
6. J. F. Orsborn and M. N. Sood. Technical Supplement to the Hydrographic Atlas. Washington Department of Ecology, State Water Program, Lewis River Basin Study Area, 1973.
7. H. C. Riggs. The Relation of Discharge to Drainage Area in the Rappahannock River Basin, Virginia. U.S. Geological Survey, Professional Paper 501B, 1964, pp. B165-B168.
8. J. F. Orsborn and others. Relationships Between Low, Average and Flood Flows in the Pacific Northwest. Department of Civil and Environmental Engineering, Washington State Univ., Pullman, OWRT Project A-074-WASH, 1975.
9. J. F. Orsborn and others. Surface Water Resources of the Coeur d'Alene, St. Joe and St. Maries Rivers in Northern Idaho. In Preliminary Investigation of the Water Resources of the Northern Part of the Coeur d'Alene Indian Reservation, Department of Civil and Environmental Engineering, Washington State Univ., Pullman, 1975, pp. 160-197.
10. H. Cönturk. Mean Discharge as an Index to Mean Maximum Discharge. Proc., Leningrad Symposium on Floods and Their Computation, IASH-UNESCO-WHO, Vol. 2, 1967, pp. 826-833.
11. H. P. Chrostowski. Stream Habitat Studies on the Uinta and Ashley National Forests. U.S. Forest Service, Intermountain Region, Ogden, UT, 1972.
12. E. R. Hedman and W. M. Kastner. Progress Report on Streamflow Characteristics as Related to Channel Geometry of Streams in the Missouri River Basin. U.S. Geological Survey, Open File Rept., Feb. 1974.
13. J. F. Orsborn and F. D. Deane. Investigation Into Methods for Developing a Physical Analysis for Evaluating Instream Flow Needs. Department of Civil and Environmental Engineering, Washington State Univ., Pullman, OWRT Project A-084-WASH Completion Rept., Sept. 15, 1976.

Publication of this paper sponsored by Committee on Hydrology, Hydraulics, and Water Quality.

Rainfall Intensity-Duration-Frequency Curves Developed From (not by) Computer Output

Brian M. Reich, Pima County Flood Control District, Tucson

Thirty-two years of maxima observed at Tucson International Airport from the National Oceanic and Atmospheric Administration's recording raingage are used to prepare a sheet of intensity-duration-frequency curves commonly used in the design of storm drainage for small urban areas. The example is employed to stress the need for examining computer printouts of mathematical statistical analysis of the rains and their logarithms by plotting data on four types of probability paper. Stress is laid on dangers of blindly extrapolating a mathematical distribution that does not fit recorded amounts for the long return periods in which engineers are usually interested. Misapplication of scales involving a logarithmic transformation are discussed. The fact that longer durations may require a different type of frequency paper than do shorter durations is illustrated and rationalized on the basis of the physical process. Internal compatibility of results for 2-, 5-, 10-, 50-, and 100-year estimates of 5-, 10-, 20-, 30-, 45-, 60-, 120-, and 180-min rainfalls is preserved when examining a tabular array of as many as five frequency analyses on one of these 48 cells.

Intensity-duration-frequency (IDF) curves are a long-standing tool of the storm-drain designer (1, 2, 3). A U.S. Weather Bureau publication (4) gave depths of maximum rainfall for various durations and return periods on many separate maps. Since then, recording gages have provided additional data on rainstorms, often more than doubling record lengths at newer sites.

Local governments and consulting engineers may wish to prepare their own intensity-duration-frequency curves, like Figure 1, from their most up-to-date gage records. The purpose of this paper is to discuss topics that an engineer must consider while preparing such design curves.

There is an urgent need for engineers to gain at least a "feel" for statistical techniques. The availability of canned digital computer programs to fit preselected statistical distributions places the responsibility on the user for testing the validity of those automated analyses with respect to his or her particular data or engineering application. In outlining various means for exercising necessary discretion, this paper will refer to common statistical terms, concepts, and equations. They will be introduced in an informal, intuitive vein. Readers desiring additional pragmatic explanations of these extreme value statistics may wish to study Magnitude and Frequency of Floods (5). That 50-page review of terms and methods also contains complete tables needed in computation and various graph papers needed in plotting extreme rainfall data. Two excellent texts (6, 7) were recently published for engineers with deeper and wider interests in statistics.

Figure 1. Rainfall IDF curves from U.S. Weather Service recording gage, Tucson.

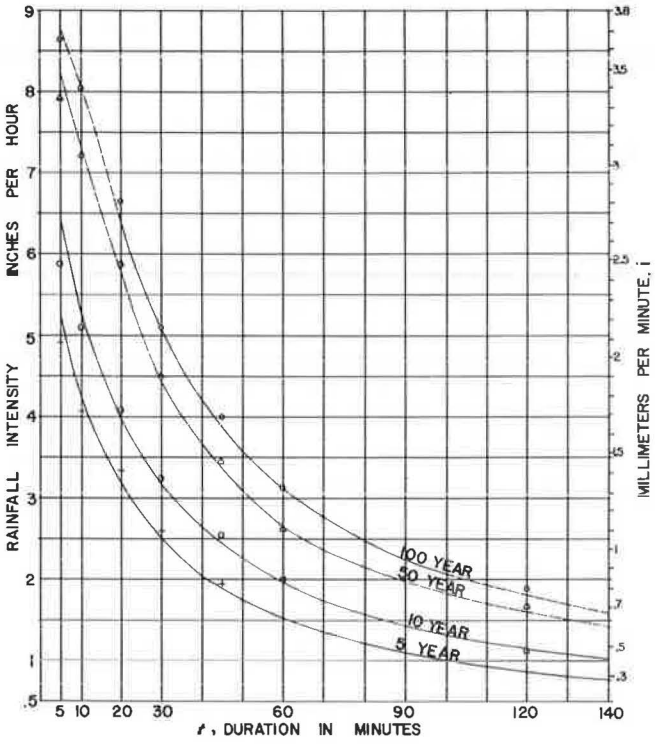

Table 1. Maximum rainfalls of various duration for each year at the Tucson Airport U.S. Weather Service recording gage.

	Maximum Rainfall (mm)							
	Duration of Maxima (min)							
Date[a]	5	10	20	30	45	60	120	180
9/24/1943	14.0	26.7	47.5	57.4	59.2	59.7	62.5	64.5
9/15/1944	10.2	15.2	22.9	26.4	26.9	27.2	30.0	31.0
7/27/1945	6.9	10.2	30.0	39.4	46.7	47.5	51.8	54.1
7/17/1946	9.4	13.5	19.6	21.1	21.3	24.1	26.9	26.9
8/8/1947	4.1	6.1	9.7	14.2	15.2	18.3	18.3	18.3
7/24/1948	14.0	23.6	34.0	40.1	45.0	46.2	47.0	47.5
8/8/1949	8.4	11.7	16.0	17.0	18.0	21.8	27.7	32.8
9/7/1950	8.1	12.2	17.3	19.3	21.1	21.1	24.4	26.7
8/2/1951	5.6	9.1	13.2	15.2	16.5	16.8	17.0	17.0
7/5/1952	9.4	12.2	22.1	23.9	25.1	25.4	25.7	25.7
7/29/1953	5.1	7.6	13.0	17.0	18.0	18.3	18.5	18.5
6/24/1954	9.9	15.7	26.7	30.2	30.5	30.5	31.5	32.0
8/3/1955	17.5	30.7	48.0	53.1	55.9	56.4	57.2	57.9
8/12/1956	7.4	10.2	11.7	11.7	17.0	18.0	18.5	18.5
8/3/1957	5.6	8.6	11.9	14.2	15.7	16.0	19.1	25.4
7/29/1958	10.7	18.8	29.0	34.5	38.9	42.2	68.8	79.2
7/3/1959	11.9	17.0	22.9	29.7	33.8	34.3	34.3	34.3
8/21/1960	4.8	7.6	9.4	10.7	11.7	12.2	12.4	12.4
8/22/1961	11.7	20.8	35.6	41.7	52.8	56.4	59.4	62.2
9/26/1962	3.6	5.1	10.2	11.9	14.2	15.7	17.5	17.5
9/4/1963	6.6	11.2	17.0	19.1	19.3	19.6	19.6	19.6
7/24/1964	11.4	17.5	19.8	22.9	25.9	28.7	45.0	45.2
7/25/1965	5.6	10.2	15.5	16.3	16.5	16.8	18.3	18.3
7/24/1966	7.6	13.0	17.5	22.1	26.2	28.2	34.5	35.1
7/29/1967	5.3	7.4	9.9	13.0	13.7	13.7	15.7	16.0
7/16/1968	7.1	8.4	11.7	11.9	12.2	14.0	14.7	15.0
8/1/1969	6.4	11.4	14.0	14.0	15.0	16.8	16.8	16.8
10/2/1970	8.1	15.2	29.0	29.7	29.7	30.5	30.5	40.9
8/12/1971	8.4	12.4	14.5	14.7	15.2	15.7	18.0	20.6
7/16/1972	10.2	14.0	25.1	34.0	36.8	37.6	39.4	39.4
8/23/1973	3.8	5.6	5.8	7.4	7.9	7.9	7.9	11.4
7/7/1974	9.4	11.4	21.3	25.7	26.9	27.9	30.7	31.8

Note: 1 mm = 0.039 in.

[a]Date refers to largest rainfall with shortest duration for that year. Maximum of longest duration often fell on a different day.

Figure 2. Pluviograph showing temporal variation of rainfall intensity within a convective storm.

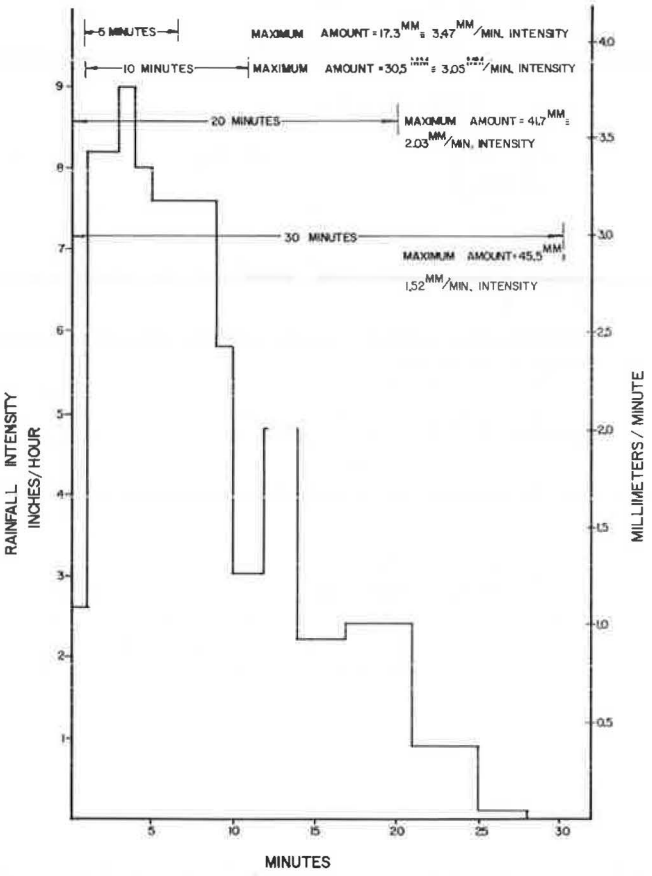

With a view to side-stepping a dry discourse on probability theory and the many mathematical constraints on its application, I have adopted a "how-to" format here. An example of deriving IDF curves for Tucson is pursued as a setting for introducing discussions on the various decisions.

EXAMINING THE DATA

The speed of an electronic computer may stimulate the impulse to keypunch the data. After running the cards through one of the readily available statistical programs, such as the Water Resources Council's (8) log-Pearson Type III package, the engineer can look at the printout to see what, say, the 100-year value "is". However, this neglects one of our best resources, observed measurements. In addition to revealing erroneous entries, examination of raw data can provide useful clues to understanding the physical process of interest.

Origins of the Data

Table 1 presents the information on which the Tucson analysis was based. To eliminate any ambiguity, Figure 2 has been developed to illustrate where tabulated rainfall amounts typically come from.

In this sample storm, the largest amount of rain in any continuous 5-min period was the 17.3 mm (0.68 in) that fell in the second, third, fourth, fifth, and sixth minutes. If this had been the largest 5-min amount in one calendar year it would have been published by the National Weather Service and entered in Table 1. Fur-

thermore, the maximum 10-min amount for the year can fall during the same rainstorm. The maximum rain for a longer duration, say, 20 min in the example of Figure 1, can also begin at a different time than that for 5 min.

Annual maximum amounts recorded in Table 1 for long durations such as 180 or 120 min can occur on different days or even in other seasons than that year's very short-duration extremes.

Unfortunately, digital recorders, which only punch their paper tape every 15 min, have recently been replacing many pen-and-chart recording raingages. The high intensities of very short duration will no longer be recorded, and underestimation will be accentuated by the random asynchrony between clock time and pulses of heavy rain.

Before 1935 the U.S. Weather Bureau analyzed tipping-bucket charts from first-order stations onto "excessive precipitation" forms. The latter quantity was defined as any portion of storm rainfall whose intensity exceeds 0.25 mm/min (0.01 in/min) with a threshold of 5.08 mm (0.20 in) of storm total. Even in the humid regions of the United States such storms have generally high-intensity rainfalls lasting 2 h or less. After 1935 the format was changed so that the most intense period of a storm was listed first, followed by its next most intense period, followed by its next, until the entire period of excessive precipitation was accumulated. An engineer fortunate enough to be working with records that go back so far should be aware of the difference.

Sampling Error

Returning to the real Tucson data in Table 1, we first observe that the highest values for short durations occurred in 1955. They were 50 percent greater than any extreme occurring in the subsequent 20 years. The second highest values had been encountered in the first year of recording, 12 years before 1955.

It is easy to realize how drastic the influence would be on the mean, or on other statistical computations, if one began the observations one year later. This should force us to see that even a 30-year record could, by chance, miss the high values that are of great significance to designs for 100-year or even 25-year floods.

These obvious comments derive from the statistical notion of sampling error, which simply states that any finite record length is merely a sample of a hypothetically infinite "population" of values. The mean of the population, μ, will never be known; all we can do is estimate it by the sample mean, $\overline{X}$. Greek symbols are reserved for population values, while Roman symbols are used for variables comprising samples, like X, and sample estimates derived from them.

The mathematical statistician will use population parameters when writing equations to describe, say, the distribution of 5-min annual maximum rainfalls throughout the possible size range of this variable. The applied statistician at best will only be able to substitute a sample estimate for each parameter needed in the theoretical equation. Some parameters or statistics are estimated fairly well from a sample; others are not. For example, if we only had the latest 16 years of this 5-min rainfall maximum, our estimate of the mean would be 7.62 mm (0.300 in). Had our father used only the first 16 years, his sample estimate would have been 9.12 mm (0.359 in), almost 20 percent greater than ours. The 32 years of data give 8.38 mm (0.330 in), which is a better estimate of the mean, but the population mean, μ, remains ellusive.

Plotting the Data

The human mind is limited in its ability to digest a column of numbers and can be greatly aided by a graphic display of the same information (see Figure 3). If points lie approximately on a straight line, then a straight line should be fitted through them by eye, and so labeled. In this way one may estimate a longer return period rain on the basis of many observations rather than simply on the largest rain recorded so far. Extrapolation is strictly justified only if the plotted set of data points displays no systematic deviation from a line. Implicit is the assumption that the distribution of these rainfall values follows the mathematical equation used in generating this particular type of probability paper. If the data exhibit a distinct curve away from the line or a marked s-shape, analysis with this type of paper or corresponding mathematical equation should be abandoned. Different types of probability paper should be tried until approximate linearity is achieved (5).

The horizontal placement of each point is achieved by assigning a rank m to each value in a list of the N observations rearranged from largest (m = 1) to smallest (m = N). These ranks enable us to assign a P_e value to each data point according to a plotting position formula. When using extreme value paper, sometimes called Gumbel for the man who introduced this statistical distribution in the United States, the best plotting position was shown by Gringorten (9) to be approximately

$$P_e = (m - 0.44)/(N + 0.12) \quad (1)$$

P_e is the probability that a rainfall equal to or larger than the specified number of millimeters will occur in one year. The return period in years for such an extreme is

$$T = 1/P_e \quad (2)$$

This cumulative probability, P_e, appears as the axis of Figure 3. It is seen to have a value of 0.01 toward the right. Commercially available paper may have high probability values, like 0.99, on the right that decrease toward the left. In that case, the numbers correspond to the probability of nonoccurrence,

$$P_n = 1 - P_e \quad (3)$$

Mathematically Fitting a Line

A generalized formula for hydrologic frequency analysis is

$$X = \overline{X} + K s_X \quad (4)$$

in which the mean is

$$\overline{X} = \Sigma X/N \quad (5)$$

and the standard deviation is

$$s_X = [(X - \overline{X})^2/(N - 1)]^{1/2} \quad (6)$$

Both $\overline{X}$ and s_X can be obtained from the series of annual maxima. K is the frequency factor that depends on the length of record used to estimate $\overline{X}$ and s_X, as well as on the probability paper selected, whose capital initial is subscripted. Table 2 gives K_ϵ for use when the plot of data exhibits satisfactory linearity on extreme value

Figure 3. Plot of 1943 through 1974 annual maximum series of 5-min rainfall on EV probability paper.

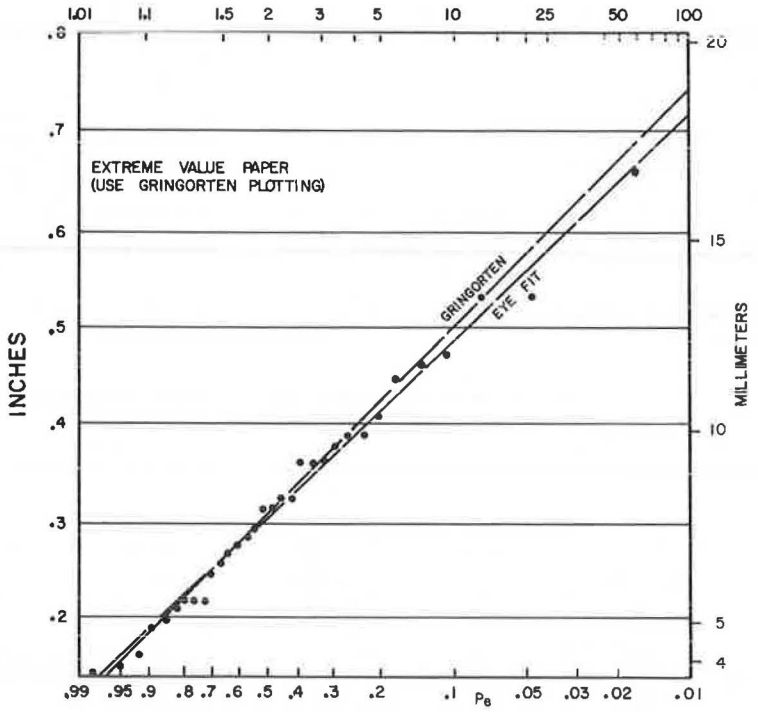

Table 2. Flood frequency factor (K_E) for extreme value line through Gringorten plotting.

Return Period	Frequency: Recording Length (years) 15	20	30	50	100	200
1.111	-1.167	-1.154	-1.140	-1.127	-1.116	-1.110
2	-0.155	-0.158	-0.160	-0.162	-0.163	-0.163
2.33	0.023	0.018	0.013	0.009	0.005	0.004
10	1.431	1.404	1.376	1.352	1.332	1.320
50	2.832	2.775	2.724	2.680	2.643	2.622
100	3.411	3.354	3.294	3.242	3.197	3.172
200	3.997	3.931	3.862	3.801	3.750	3.720
500	4.771	4.693	4.611	4.539	4.479	4.443

paper (see Figure 3). Earlier published tables had assumed Gumbel's mathematical fitting through data plotted according to the Weibull formula

$$P_e = m/(N + 1) \quad (7)$$

which has been in popular use for normal and log-normal paper as well. After this Tucson study a compromise formula

$$P_e = (m - 0.4)/(N + 0.2) \quad (8)$$

has been shown (10) mathematically to suit all four flood frequency papers considered here.

Application of Table 2 and Chow's Equation 4 to our 32 years of 5-min annual maximum rainfalls is simple. The 100-year estimate becomes

$$X_{100\,yr} = \bar{X} + 3.284 s_X = 8.374 + 3.284(3.251) = 19.051 \text{ mm} \quad (9)$$

The mean and standard deviation, s_x, can be obtained from pocket calculators. Similarly,

$$X_{2.33\,yr} = 8.374 + 0.012(3.251) = 8.413 \text{ mm} \quad (10)$$

This is virtually equal to the mean of the series of annual maxima, $\bar{X} = 8.382$. The equality would be perfect for an infinitely long theoretical population. Computation of a third point with Equation 4 and Table 2 should verify the mathematical straight line (Gringorten) in Figure 3.

Attention should be drawn to the fact that the mathematically fitted extreme value line results from substituting $\bar{X}$ and s_x into Equation 4. It is simple to program a computer to print out estimated rain with 25-, 100-, or even 500-year return periods. The simple computer did not, however, examine a plotted data for linearity. If that criterion is violated, the computer output is misleading; that is, errors would result from using the wrong model.

Other Probability Papers

The extreme value distribution was introduced because it has long been used by the U.S. Weather Service in analyzing short-duration rainfall maxima. They have just produced maps (11) for 5- through 60-min rains for the 37 eastern states from mathematically fitting this distribution, which has the synonym Fisher-Tippett Type I. Their analysis comes close to the application of Equation 4, without the influence of Gringorten's theory. Vast amounts of hourly data were analyzed from about 1900 stations with 25 years of data, and minute-by-minute examinations were made for an additional 200 stations averaging 60 years' record length.

For such short durations there is also a theoretical justification for applying the EV, or Gumbel, distribution. This will be discussed later with respect to the Tucson data, where Figure 3 shows how close the 5-min annual series plots to a straight line. The Gringorten mathematical fit is also seen to closely approximate my own eye fit.

Local preparation of IDF curves will usually involve

frequency analysis of only one raingage, so the engineer will be able to rapidly analyze the data graphically and with different types of probability distributions. Moreover, the search for IDF curves often necessitates the frequency analysis of rains for such long durations that the theoretical justification for the EV distribution is no longer valid. Figure 4 shows how systematic nonlinearity of plotted 180-min rainfall maxima shows the invalidity of extrapolating a Gringorten line, or use of Gumbel-type equations. It thus behooves an investigator to try other statistical or probability distributions that may suit those data better. The simple way to achieve this is to plot the annual series on different probability papers.

Log-extreme value paper is seen in Figure 5 to remove the curved toe exhibited by points with P_e greater than 0.2 on Figure 4. The horizontal grid of log-extreme value paper is basically the same as it is on EV paper. A theoretical line can be fitted by applying Equation 4 and Table 2 to the statistics computed from the logarithms of individual annual maxima. After replacing each annual maximum X by L = log X, one may proceed to obtain the mean and standard deviation of the transformed series $\bar{L}$ and s_L. The modified application of Equation 4 gives an estimate

$$\log X = \bar{L} + K_E s_L \qquad (11)$$

This produces the theoretical straight line in Figure 5.

Figure 4. S-shape of data plotted by Gringorten's formula showing EV distribution invalid for 180-min rainfalls in Tucson.

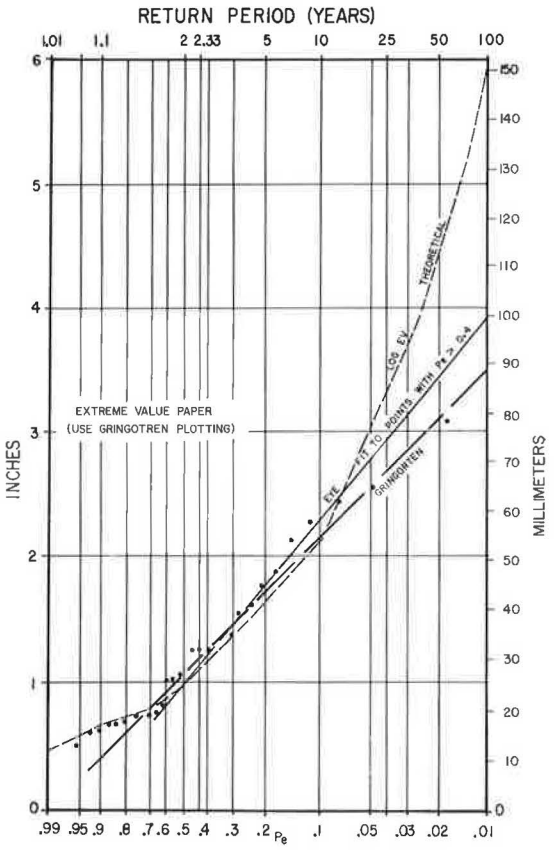

Log Scales

Data points may appear to be closer to the straight line in Figure 5 than to that in Figure 4. One should recognize the deceptive tendency for log-paper to apparently reduce the scatter of large values. The second-largest and largest appear closer to the logarithmic straight line in Figure 5 than to the eye-fit straight line in Figure 4. In fact, they are progressively 12.7 and 40.6 mm (0.5 and 1.6 in) of rain from the theoretical log-extreme value prediction. To emphasize this point the log-EV line, computed from Equation 11, was transformed back to linear units and added onto Figure 4 as a dotted curve.

A second problem of straight-line extrapolation on log paper is also emphasized by this dotted curve in Figure 4. The larger six or ten data points suggest a curve whose slope decreases with progressively longer return periods. The theoretical log-EV curve must, by definition, always have a constantly increasing slope. This is a violation of observations of large rains that particularly relate to our engineering interest in predicting for large return periods. Moreover, our understanding of the physical world suggests that the data should curve toward a horizontal asymptote representing a probable maximum precipitation (PMP) of all the moisture than can be drawn out from the finite overlying atmosphere. No one will deny that the log-EV curve gives the best representation of the 27 smaller data values in Figure 4, but that is not generally the domain of engineering interest.

Log-Normal and Normal Distributions

The classic log-normal (LN) paper, still favored by the Soil Conservation Service, is shown in Figure 6. This type of paper should always be tried in the search for the model that best fits a set of data. The attention that the Water Resources Council (WRC) has forced (8) on the log-Pearson Type III (LP III) makes it im-

Figure 5. Log-extreme value paper improving linearity of 180-min rainfalls from Tucson.

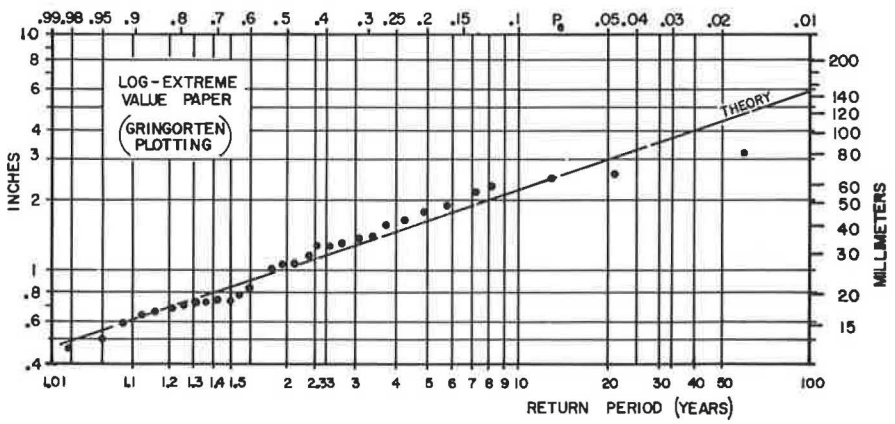

portant for engineers to understand the LN distribution, which is a special case of the LP III.

In Figure 6, the eye fit of this LN to 180-min rains was an acceptably straight line in the range around 5 to 10 years, for which it was used in Table 3. Graphically small deviations of points plotted at 20 and 40 years are actually more significant because the log transformation squeezed the vertical scale. True deviations were less when plotted on normal (N) paper. Extrapolation to the right side gave the best 50- and 100-year 180-min estimates, as signified by the arrows on the eye N line in Table 3.

One of the earliest probability distributions used was this so-called normal distribution. Its characteristic can be seen from Figure 7 to be a symmetrically changing spacing of the probability lines on either side of $P_e = 0.5$. This symmetry is due to its assumption that data will have a zero skewness coefficient, CSX. The latter statistical parameter can be evaluated, albeit with considerable trouble and risk of error, by hand computation as follows:

$$CSX = [N \Sigma (X - \bar{X})^3] / [(N - 1)(N - 2)(s_x)^3] \quad (12)$$

Engineers soon found that much of their hydrologic data had positive skewness. For instance, the highest floods were often of an order of magnitude greater than floods that occurred rather frequently. This relative largeness in the numerator of Equation 12 was greatly amplified by cubing the terms before summing. An escape from this problem was sought by making a log transformation; this was accomplished through the nonlinear spacing along the vertical axis of Figure 6. The apparent scaling down of larger values was to have drawn the entire annual series of the logarithms into a straight line. If this were perfectly achieved, then the data set would have a zero value for the coefficient of skewness of the logs, where

$$CSL = [N \Sigma (L - \bar{L})^3] / [(N - 1)(N - 2)(s_L)^3] \quad (13)$$

The advantage of the LN or N distributions is the extreme simplicity of fitting a mathematical curve. If a straight line effectively passes through a whole set of points on N paper, the theoretical line could be fitted as follows:

$$\bar{X} \text{ at } P_e = 0.5,$$

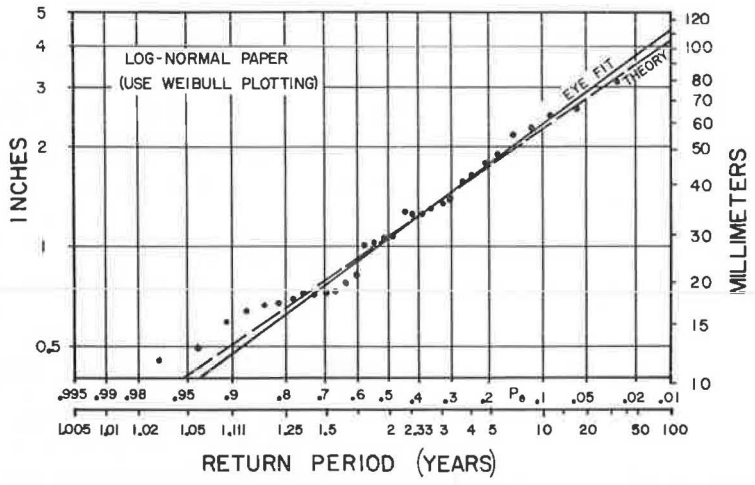

Figure 6. Example of classical log-normal analysis for 180-min rainfalls.

Table 3. Array of rainfalls expected for eight durations and four return periods from various curves.

Duration (min)	Curve	Preferred Order or Comment	Return Period (years) 5 mm	5 mm/min	10 mm	10 mm/min	50 mm	50 mm/min	100 mm	100 mm/min
5	Eye EV	Good	10.4	→ 3.08	13.4	→ 3.49	16.8	→ 3.35	18.3	→ 3.65
10		Good	17.3	→ 1.73	21.6	→ 2.16	30.5	→ 3.05	34.0	→ 3.40
20		Fair	28.2	→ 1.41	34.5	→ 1.73	49.8	→ 2.49	56.4	→ 2.82
30		S-shape	33.0	→ 1.10	41.1	→ 1.37	57.2	→ 1.90	64.8	→ 2.16
	Gringorten	Unacceptable	36.3		44.7		63.3		69.6	
	Eye EV		37.3	→ 0.83	47.5		71.4		80.8	
45	Eye LN		38.1		48.3	→ 1.07	74.4	→ 1.46	86.4	→ 1.69
	Theory LN		34.8		43.4		65.5		75.7	
	Eye N		39.1		48.8		66.0		71.6	
	Gringorten	Unacceptable	37.6		46.0		64.8		72.6	
	Eye EV		37.6		47.5		70.1		79.0	
60	Eye LN		38.1	→ 0.63	51.1	→ 0.85	83.6		99.3	→ 1.32
	Theory LN		35.8		45.2		66.0		76.2	
	Eye N		-		50.8		66.5	→ 1.11	79.3	
	Gringorten	Unacceptable	41.4		51.8		68.6		82.8	
	Eye EV	3	45.0	→ 0.36	55.1		73.2		92.7	
120	Eye LN	2	43.2		56.6	→ 0.47	94.0	→ 0.71	111.8	→ 0.80
	Eye N	1	45.5		56.9		76.7		83.6	
	Theory LN		40.6		51.1		76.7		88.7	
	Gringorten		43.4		55.1		78.2		88.9	
	Eye EV		45.2		57.7		87.4		99.1	
180	Eye LN		45.7	→ 0.25	60.2	→ 0.33	96.5		114.3	
	Eye N	1	46.2		59.5		81.8	→ 0.45	89.7	→ 0.50
	L-Gringorten	Unacceptable	41.4		55.1		112.0		149.9	

Notes: 1 mm = 0.039 in.
Arrows point to intensity corresponding to selected value.

$\overline{X}$ + s_X at P_e = 0.159, and
$\overline{X}$ - s_X at P_e = 0.841.

When fitting a theoretical LN line, antilogs must be taken, before plotting the line, according to

$\overline{L}$ at P_e = 0.5,
$\overline{L}$ + s_L at P_e = 0.159, and
$\overline{L}$ - s_L at P_e = 0.841.

Log-Pearson Type III

Nonlinearities of data, such as those seen in Figures 6 and 7, persisted to frustrate the mathematician. In 1923 Pearson developed a system of twelve types of curves to fit various degrees of upswing or flattening of data. The very next year this empirical system of curve fitting was applied to New York flood problems by H. A. Foster (12). Pearson's curve fitting was again discussed in E. E. Foster's excellent text (13) in 1948.

When the U.S. Army Corps of Engineers (14) proposed using Pearson's Type III (LP III) curve in 1962, they suggested that the log transformation be made to floods before proceeding with the computations. The procedure promulgated by the U.S. Water Resources Council first in 1967 and again in 1976 (8) requires the user to first take the log of each piece of data and then calculate their statistics: $\overline{L}$, s_L, and CSL. The last value is used to select K_P for various return periods, T, from Table 4. Substituting K_P values into Equation 14 and taking antilogs yield the LP III curve

$$\log X = \overline{L} + K_P s_L \quad (14)$$

The introduction of the third parameter, CSL, gives additional flexibility for closer fitting through observed points. Unfortunately, CSL is highly susceptible to sampling error caused perhaps by the presence of an abnormally large (outlier) maximum. Alternatively, another sample in time may by chance contain many values far smaller than its mean, which could cause CSL to become very negative. The great dangers of using LP III in predicting values for 100-year return periods (5, 15) lies in extrapolating curvature dictated by this error-prone CSL. The problem of determining CSL has led some authors to recommend the use of regional skewness, but that appears to be equally variable, and has led others

Figure 7. Normal paper suggesting empirical prediction line for large return periods and long duration rainfalls.

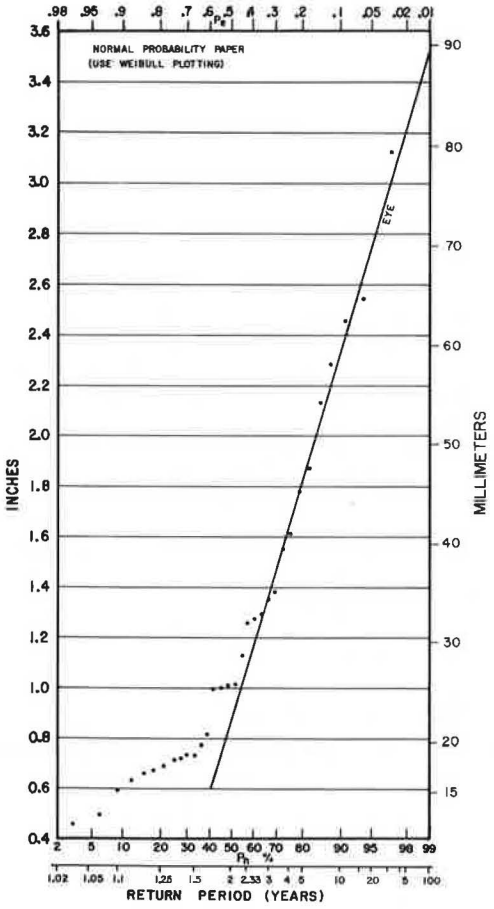

Table 4. K_p values for log-Pearson Type III analyses.

	P_e					
	0.90	0.429	0.10	0.02	0.01	0.002
	T					
CSL	1.111	2.33	10	50	100	500
3.0	-0.660	-0.284	1.180	3.152	4.051	6.205
2.9	-0.681	-0.274	1.195	3.134	4.013	6.117
2.8	-0.702	-0.263	1.210	3.114	3.973	6.017
2.7	-0.724	-0.251	1.224	3.093	3.932	5.922
2.6	-0.747	-0.238	1.238	3.071	3.889	5.825
2.5	-0.771	-0.226	1.250	3.048	3.845	5.728
2.4	-0.795	-0.213	1.262	3.023	3.800	5.628
2.3	-0.819	-0.200	1.274	2.997	3.753	5.527
2.2	-0.844	-0.185	1.284	2.970	3.705	5.425
2.1	-0.869	-0.171	1.294	2.942	3.656	5.321
2.0	-0.895	-0.155	1.302	2.912	3.605	5.215
1.9	-0.920	-0.139	1.310	2.881	3.553	5.108
1.8	-0.945	-0.125	1.318	2.848	3.499	5.000
1.7	-0.970	-0.108	1.324	2.815	3.444	4.890
1.6	-0.994	-0.092	1.329	2.780	3.388	4.779
1.5	-1.018	-0.075	1.333	2.743	3.330	4.667
1.4	-1.041	-0.058	1.337	2.706	3.271	4.553
1.3	-1.064	-0.041	1.339	2.666	3.211	4.439
1.2	-1.086	-0.025	1.340	2.626	3.149	4.323
1.1	-1.107	-0.008	1.341	2.585	3.087	4.206
1.0	-1.128	0.010	1.340	2.542	3.022	4.088
0.9	-1.147	0.026	1.339	2.498	2.957	3.969
0.8	-1.166	0.042	1.336	2.453	2.891	3.850
0.7	-1.183	0.058	1.333	2.407	2.824	3.730
0.6	-1.200	0.075	1.328	2.359	2.755	3.609
0.5	-1.216	0.095	1.323	2.311	2.686	3.487
0.4	-1.231	0.111	1.317	2.261	2.615	3.366
0.3	-1.245	0.126	1.309	2.211	2.544	3.244
0.2	-1.258	0.142	1.301	2.159	2.472	3.123
0.1	-1.270	0.158	1.292	2.107	2.400	3.001
0.0	-1.282	0.177	1.282	2.054	2.326	2.878
-0.1	-1.292	0.193	1.270	2.000	2.252	2.759
-0.2	-1.301	0.208	1.258	1.945	2.178	2.639
-0.3	-1.309	0.225	1.245	1.890	2.104	2.520
-0.4	-1.317	0.240	1.231	1.834	2.029	2.401
-0.5	-1.323	0.256	1.216	1.777	1.955	2.283
-0.6	-1.328	0.268	1.200	1.720	1.880	2.171
-0.7	-1.333	0.283	1.183	1.663	1.806	2.062
-0.8	-1.336	0.299	1.166	1.606	1.733	1.953
-0.9	-1.339	0.313	1.147	1.549	1.660	1.846
-1.0	-1.340	0.327	1.128	1.492	1.588	1.741
-1.1	-1.341	0.340	1.107	1.435	1.518	1.647
-1.2	-1.340	0.353	1.086	1.379	1.449	1.556
-1.3	-1.339	0.365	1.064	1.324	1.383	1.467
-1.4	-1.337	0.405	1.041	1.270	1.318	1.383
-1.5	-1.333	0.390	1.018	1.217	1.256	1.303
-1.6	-1.329	0.400	0.994	1.166	1.197	1.233
-1.7	-1.324	0.410	0.970	1.116	1.140	1.169
-1.8	-1.318	0.419	0.945	1.069	1.087	1.107
-1.9	-1.310	0.427	0.920	1.023	1.037	1.051
-2.0	-1.302	0.439	0.895	0.980	0.990	0.998
-2.1	-1.294	0.444	0.869	0.939	0.946	0.952
-2.2	-1.284	0.451	0.844	0.900	0.905	0.909
-2.3	-1.274	0.459	0.819	0.864	0.867	0.870
-2.4	-1.262	0.465	0.795	0.830	0.832	0.833
-2.5	-1.250	0.470	0.771	0.798	0.799	0.800
-2.6	-1.238	0.473	0.747	0.768	0.769	0.769
-2.7	-1.224	0.476	0.724	0.740	0.740	0.741
-2.8	-1.210	0.479	0.702	0.714	0.714	0.714
-2.9	-1.195	0.480	0.681	0.689	0.690	0.690
-3.0	-1.180	0.481	0.660	0.666	0.667	0.667

Table 5. Parameters from fitting IDF equation through observed intensities at eight durations.

Parameter	Return Period (years) 5	10	50	100	Approximate 2-Year Partial Duration ≤120 Min
a	50.1	66.0	91.1	102.1	33.7
b	17.29	18.97	18.64	17.91	14.49
r^2	0.999	0.999	0.995	0.993	0.999

Note: 1 in/h = 25 mm/h.

to suggest using a zero skewness of the logs. This causes the LP III curve to simplify back to the log normal.

Selecting the Frequency Curve

Mathematical statisticians are developing analytical tests for deciding which type of distribution, or model, best fits the data. Unfortunately, the sampling error in determining the parameters needed by the model's equation complicates the problem, which involves the interaction between the choice of model and uncertainty as to population parameters. Without knowing for certain the type of model, e.g., EV or LN, one cannot say whether the deviations of the data from the frequency curve are reasonable to expect from such a random process. Rather than discuss confidence bands within which a population estimate of, say, a 100-year rain can be expected to lie, this paper will simply consider the purpose for which each frequency analysis is performed.

Sometimes engineers require rainfall estimates for return periods from 20 to 100 years. In such a case, importance is ascribed to fitting a line through the 16 larger rains on Figure 7. On the other hand, designs may concern nuisance water with return periods below 2 years. In this case, attention would need to be paid to the lower part of the elbow in Figure 7.

With regard to those interested in larger rains, eye-fitted evaluation should be made to points with P_e greater than 0.4. For these, Figure 7 displays smaller variability of individual points than does Figure 4, and therefore takes precedence. Simultaneous consideration must be given to Figures 5 and 6, while observing the caution recommended with log-scales. The evaluation soon becomes very complex and beyond the capabilities of an electronic computer. If, on the other hand, computer output from fitting the EV, log-EV, LN, and LP III was simply read, the 100-year estimates would be 110.5, 294.4, 121.7, and 142.2 mm (4.35, 11.59, 4.79, and 5.60 in) respectively.

OBTAINING COMPATIBLE ESTIMATES FROM VARIOUS DURATIONS

An impression of the complexity can be had by studying the pros and cons of various frequency curves in Figures 4, 5, 6, and 7 simultaneously. Studies were also needed for 120-, 60-, 45-, 30-, 20-, 10-, and 5-min durations. For each of these an estimate had to be settled upon for the return periods of 5, 10, 50, and 100 years. Each cell could have involved choices among these six frequency curves: Gringorten, eye-fitted extreme value, eye-fitted log-normal, theoretically fitted log-normal, eye-fitted normal, or log-Gringorten. The array of results is presented in Table 3. The ultimate choice in each cell is marked with an arrow pointing to the equivalent intensity in millimeters per minute. In the 5-, 10-, 20-, and 30-min cases data were plotted so linearly on EV paper that estimates for all return periods should be read from that model rather than from any other paper. As durations increase, different probability papers serve better at fitting the observed maxima. With 45-min rain the eye EV and eye LN yield the best 5- and 10-year estimates. Longer durations' estimates sometimes are an average of two or more models from which arrows emanate.

Overall consistency within the IDF displayed by four curves in Figure 1 is a logical requirement. This constraint, as well as the frequency desiderata discussed above, must also be borne in mind. Thus for each duration in Table 3 intensities must increase toward the right. Likewise there must be a systematic decrease in the selected intensities down each column.

Another advantage of consolidating information across many frequency analyses is that the final curves smoothed through various durations in Figure 1 offset some sampling error. This is exemplified by the circles around the 100-year intensity-duration curve and crosses around the 5-year one. They represent the values settled on in Table 3. Eye fitting of curves through all four such sets of points to obtain generally concentric shapes provides further reinforcement across various return periods.

Intensity Duration Equations

Generalized relations along such curves and between various return periods have been found according to the classical equation

$$i = a/(b + t) \tag{15}$$

where a and b are different constants for each curve in Figure 1. They can be evaluated by the linear regression program wired into many pocket calculators by transforming Equation 15 to

$$it + ib = a \tag{16}$$

whence

$$a/i = b + t \tag{17}$$

and

$$1/i = (b/a) + (1/a)\,t \tag{18}$$

Reciprocals of finalized intensities from Table 3 are regressed as the dependent variable against t, the specified durations, that are considered free of error. The classical intercept and slope in parentheses can be manipulated to obtain a and b for Equation 15. Results of such an analysis are shown in Table 5. The coefficient of determination, r^2, (giving the fraction of the variation in 1/i that was explained by the equation), is highly satisfactory.

Once more the computer output need not be followed slavishly. The dashed portions of two curves in Figure 1 were sketched by eye where the mathematical model seemed to deviate too far from frequency estimates selected in Table 3.

Approximating the 2-Year Estimates

The smaller rainfall intensities that are exceeded every 2 years or more could cause damage or be a nuisance with economic impact, regardless of their occurring twice in one year or not at all in others. So strictly speaking a so-called "partial duration series" containing all events above a certain threshold value should be collected for an exact analysis of their statistics. Since

Table 1 of maximum annual rains does not contain that type of observation, we will have to content ourselves with approximations that seem rational.

A 2-year partial series (16) corresponds to an annual series return period of 2.33 years. The 2.33-year estimate made by extreme value (Gringorten) analysis was shown through Equation 4 and Table 2 to almost equal the mean of the annual series. Thus it is suggested that the mean, $\bar{X}$, be used as an approximation for the 2-year partial duration rainfall. The curve was not added to Figure 1, but a and b as determined from Equation 15, in this case for i millimeters per hour and t minutes are listed on the right of Table 5.

CONCLUSION

Only through the human integration of process and probability understanding can the mass of computer output be transformed into design curves for practitioners.

REFERENCES

1. J. W. Clark and W. Viessman, Jr. Water Supply and Pollution Control. International Textbook, Scranton, PA, 1965.
2. Subcommittee on Small Water Storage Projects of National Resources Committee. Low Dams—A Manual of Design for Small Water Storage Projects. U.S. Government Printing Office, 1938.
3. Rainfall Intensity-Duration-Frequency Curves. U.S. Weather Bureau, Technical Paper No. 25, 1955.
4. D. M. Hershfield. Rainfall Frequency Atlas of the United States for Durations From 30 Minutes to 24 Hours and Return Periods From 1 to 100 Years. U.S. Weather Bureau, Technical Paper No. 40, 1961.
5. B. M. Reich. Magnitude and Frequency of Floods. CRC Critical Reviews in Environmental Control, Vol. 6, No. 4, 1976, pp. 297-348.
6. C. T. Haan. Statistical Methods in Hydrology. Iowa State Univ. Press, Ames, 1977.
7. J. R. Benjamin and C. A. Cornell. Probability, Statistics, and Decisions for Civil Engineers. McGraw-Hill, New York, 1970.
8. Guidelines for Determining Flood Flows Frequency. U.S. Water Resources Council, Bulletin No. 17 of the Hydrology Committee, March 1976.
9. I. I. Gringorten. A Plotting Rule for Extreme Probability Paper. Journal of Geophysical Research, Vol. 68, No. 3, 1963, p. 813.
10. C. Cunnane. Unbiased Plotting Positions—A Review. Journal of Hydrology, Vol. 37, 1978, pp. 205-222.
11. R. H. Frederick, V. A. Meyer, and E. P. Auciello. 5- to 60-Minute Precipitation Frequency Maps for the Eastern and Central U.S. National Oceanographic and Atmospheric Administration, Technical Memo NWF HYDRO 35, 1977.
12. H. A. Foster. Theoretical Frequency Curves. Trans., ASCE, Vol. 87, 1924, p. 142.
13. E. E. Foster. Rainfall and Runoff. Macmillan, New York, 1948.
14. L. R. Beard. Statistical Methods in Hydrology. U.S. Army Corps of Engineers, Sacramento, CA, 1962, pp. 74.
15. B. M. Reich. "Lysenkoism" in U.S. Flood Determinations. Paper presented to the American Geophysical Union, Surface Runoff Committee, San Francisco, Dec. 1977.
16. R. K. Linsley, Jr., M. A. Kohler, and J. L. Paulhus. Hydrology for Engineers. McGraw-Hill, New York, 1958.

Publication of this paper sponsored by Committee on Hydrology, Hydraulics, and Water Quality.